

Institut für Theoretische Physik  
Fakultät Mathematik und Naturwissenschaft  
Technische Universität Dresden



# Theoretical aspects of motor protein induced filament depolymerisation

**Dissertation**

Zur Erlangung des akademischen Grades  
Doktor der Naturwissenschaften  
(Dr. rer. nat.)

angefertigt am Max Planck Institut  
für Physik komplexer Systeme  
Dresden



vorgelegt von

**Gernot A. Klein**

Dresden, 2005



---

# Contents

<b>1</b>	<b>Introduction</b>	<b>1</b>
<b>2</b>	<b>The cytoskeleton and motor proteins</b>	<b>5</b>
2.1	Cytoskeletal filaments . . . . .	5
2.1.1	Structure and organisation of actin and intermediate filaments . . . . .	6
2.1.2	Assembly and structure of microtubules . . . . .	8
2.2	Cytoskeletal motor proteins . . . . .	10
2.2.1	Myosin and dynein . . . . .	11
2.2.2	Kinesin . . . . .	12
2.3	Microtubule dynamics and structures . . . . .	14
2.3.1	Force generation by polymerising filaments . . . . .	14
2.3.2	Dynamic instability of growing microtubules . . . . .	16
2.3.3	Reorganisation of microtubules during mitosis . . . . .	17
2.4	Microtubule-depolymerising motor proteins . . . . .	18
2.4.1	Properties of kinesin-13 motors . . . . .	19
2.4.2	Mechanism of microtubule depolymerisation . . . . .	20
2.4.3	Cellular functions . . . . .	22
2.5	Theoretical description of motor proteins . . . . .	23
2.5.1	Phenomenological approach . . . . .	23
2.5.2	Isothermal ratchet models . . . . .	25
2.5.3	Stochastic models on discrete lattices . . . . .	26
<b>3</b>	<b>General description of motor induced filament depolymerisation</b>	<b>29</b>
3.1	Filament depolymerisation . . . . .	29

## ii Contents

3.1.1	Dynamics of motor densities . . . . .	30
3.1.2	Motor induced filament depolymerisation . . . . .	31
3.1.3	Processive subunit removal . . . . .	32
3.2	Steady-state solutions . . . . .	32
3.2.1	Density profiles of motor proteins . . . . .	33
3.2.2	Stability of solutions . . . . .	34
3.3	Dynamic accumulation of motor proteins . . . . .	36
3.3.1	Mechanisms of motor accumulation at filament ends . . . . .	36
3.3.2	Influence of collective effects . . . . .	37
3.3.3	Role of processivity . . . . .	41
3.4	Instabilities due to collective effects . . . . .	42
3.5	Summary . . . . .	45
<b>4</b>	<b>Microscopic mechanisms and fluctuations</b>	<b>47</b>
4.1	Lattice description of motor dynamics . . . . .	47
4.1.1	Microscopic interactions . . . . .	48
4.1.2	Influence of crowding . . . . .	49
4.2	Master equation approach . . . . .	51
4.3	Mean-field approximation . . . . .	52
4.3.1	Continuum limit and mean-field approximation . . . . .	52
4.3.2	Connection to generic description . . . . .	54
4.4	Depolymerisation mechanisms influencing accumulation . . . . .	56
4.4.1	Crowding hindering depolymerisation . . . . .	57
4.4.2	Crowding reducing processivity . . . . .	58
4.5	Effects of fluctuations . . . . .	60
4.6	Summary . . . . .	60
<b>5</b>	<b>Effects of multiple protofilaments</b>	<b>63</b>
5.1	Coupling of sublattices by motor dynamics . . . . .	63
5.2	Effects on accumulation . . . . .	66
5.2.1	Effects of inter-sublattice processivity . . . . .	67
5.2.2	Regimes of accumulation . . . . .	68
5.3	Edge structure of multiple sublattices . . . . .	69
5.3.1	Uncoupled sublattices . . . . .	70

5.3.2	Coupled sublattices . . . . .	71
5.4	Ring currents of motors . . . . .	75
5.5	Mean-field description with effective parameters . . . . .	76
5.6	Summary . . . . .	80
<b>6</b>	<b>Motor induced filament depolymerisation under applied forces</b>	<b>81</b>
6.1	Generic description . . . . .	81
6.1.1	Collective effects of bound motors . . . . .	82
6.1.2	Dynamics of unbound motors . . . . .	84
6.1.3	Force balance . . . . .	84
6.2	Force-velocity relationships . . . . .	85
6.2.1	Depolymerisation velocity . . . . .	85
6.2.2	Critical detachment force . . . . .	88
6.3	Role of fluctuations . . . . .	88
6.3.1	Evolution equations . . . . .	88
6.3.2	Comparison with generic theory . . . . .	91
6.4	Summary . . . . .	94
<b>7</b>	<b>Summary and Perspectives</b>	<b>97</b>
<b>A</b>	<b>Parameter determination in the generic description</b>	<b>101</b>
<b>B</b>	<b>Master and evolution equations for the one-dimensional discrete model</b>	<b>107</b>
<b>C</b>	<b>Subunit labelling and rate determination on an array of sublattices</b>	<b>109</b>
<b>D</b>	<b>Master equations for the two-dimensional discrete model</b>	<b>113</b>
<b>E</b>	<b>Random deposition model</b>	<b>117</b>
	<b>Bibliography</b>	<b>119</b>



---

# Introduction

Many active biological processes, for example cell locomotion, the transport of organelles inside the cell, and cell division, are driven by highly specialised motor proteins which interact with the cytoskeleton. The cytoskeleton is a network of filamentous structures which are linear aggregates of proteins, for example actin and tubulin. In a living cell, actin filaments and microtubules are dynamic structures and can rapidly change their lengths by addition and removal of subunits at the ends, allowing their use for a wide range of different tasks. Because they have two structurally distinguishable ends, these filaments exhibit an asymmetry along their lattice, determining the direction of motion of, and force generation by bound motor proteins. These motor proteins are able to transduce the chemical energy of a fuel called ATP to do mechanical work while interacting with a filament.

In addition to generating forces along filaments, it is now a well-established fact that certain motor proteins can also interact with filament ends, where they influence polymerisation and depolymerisation. Examples of depolymerising proteins are certain members of the kinesin family, with members of the KIN-13 subfamily being the best-studied so far, which are capable of depolymerising microtubules and regulating microtubule lengths in a cell. One role for KIN-13 family members is thought to be in the mitotic spindle, a microtubule structure that is formed in the process of cell division and is responsible for separation and distribution of the duplicated genetic material to the forming daughter cells. The accurate distribution of the genetic material to daughter cells is essential for the survival of the cells and the whole organism. During the process of division, shortening microtubules generate forces which pull the chromosomes to which they are attached towards the opposing poles of the cell.

Recent experimental studies have started to illuminate the essential contributions of members of the KIN-13 subfamily to the assembly of the mitotic spindle and subsequent chromosome segregation, for example correcting the erroneous attachment of microtubules to chromosomes and producing chromosome movement towards the poles of the cell. In addition, *in vitro* assays have elucidated kinetic properties of these proteins and have produced astonishing results, notably protein accumulation at depolymerised filament ends, the possibility of processive subunit removal and surprisingly fast filament end finding by these proteins. These and further aspects of the biological background to this work is given in chapter 2.

In contrast to the ongoing experimental engagement, no theoretical attempts to find underlying mechanisms and principles, which could help explain these phenomena, has been made so far. The aim of this work therefore is to develop a theoretical framework capable of describing experimentally observed behaviour, shed light on underlying principles of motor induced subunit removal and, going a step further, make predictions about how these proteins may behave in situations not yet experimentally investigated. As these motor proteins consume energy in order to induce subunit removal, they represent a non-equilibrium system and the observed phenomena cannot be described with the standard concepts of equilibrium statistical mechanics. In the following work we will therefore use two different theoretical approaches to describe motor dynamics, introduced in chapter 3 and chapter 4.

In chapter 3 we will describe motor dynamics by phenomenological continuum equations. Here, instead of describing individual motor proteins, motor densities are considered and fluctuations due to the discrete number of proteins are neglected. In general, this kind of description is applicable for spatially extended systems and for describing dynamic behaviour on length scales which are large compared to the underlying molecular length scales. One of the main advantages of this approach is the minor amount of microscopic information needed, in order to formulate equations which correctly describe the system. Therefore, the continuum equations themselves are to a large extent independent of the underlying molecular details of the system, whereas the specific values of the macroscopic parameters entering the equations are determined by these details.

In chapter 4 on the other hand, we take the discrete nature of the motor proteins explicitly into account, leading to a stochastic description of motors on a filament. Here, motor proteins are represented by identical particles moving stochastically on a discrete lattice. This kind of description is part of a class of driven lattice gas models which are used to study a broad range of transport phenomena, including the movement of motor proteins on filaments, the diffusion of ions in channels and the traffic flow of cars on highways. This kind of description enables us to discuss the effects of different microscopic mechanisms of subunit removal and to investigate the role of fluctuations on the dynamic behaviour of motor proteins. These are expected to become important if motor dynamics are observed on length scales comparable to the underlying molecular length scales, or if the number of observed proteins becomes small.

A discrete stochastic description of motor dynamics in two dimensions is formulated in chapter 5. By approximating a microtubule, which is consisting of several parallelly aligned protofilaments, to an array of periodically aligned lattices, we can investigate how the presence of multiple protofilaments influences subunit removal. Additionally, this stochastic model allows us to examine motor behaviour arising due to the structure of a microtubule lattice. As most microtubules exhibit a seam between two of the protofilaments, breaking the cylindrical symmetry of the microtubule, and motor proteins consume energy in order to induce subunit removal, thus operating in a non-equilibrium regime, ring currents of motor proteins on the circumference of a microtubule can occur. We also address how subunit removal, and consequently the structure of the edge of the lattice array, is influenced by motor dynamics and how it evolves in time. The interpretation of subunit removal as an inverse growth process is discussed in relation to descriptions of the growths of surfaces.

In a cell, certain members of the KIN-13 subfamily are linked to chromosomes, while

interacting with the ends of microtubules belonging to the mitotic spindle. Due to the linkage, motors are not free to move but are mechanically coupled and remove subunits under the influence of external forces. This can be mimicked by experiments in which motors are linked to beads on which forces can be exerted. In chapter 6 we discuss this collective behaviour of motor proteins which are linked to such a common anchoring point and examine the influence of an externally-applied force on motor-induced subunit removal.



---

# The cytoskeleton and motor proteins

In this chapter we will provide the biological background required for assessing the following work. We will focus on the cytoskeleton of living cells and associated motor proteins. For a general and comprehensive introduction to the area of molecular cell biology, we refer the reader for example to Alberts et al. (2002); Lodish et al. (2003) or Bray (2001). An introduction to this field from a more physical point of view can be found in Howard (2001) and Nelson (2004).

## 2.1. Cytoskeletal filaments

One of the most fascinating and essential capacities of living cells is the ability to actively migrate in multicellular organisms or even outside them, for example on a substrate. In addition to this dynamic property, the soft bodies of cells also show remarkable mechanical properties, e.g. cells are able to recover their original shape after an external stress has been imposed on them. The structural element responsible for these extraordinary properties is the cytoskeleton, a three-dimensional system of protein fibres extending throughout the cytoplasm of all eucaryotic cells. The cytoskeleton is composed of three types of fibres - actin filaments (also called microfilaments), intermediate filaments and microtubules. These filaments are organised by a variety of accessory proteins into discrete structures like bundles, networks and gel-like lattices and are linked to organelles and the plasma membrane of the cell. In a living cell, these structures are highly dynamic and continuously assemble and disassemble in order for the cell to move and change shape.

Besides its importance for the movements of entire cells, the cytoskeleton is also critical for the movements taking place within cells, e.g., the transport of membrane vesicles and molecular materials or the active separation of chromosomes during cell division. This internal movement additionally requires a special class of proteins, the so-called molecular motors (see below), which are able to use actin filaments and microtubules as tracks, along which they can move, carrying different kinds of cargo with them.

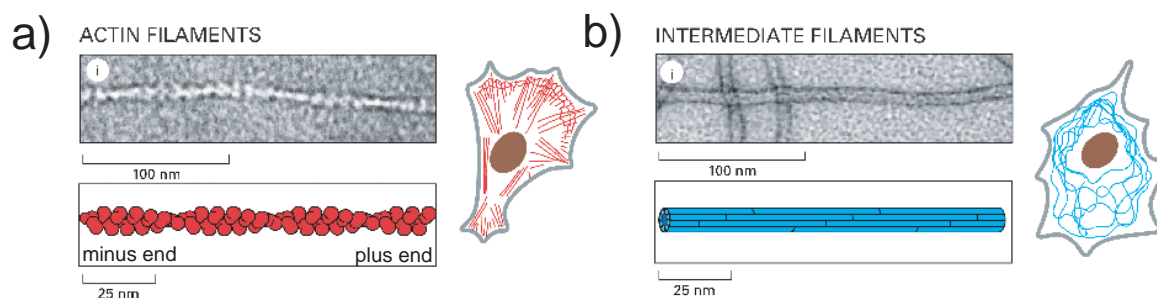


**Figure 2.1:** a): Illustration and micrograph of an actin filament. Actin filaments are polar, with two structurally distinguishable ends. Their diameter is between 5 – 9nm and their highest concentration can be found just beneath the cell membrane. b): Illustration and micrograph of intermediate filaments. Intermediate filaments are ropelike fibers with a diameter of approximately 10nm. In contrast to actin filaments and microtubules they do not exhibit a structural asymmetry. Adopted from (Alberts et al., 2002).

### 2.1.1. Structure and organisation of actin and intermediate filaments

#### Actin filaments

In eukaryotic cells, actin is found in two forms: as an approximately globular monomer, called G-actin; and as an elongated linear polymer, called F-actin which is build up of G-actin monomers. The diameter of the monomers is roughly 6nm and each monomer has a deep cleft, which is used for binding and hydrolysis of ATP. The dynamics of polymerisation and depolymerisation of F-actin filaments is governed by ATP hydrolysis<sup>1</sup>. An actin filament can be imagined as a two-stranded helix of identical globular G-actin monomers. The diameter of the filament is between 7 – 9nm and due to this thin structure actin filaments are highly flexible in comparison for example to microtubules. The average persistence length is 9–12 $\mu$ m (Yanagida et al., 1984; Gittes et al., 1993; Riveline et al., 1997). All monomers are oriented in the same direction and thus the whole filament itself exhibits polarity. The two structurally different ends are called the plus and minus end, where by convention the end of the filament where the cleft for ATP binding is exposed, is called the minus end. The individual actin filaments are normally organised into filament bundles and networks. In order for these bundles and networks to be stable and resistant, so-called actin cross-linking proteins are required.

Actin filaments are highly dynamic and are constantly growing or shrinking. As a first step for actin filaments to polymerise, G-actin monomers have to form stable aggregates of 3 to 4 monomers. These oligomers can then act as nucleation seeds which are then rapidly elongated by addition of subunits to either side of the seed. Because of the structural differences of the ends, the growth rate of the plus end is five to ten times faster than that of the minus end. As filament sizes increase, the concentration of monomers drops, until an equilibrium situation is reached. In this equilibrium, actin filaments still exchange subunits at the end, but no net mass change occurs. In this situation *treadmilling* can occur, where subunits are added at the plus side of the filament and are lost with at same rate at the minus end of the filament. The total length of the filament thus stays the same, but individual subunits move from the minus end through the filament to the plus end, reaching speeds around 0.03 $\mu$ m/*min*.

<sup>1</sup>Note that the onset of polymerisation depends strongly on the ionic strength of the solution

Actin contributes to cell and intracellular motion in a variety of contexts. Certain bacteria (e.g. *listeria monocytogenes*) are thought to move through the cytoplasm of infected cells by polymerising actin filaments at the base of the bacterium, thus being pushed forward by the forces generated by the actin meshwork assembly at the tail of the bacteria (reaching speeds up to  $11\mu\text{m}/\text{min}$ ). In fibroblasts or keratinocytes actin filaments play a key role in the protrusion of lamellipodia and filopodia, where they form a network of crosslinked filament bundles which is able to produce forces, pulling the cell forward. Actin filaments also take part in the process of cell division, when the so called contractile ring, a structure of parallel and anti-parallel aligned actin filaments cleaves the cell in the middle and finally physically divides it. In combination with myosin motor proteins, actin filaments are the crucial component of contraction and force production in muscle cells.

### Intermediate filaments

Intermediate filaments are rope-like structures with a diameter of about 10nm, thus lying between the diameter of actin filaments and microtubules, giving rise to their name. The subunits of these filaments are elongated fibrous proteins consisting of a globular head, a globular tail and a central elongated helical rod domain. Although the exact structural build up of intermediate filaments from these subunits is not yet absolutely clear, it is thought that two subunits form a homodimer, which then can form anti-parallel tetramers. These are then thought to align head-to-tail and side-by-side to form the final rope-like intermediate filament. The structural diversity of the proteins forming the intermediate filaments is much higher than of the proteins forming actin filaments and microtubules. They can be roughly grouped in four subfamilies, forming different intermediate filaments: *Keratin*-filaments occurring in epithelial cells, *vimentin*-filaments in muscle cells and neuroglial cells, *neurofilaments* in nerve cells and *nuclearlamins*, occurring in the nuclear membrane of animal cells.

Besides all the differences of the underlying subunits of these filament, they share a few common properties. All of them are highly stable structures and because of this stability, they are unable to contribute to cellular motility the way that actin filaments and microtubules do by polymerisation and depolymerisation. Due to the symmetric non polar structure of the subunits, the overall structure of intermediate filaments is also nonpolar. Thus intermediate filaments cannot be used as tracks for motor proteins (see chapter theoretical description of motors). Another common property of intermediate filaments, which also distinguishes them from actin filaments and microtubules, is their inability to bind nucleotides. Their assembly takes place without the hydrolysis of ATP or GTP.

The main role of intermediate filaments, very generally speaking, is the reinforcement of cells, or certain delicate parts of these cells, that are subject to stress. Examples are muscle cells and skin cells, where these filaments, by stretching and distributing the applied forces, circumvent the disruption or damage of the cell membrane.

### 2.1.2. Assembly and structure of microtubules

#### Microtubule structure

Microtubules are straight hollow cylindrical nanotubes with an approximate outer diameter of 24nm and a varying length ranging from a fraction of a micrometre to a few hundred micrometres. Due to the cylindrical build-up, microtubules are very stiff structures, with a persistence length of 2 – 3mm (Gittes et al., 1993; Venier et al., 1994). Each microtubule in a cell generally consists of 13 protofilaments arranged in parallel<sup>2</sup>, linear aggregates that are composed of heterodimeric subunits, called tubulin dimers, which themselves consist of two closely related globular proteins,  $\alpha$ -tubulin and  $\beta$ -tubulin (see Fig.2.2). Each of these monomers are approximately 4nm in diameter. The  $\alpha$ -tubulin and  $\beta$ -tubulin in a dimer are very stably bound together by noncovalent interactions, so that the dimer under normal conditions rarely dissociates into individual  $\alpha$ -tubulin and  $\beta$ -tubulin monomers. Each dimer is capable of binding two molecules of GTP nucleotide, one at the  $\alpha$ -tubulin and one at the  $\beta$ -tubulin. The GTP binding site of  $\alpha$ -tubulin is blocked by the  $\beta$ -tubulin of the dimer, so that a bound GTP molecule cannot be released and is also never hydrolysed. The nucleotide bound to the  $\beta$ -tubulin may be exchanged and it can also be hydrolysed to GDP, strongly influencing the dynamic behaviour of microtubules. In a protofilament all these dimers are arranged with the same orientation, the free side of the  $\beta$ -tubulin of a dimer forms an interface with the free side of an  $\alpha$ -tubulin of another dimer, resulting in an overall polarity of the protofilament. As all protofilaments in a microtubule are aligned in parallel, the whole microtubule shows the same polarity, with  $\alpha$ -tubulin being exposed on one side and  $\beta$ -tubulin on the other, resulting in two structurally different ends. Due to the structural difference between the ends of a microtubule, the rate constants for association and dissociation of subunits can differ at both ends, thus leading to different dynamic behaviour. The end showing faster growth and shrinkage is often called the plus end, while the slower growing and shrinking end is called the minus end. It has been shown, that the  $\beta$ -tubulin side is the one with the faster dynamics. In a microtubule, each protofilament is slightly shifted longitudinally in respect to its neighbouring protofilaments, giving the microtubule in addition to its polarity a helical structure, see Fig.2.2. In addition to forming singlet microtubules, protofilaments may also form doublet or triplet microtubules, as found in cilia or flagella and centrioles or basal bodies respectively.

#### Microtubule dynamics

In living cells microtubules are formed by nucleation of  $\alpha$ -tubulin and  $\beta$ -tubulin at a specific location in the cell, called the microtubule-organizing center (MTOC). In most animal cells there is only one MTOC, the centrosome, which is located close to the cell nucleus. In fungi and higher plant cells microtubules are nucleated at several places, called the spindle pole body, a small plaque embedded on the nuclear envelope. While differing in many respects, all MTOCs contain a third type of tubulin, the so called  $\gamma$ -tubulin, that is present in a ring-like structure and acts as a nucleation seed. The  $\alpha$ ,  $\beta$ -tubulin add to the  $\gamma$ -tubulin -

---

<sup>2</sup>there are however also microtubules with 3, 7 and 15 protofilaments.

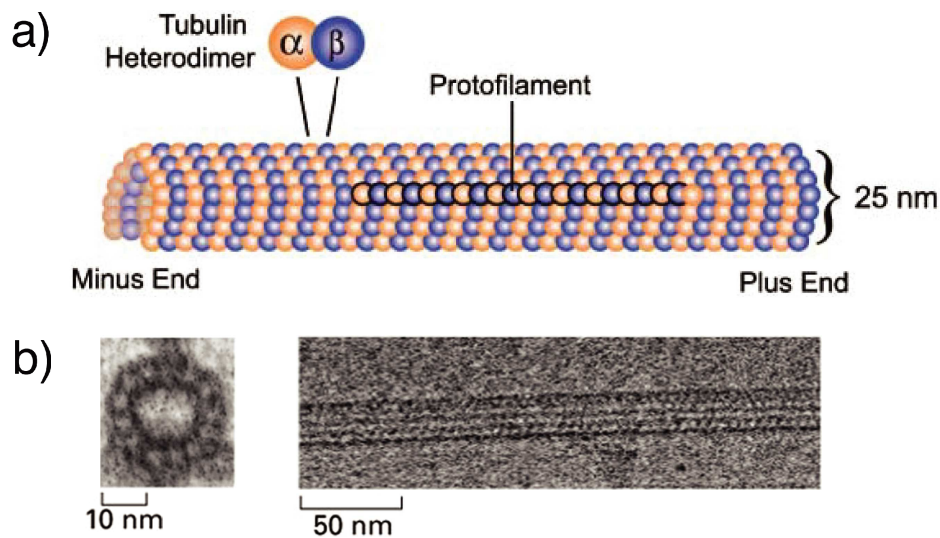


**Figure 2.2:** a): Illustration of microtubule structure. Microtubules are hollow cylinders composed of parallel aligned protofilaments. Each protofilament is a linear aggregation of approximately 8nm long heterodimers, consisting of two distinct proteins,  $\alpha$ -tubulin and  $\beta$ -tubulin. All heterodimers are arranged in the same orientation in a protofilament, leading to an overall polarity of the microtubule with two structurally different ends. The minus end exhibits slower growth and shrinkage than the plus end. Taken from (Kline-Smith and Walczak, 2004). b): Electron micrograph of a cross section of a microtubule and of a microtubule lattice. Adopted from (Alberts et al., 2002).

ring in such a way, that the  $\alpha$ -tubulin end is located in the MTOC, while the  $\beta$ -tubulin end is growing outwards to the cell periphery. The spontaneous nucleation of  $\alpha, \beta$ -tubulin without a  $\gamma$ -tubulin acting as a nucleation seed is under normal conditions only possible at much higher concentrations of free  $\alpha, \beta$ -tubulin than present in a living cell. This way, by providing  $\gamma$ -tubulin as a nucleation side, cells can control where microtubules form in the cell.

### The role of microtubules in cells

One of the key functions of microtubules is the formation of the mitotic spindle during cell division (mitosis). In mitosis, the chromosomes that have been duplicated are equally separated into the opposing parts of the cell, before the cell is divided in the middle to form two new daughter cells. The role of the mitotic spindle is to capture and attach to chromosomes in order to align them in the equatorial plane of the cell so that they can be evenly separated to each daughter cell.

Besides their role in cell division, where microtubules have to be constantly remodelled, they can also play an important role in cells where they need to be highly stable. Examples are eukaryotic cilia and flagella, where microtubules form the key structure that due to the action of motor proteins is able to bend and thus for example is used to propel sperm cells.

As already mentioned, microtubules also provide the tracks for active transport by motor proteins, as for example the organisation and distribution of organelles like mitochondria and the endoplasmic reticulum or the transport of proteins from neurons to the axon terminals.

## 2.2. Cytoskeletal motor proteins

Motor proteins are specialised enzymes that are involved in many cellular movements. Some motor proteins generate rotary movement, e. g. the  $F_0F_1$  complex, which is involved in the beat of bacterial flagella or the packing of DNA into the capsid of a virus. Others generate linear motion, like RNA polymerases which translocate along DNA during transcription, or cytoskeletal motor proteins that are able to bind to and move along cytoskeletal filaments. Cytoskeletal motor proteins which move along polarised cytoskeletal filaments can be divided in three families: myosins, kinesins and dyneins. Each family is defined by sequence similarity in the motor domains, where proteins of each family on average share 50% identical amino acid sequence. Additionally, motor proteins of a single family always interact with the same kind of filaments: kinesin and dynein motors bind to microtubules, while myosin motors interact with actin filaments. Up to now, there are no motors known to move on the non-polar intermediate filaments.

Axonemal dyneins, conventional kinesin and muscle myosin have been visualised using electron microscopy, as elongated molecules, with lengths between 40 – 100nm. Despite the unique features of each of these motor proteins, enabling them to fulfil particular tasks in the cell, all motor proteins have two structurally different parts: a globular head domain (also called motor domain), able to bind to congruent filaments and ATP molecules. Myosin and kinesin motors can have one or two motor domains, while dyneins can have up to three heads (Alberts et al., 2002); the second part is an elongated tail region that is used to attach the protein to its cargo or other motor proteins. While the sequence of the motor domains is highly conserved between members of one family, the tail sequences can differ greatly. Due to this difference in the tail region, different proteins are able to transport a wide variety of different cargos. Motors of the three families not only work as monomers, but they can oligomerise to dimers, trimers and tetramers (Howard, 2001).

One of the key features common to all proteins of the myosin, kinesin and dynein families is the ability to hydrolyse ATP molecules, which are bound to the motor domain of the protein, to ADP and phosphate and convert the free energy gained in this reaction to mechanical work. Microscopically, this is achieved by a conformational change of the ATP-binding structure, subsequent to the loss of the phosphate group from ATP. This first, tiny structural rearrangement<sup>3</sup> is then mechanically amplified to a step of the motor protein of several *nm* (Schliwa, 2003). Exactly how the cycle of ATP hydrolysis is coupled to the mechanical cycle of protein motion is still under strong debate and may also vary for different kinds of motor proteins.

Due the structure of the motor domain, motors of the three families only attach at specific binding sites to their associated filaments and always with a specific orientation. The forces generated by motors will therefore always lead to a directed movement on the filament, determined by the polar structure of the filament. Initially it was believed that motors of one family move in one direction only, namely kinesin motors to the plus end and dynein motors to the minus end of microtubules and myosin to the plus end of actin filaments. This belief had to be abandoned, after kinesin and myosin motors were discovered that move unidirectionally to the respective opposite end of the filament. The directionality of motor proteins could be observed through the use of *in vitro* motility assays. In general, one can

---

<sup>3</sup>The loss of the phosphate group is thought to leave a space of approximately 0.5*nm*

distinguish two different kinds of assays: the bead assay and the gliding assay. In the bead assay, filaments are attached to a surface, while the motor proteins are fixed to a bead. The motion of the bead due to the interaction of proteins with the filaments can then be observed using light microscopy. In the gliding assay, motor proteins are fixed to a surface, and the filaments are observed to glide along the motor coated surface, after attachment of motors to the filaments. Besides the directional motility of proteins, another important feature of motor protein dynamics was discovered with in vitro motility assays, namely the processivity of proteins. Some motor proteins are able to move continuously along the filament over distances, that correspond to several hundred individual steps. These motor proteins are described as working processively, while proteins which detach rapidly from the filament and thus only perform a few single steps, are called non-processive (Howard, 2001).

### 2.2.1. Myosin and dynein

#### Myosin

Myosin motors are the only cytoskeletal motor proteins that associate with actin filaments. The first member of this family (and also the first motor protein to be discovered at all) was discovered in complex with actin filaments already in 1864 (Kuehne et al., 1864) and first isolated in 1941 (Szent-Gyorgyi, 1941). This founding member, now labelled sarcomeric myosin II, was later then identified as forming crossbridges between thin and thick filaments of muscle (Huxley, 1957) and thus being responsible for the contraction of muscles. Being the first myosin motor to be discovered, myosin II is often also referred to as *conventional* myosin and all other types of myosin as *unconventional* myosins. Today, myosin motors are grouped in a total of 18 classes with each class consisting of several different isoforms. In spite of sharing a well conserved motor domain, myosin motors show a broad diversity of structure and kinetic properties like the directionality of their movement and the processivity: some myosin motors are two headed, for example myosin II, V and myosin VI while others only have one head, for example myosin I and myosin IXb (Schliwa, 2003). While most myosin motors show plus-end directed motion, myosin VI and myosin IX exhibit minus-end directed motion. The motion on the filaments can be non-processive as in the case of myosin II, or processive as in the case of myosin V<sup>4</sup> and myosin IXb. As non-processive or low-duty motors detach after a single step, they normally work coordinately in large assemblies, like myosin II during muscle contraction while processive motors like Myosin V are able to move large distances on their own.

Myosin motor proteins are involved in a wide range of biological functions. Examples apart from the role of myosin II in the contraction of muscles are for example vesicle transport via myosin V and the organisation of stereocilia in sensory hair cells through myosin VII (Schliwa, 2003). For newest developments in myosin research, see (Myosin-Homepage).

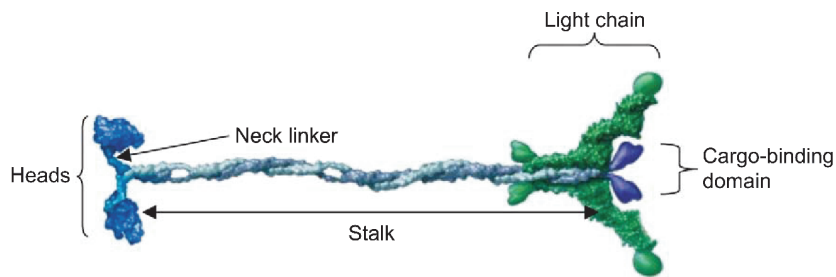


**Figure 2.3:** Structure of kinesin I. The two identical heads are able to bind microtubules and ATP molecules. Each head is connected to a neck linker which can undergo nucleotide-dependent conformational changes and thus allows for stepping. At the other end of the roughly  $70nm$  long coiled-coil stalk, kinesin has a cargo-binding domain, allowing it to bind to distinct organelles and vesicles. From, (Vale, 2003; Yildiz and Selvin, 2005).

## Dynein

Although dynein was the second motor protein to be discovered in 1965 (Gibbons and Rowe, 1965), where it was shown to be a force-generating crosslinker between microtubules in cilia, less is known about it than about myosin and kinesin. In comparison to myosin and kinesin motors, dynein motors are between two and four times larger, they are constructed of several smaller proteins, which are generally labelled heavy, intermediate and light chains, to indicate their differences in weight and they can have up to three heads (Schliwa, 2003). Dynein seems to be the only family of cytoskeletal motor proteins with all its members showing the same directionality of their movement, namely towards the minus end of microtubules although dynein with oscillatory behaviour has been reported (Shingyoji et al., 1998). The average speeds of dyneins range from  $2 - 7\mu m/s$ . Today, dyneins are categorised into two major groups: axonemal and cytoplasmic dynein (Oiwa and Sakakibara, 2005). Axonemal dyneins are found in eukaryotic cilia and flagella (Gibbons, 1981) where they produce bending motion by sliding microtubules relative to each other. The group of axonemal dyneins can be further divided into inner and outer arm dyneins. While it seems that inner arm dynein, for example dynein-c, works processively (Sakakibara et al., 1999), outer arm dynein showed processive motion at low ATP concentrations, but non-processive behaviour, similar to muscle myosin, for higher ATP concentrations (Hirakawa et al., 2000). Cytoplasmic dynein, thought to have two identical head regions, is a processive protein and involved in a variety of cellular processes, like transport of intracellular organelles, organisation of the mitotic spindle and chromosome separation (Hirokawa, 1998).

### 2.2.2. Kinesin

Kinesins associate, like dyneins, with microtubules and are involved in cargo transport and mitosis. The first member of this superfamily was identified in 1985, (Brady, 1985; Vale et al., 1985) in squid axons where it transports membrane-enclosed organelles from the neuronal

<sup>4</sup>Interestingly, not all members of this class show the same behaviour, as mammalian myosinV is highly processive, but in yeast it is not. (Mehta et al., 1999; Reck-Peterson et al., 2001).

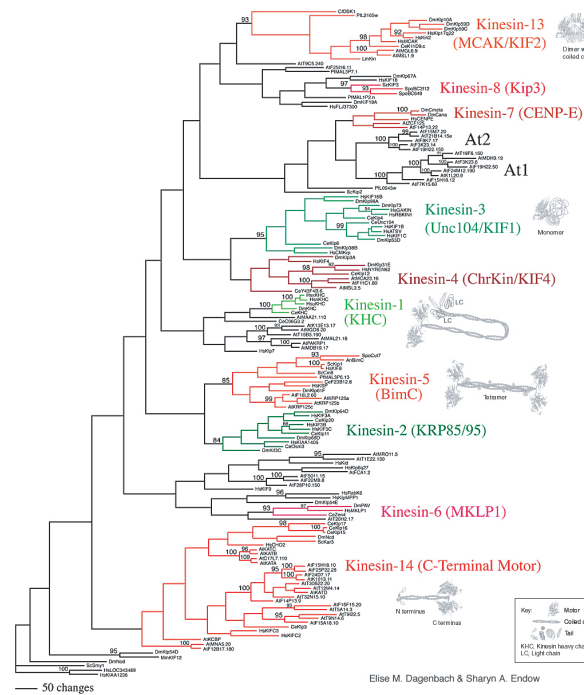


**Figure 2.4:** Kinesin-family tree. The kinesin superfamily is divided in 14 subfamilies, according to alignment of motor domain sequence. Taken from the kinesin homepage (Kinesin-Homepage).

cell body towards the axon terminal. This founding member has since then been found in a wide range of organisms and cell types and additionally 45 different kinesin motors could be identified in humans (Miki et al., 2001). The kinesin family has been divided in 14 subfamilies, denoted KIN-1 to KIN-14, and a group of *orphans*, that are not yet grouped. Kinesin motors are in general highly processive and therefore play an important role in intracellular cargo transport. The above mentioned transport of membranous vesicles in neurons would take, due to the extreme length of up to 1m of the neurons, several years if it would rely on diffusion but can be achieved in a couple of minutes by kinesin. The maximal velocity is about  $2\mu\text{m/s}$  *in vivo* (Howard, 2001), forces generated are approximately 6pN (Svoboda et al., 1993) and the motion is in general directed towards the plus-end of microtubules. Recently it could be shown that KIN-1 is moving in a hand-over-hand fashion along a microtubule (Asbury et al., 2003). Exceptions to the plus-end directionality are some members of the subfamily KIN-14, which show minus-end directed motion, and members of the subfamily KIN-13, which seem to show no directed motion at all. These two subfamilies also differ from the other subfamilies, by the sequence position of their motor domains. KIN-13 proteins have an internally and KIN-14 proteins an C-terminus located motor domain, while all the other kinesin proteins have an N-terminus located motor domain. In addition to their important role in intracellular transport, some members of the kinesin family, e. g. Ncd, contribute substantially to the formation of mitotic spindles and the poleward motion of chromosomes during cell division (Hatsumi and Endow, 1992; Endow et al., 1994a).

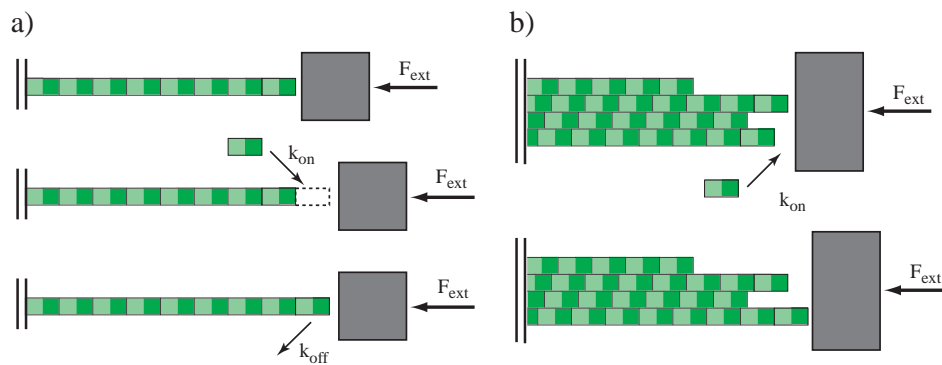


**Figure 2.5:** **a)** Illustration of Brownian ratchet models of force generation by polymerisation of filaments. Even though an external force opposes the growth of the filament, new subunits can add to the filament end (with rate  $k_{on}$ ) due to thermal fluctuations of the load, if the occurring gap is larger than the adding subunit. The removal of subunits (with rate  $k_{off}$ ) is unaffected by the opposing force. **b)** The same ratchet model as in a), but generalised to filaments consisting of many protofilaments, e. g. microtubules. In this case, the gap can be smaller compared to a) in order for a subunit to add. Adopted from (Dogterom et al., 2005).

## 2.3. Microtubule dynamics and structures

### 2.3.1. Force generation by polymerising filaments

The possibility, that polymerising filaments could generate forces, was suggested by experiments on the motion of chromosomes during cell division for microtubules (Inoue and Salmon, 1995) and for actin filaments by observations on the growth of protrusions of liposomes (Miyata et al., 1999). Other examples, where the force generating potential of polymerising filaments has been observed, include organelles and membranes (Waterman-Storer et al., 1995; Waterman-Storer and Salmon, 1998) being moved by assembling microtubules and the intracellular propulsion of *Listeria* or the deformation of membranes by actin polymerisation (Pantaloni et al., 2001; Pollard and Borisy, 2003). The first quantitative measurements with individual growing microtubules utilised the deformation of membranes due to interaction with assembling microtubules or the buckling of growing microtubules interacting with rigid obstacles, to deduce the exerted forces (Fyngenson et al., 1997; Dogterom and Yurke, 1997) (see (Dogterom et al., 2005) for recent review). From a theoretical view point, one can distinguish roughly two approaches used to discuss force-velocity relationships and stall forces of growing filaments against an external force. One, based on thermodynamic arguments (Hill, 1987; Dogterom, 2001) and one based on microscopic kinetic models (Peskin et al., 1993).

#### Thermodynamic arguments

Denoting the on-rate and off-rate of subunits to a filament end with  $k_{on}$  and  $k_{off}$  respectively, one can write for the growth velocity in case of constant subunit concentration,

$$v = \delta(k_{on} - k_{off}) \quad . \quad (2.1)$$

In order for  $v \geq 0$ , one additionally assumes  $k_{on} \geq k_{off}$  and the average change in the length of the filament due to subunit addition or removal is given by,  $0 \leq \delta \leq a$ , where  $a$

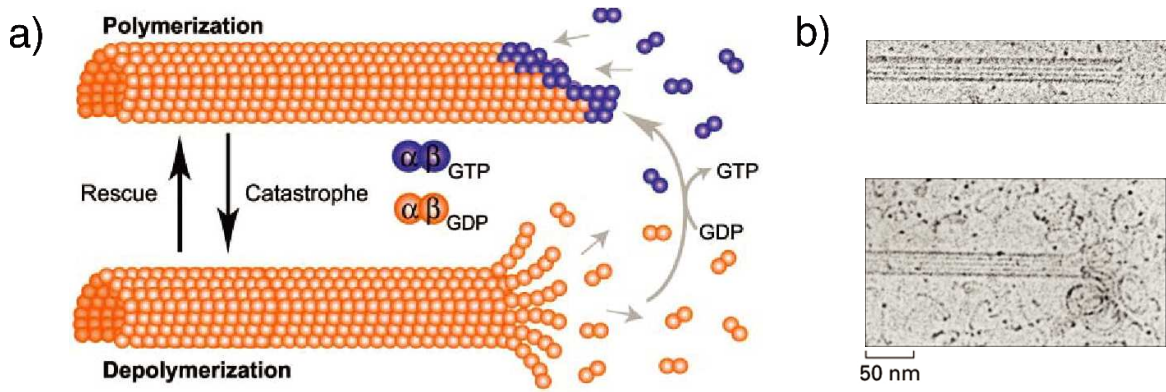


**Figure 2.6:** **a)** Illustration of dynamic instability in microtubule growth. Microtubules can switch rapidly between a stage of polymerisation and a stage of fast depolymerisation. While GTP-bound tubulin dimers favour a straight conformation of protofilament ends, leading to growth and stable microtubules, GDP-bound tubulin dimers favour a curved conformation, enabling protofilaments to rapidly depolymerise. Note, that dynamic instability can occur at both ends of microtubules, although not shown here. Taken from (Kline-Smith and Walczak, 2004). **b)** Electron micrographs of microtubules in each of these two states. Taken from (Alberts et al., 2002).

is the size of one subunit. The ratio of the on- and off-rate is given by a Boltzmann factor,  $\exp(\Delta G/k_B T)$ , where  $\Delta G$  denotes the free energy difference between the on- and off-state of a subunit and  $k_B T$  the thermal energy. In the case of an applied force, this factor has to be modified in order to account for the work performed against the external force  $F$ , leading to  $\exp(-q F d_1/k_B T)$ , where  $F d_1$  represents the most probable work needed to add a subunit against the external force  $F$  (Kolomeisky and Fisher, 2001) and  $q$  determines how much more the on-rate is affected by the external force than the off-rate. Values of  $q$  and  $d_1$  can be estimated from experimental data (see Kolomeisky and Fisher (2001); Dogterom and Yurke (1997) for explicit appraising of values). In the case of an applied external force opposing the polymerisation, this force-velocity relationship can be written as (Kolomeisky and Fisher, 2001):

$$v(F) = \delta \left( k_{\text{on}} e^{-q F d_1/k_B T} - k_{\text{off}} e^{(1-q) F d_1/k_B T} \right) . \quad (2.2)$$

From the above equation one can deduce the stall force, for which polymerisation stops:

$$F_s = \frac{k_B T}{d_1} \ln\left(\frac{k_{\text{on}}}{k_{\text{off}}}\right) . \quad (2.3)$$

### Kinetic models

The first description based on a more mechanistic view of force generation by polymerising filaments was introduced by Peskin et al. (1993) for individual actin filaments. It was followed by more elaborate models, for example taking into account filaments consisting of many protofilaments (Mogilner and Oster, 1999; van Doorn et al., 2000; Stukalin and Kolomeisky, 2004), but leaving the basic principle of the original work by Peskin et al. unaltered. In this so called thermal ratchet model, subunits can add to the filament end which is in contact with a load only if thermal fluctuations create a gap between the filament end and the load, large

enough for a subunit to fit in the gap (see Fig.2.5). The removal of subunits is unaffected by the force exerted through the load on the filament end. The force-velocity relationship therefor depends in this model on the probability  $p(F, x \geq \delta)$ , for a gap large enough for subunit addition to occur and can be written as:

$$v(F) = \delta (k_{\text{on}}p(F, x \geq \delta) - k_{\text{off}}) \quad . \quad (2.4)$$

The stall force can be calculated from a reaction-diffusion equation, given by (Peskin et al., 1993):

$$\partial_t c(x) = D\partial_x^2 c(x) + \frac{DF}{k_{\text{BT}}}\partial_x + k_{\text{on}}c(x + \delta) - k_{\text{off}}c(x) \quad (x < \delta) \quad (2.5)$$

$$\partial_t c(x) = D\partial_x^2 c(x) + \frac{DF}{k_{\text{BT}}}\partial_x + k_{\text{on}}(c(x + \delta) - c(x)) - k_{\text{off}}(c(x - \delta) - c(x)) \quad (x > \delta) \quad (2.6)$$

Here,  $x \geq 0$  is the distance from the filament end to the load and  $c(x)$  is a distribution of these distances. The resulting stall force equals the expression retrieved from thermodynamic arguments, Eq.(2.3), for  $d_1 = \delta$ .

### 2.3.2. Dynamic instability of growing microtubules

As introduced before (see page 8), microtubules can show a distinctive dynamic behaviour: they can switch rapidly between a phase where the average number of subunits being added to the plus end exceeds the average number of subunits being removed, thus resulting in a net growth of the microtubule, and a phase where subunits quickly dissociate from the plus end, resulting in a rapid shrinkage of the microtubule (see Fig.2.7b) This so called dynamic instability of microtubule growth, consists of the onset of rapid depolymerisation (called catastrophe) and the starting of a new growth phase after a catastrophe (called rescue) (see Fig.2.6). The underlying reason for this unique dynamic behaviour is thought to lie in the different binding and the structural properties of the GDP and GTP state of tubulin subunits at microtubule ends (Mitchison and Kirschner, 1984). GTP-tubulin subunits bound at microtubule ends favour a straight confirmation of protofilaments. Protofilaments are therefore able to keep strong lateral bonds between each other and steady filament growth is facilitated due to this confirmation. The hydrolysis of GTP to GDP however, goes along with a conformational change, that results in curved protofilaments at microtubule ends, with weak lateral bonds between them, facilitating the rapid desintegration of the microtubule. In a living cell most free tubulin subunits are GTP bound, as the concentration of GTP is normally much higher than that of GDP and the hydrolysis proceeds only slowly in free tubulin subunits. This hydrolysis is accelerated once the tubulin dimer is bound to a microtubule end, thus most of the subunits in a microtubule will be in their curved GDP bound state. Nevertheless, in the case where the association rate of GTP bound tubulin is higher than the hydrolysis rate, a microtubule will have a so-called GTP-cap, that is forcing the protofilaments into a straight and stable conformation. If this cap is lost, protofilaments can start curling and microtubules rapidly depolymerise.

Theoretically, the dynamic instability of microtubules has been first described by Flyvbjerg et al. (1994). The used phenomenological description is summarised by a master equation for the distribution of cap-lengths,  $p(x, t)$ , given by:

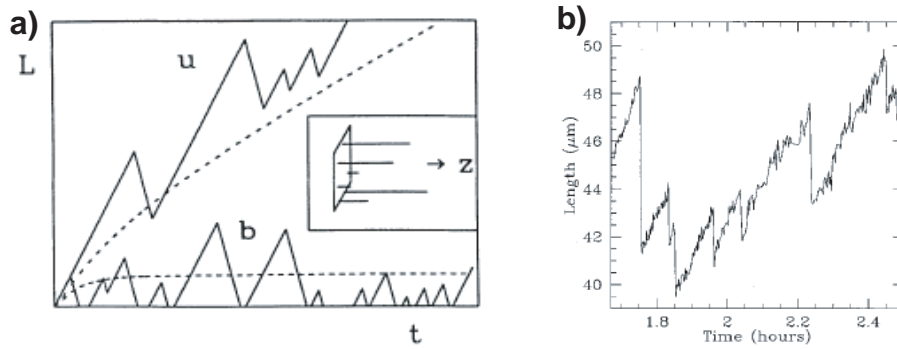


**Figure 2.7:** a) Time sequence for a microtubule undergoing dynamic instability: unbounded growth (u) and bounded growth (b). Dotted lines represent averages over many microtubules. Taken from (Dogterom and Leibler, 1993). b) (Single) Microtubule length as a function of time. Taken from (Flyvbjerg et al., 1996).

$$\partial_t p = -v \partial_x p + D \partial_x^2 - r x p + r \int_x^\infty dyp(y, t) . \quad (2.7)$$

Here, the right hand side consists of terms describing the average growth,  $v$ , of the cap's length during the rescue period, the fluctuation of this average growth, the rate  $r$  with which caps of length  $x$  are shortened and the rate with which caps longer than  $x$ , reduce to length  $x$ . With this description, observed catastrophe rates and waiting times for catastrophes could be reproduced.

Analysis of the distribution of microtubule lengths due to the dynamic instability was done by (Dogterom and Leibler, 1993). In the case of an isolated microtubule, a mean field approximation for the dynamics of the probability distributions for growing and shrinking microtubules, leads to either bound or unbound growth of the microtubule (see Fig. 2.7a). This mechanism of rapidly switching between polymerisation and depolymerisation does not only allow the microtubule network to quickly alter its structure, but is also a highly effective search mechanism in space (needed e.g. for the capture of chromosomes during cell division) as was demonstrated in (Holy and Leibler, 1994).

### 2.3.3. Reorganisation of microtubules during mitosis

After the genetic material of a cell has been duplicated and condensed, it has to be faithfully separated and distributed into the two newly forming daughter cells. In eucaryotic cells this is achieved during the process of mitosis by the so called mitotic spindle. This spindle is composed of microtubules and a variety of proteins binding and interacting with them.

During prophase the centrosome duplicates and the two asters move apart to opposing sides of the cell. Microtubules nucleate and protrude from each centrosome into the cell centre. After the breakdown of the nuclear envelope which shields the chromosomes from the rest of the cell, microtubules can capture chromosomes and attach to the kinetochores. Dynamic instability is critical for the chromosomes to be captured by spindle microtubules, as the rapid shortening and lengthening allows the microtubules to probe a larger space in the cell (Holy and Leibler, 1994)

One can distinguish three kinds of microtubules in the mitotic spindle during metaphase:

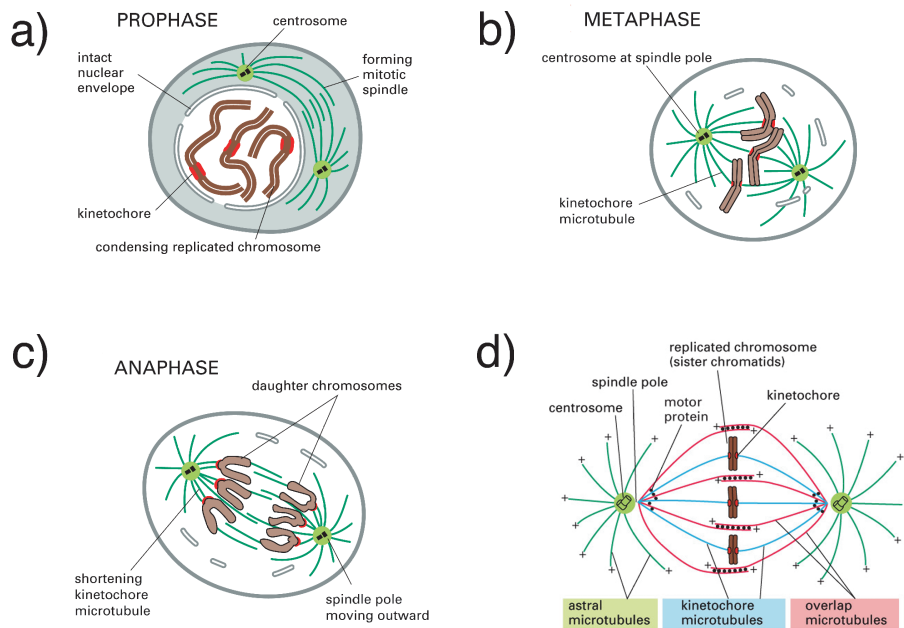


**Figure 2.8:** a)-c): Illustrations of the role of the mitotic spindle in different stages of cell division. d): Illustration of the three classes of microtubules of the fully formed mitotic spindle. Adapted from (Alberts et al., 2002).

(i) microtubules growing from the centrosome towards the cell cortex and attaching there (astral microtubules). These microtubules are involved in the transmission of forces leading to spindle positioning and spindle oscillations. (ii) microtubules growing towards the middle of the cell and connecting to chromosomes (kinetochore microtubules). Each kinetochore is connected to a whole microtubule bundle, consisting of several individual microtubules. (iii) microtubules growing towards the cell centre and overlapping with microtubules projecting from the opposite centrosome. These microtubules, are responsible for structure and bipolarity of the mitotic spindle. In anaphase, the kinetochore chromosomes start to depolymerise while keeping attached to the chromosomes, thus driving the poleward movement of the chromosomes. In addition also the spindle poles start to move further apart. Finally, after complete separation, a new nuclear envelope is formed around the chromosome in each part of the cell and the cell is divided by the so called contractile ring.

## 2.4. Microtubule-depolymerising motor proteins

In addition to the wide spectrum of biological tasks, e. g. cargo translocation along microtubules and spindle organisation, that kinesin motors are involved in, some members of the kinesin superfamily have the astonishing ability to destabilise microtubules directly from their ends. For example Kar3 in yeast, a minus-end directed motor, belonging to the KIN-14 subfamily, was reported to depolymerise microtubules *in vitro* specifically from minus ends (Endow et al., 1994b). Other examples are members of the KIN-8 family, for example Klp67A,

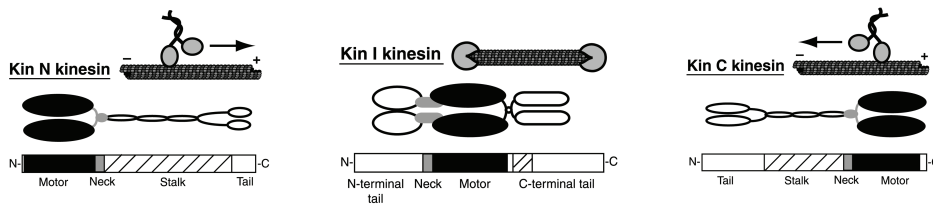


**Figure 2.9:** Schematic illustration of kinesin structure. Kinesins are classified here in three classes based on the position of their motor domain within their peptide sequence. Kin-N kinesins have a N-terminal, Kin-C a C-terminal, and Kin-I an internal motor domain. Kin-N and Kin-C proteins have a high affinity to microtubule lattices, while Kin-I proteins show high end binding. Respective directionality of members of the different classes is indicated (Ovechkina and Wordeman, 2003). Note that Kin-N kinesins include the subfamilies KIN-1 to KIN-12, Kin-C of the subfamily KIN-14 and Kin-I of the subfamily KIN-13 (Lawrence et al., 2004).

a kinesin motor in *Drosophila* which was shown to move towards plus-ends of microtubules in an *in vitro* motility assay. There are also indications that the protein is also capable of destabilising microtubule ends (Gandhi et al., 2002). The depolymerising motor proteins best studied so far are members of the kinesin subfamily KIN-13 (Desai et al., 1999; Maney et al., 2001; Moores et al., 2002; Hunter et al., 2003). Members of this subfamily include, MCAK in hamster (Wordeman and Mitchison, 1995), XKCM1 in *Xenopus* (Frog) (Walczak et al., 1996) and KIF2 in mouse (Noda et al., 1995). We will from now on concentrate on members of this subfamily (see Hunter and Wordeman (2000); Ovechkina and Wordeman (2003); Moore and Wordeman (2004); Wordeman (2005) for a more elaborate review of the field).

### 2.4.1. Properties of kinesin-13 motors

The ability to depolymerise microtubules from the ends is not the only factor which distinguishes KIN-13 proteins from other kinesin proteins. They are also structurally distinct, as the conserved core motor domain of the kinesin superfamily is generally located in the middle of the peptide sequence, instead of at either end of the sequence as in other kinesin proteins (see Fig.2.9).

While most kinesin motor proteins use ATP hydrolysis to move unidirectionally on microtubules, there is no evidence for directed motion of KIN-13 motors<sup>5</sup>. Instead it seems that depolymerising motor proteins perform unbiased diffusional motion once they are bound to microtubule lattices (Helenius et al., submitted). The absence of directed motion and the observed diffusion, are also in accordance with observed accumulation (*in vitro*) of KIN-13 motors at both ends of microtubules (see Fig. 2.10), even in the absence of hydrolysable ATP. Additionally, the times observed for MCAK to target microtubule ends are too fast to be accounted for by a three-dimensional search process in the microtubule containing solution. An cooperation of one-dimensional lattice diffusion and three-dimensional diffusion was therefore proposed to explain the fast end-targeting observed by (Hunter et al., 2003).

Depolymerisation speeds of up to  $1\mu\text{m}/\text{min}$  have been reported (Hunter et al., 2003) with

<sup>5</sup>The reported directionality of Kif2A in mouse (Noda et al., 1995) could not be replicated (Desai et al., 1999), and it is likely that contamination with a plus-end directed motor was responsible for the observed motion.

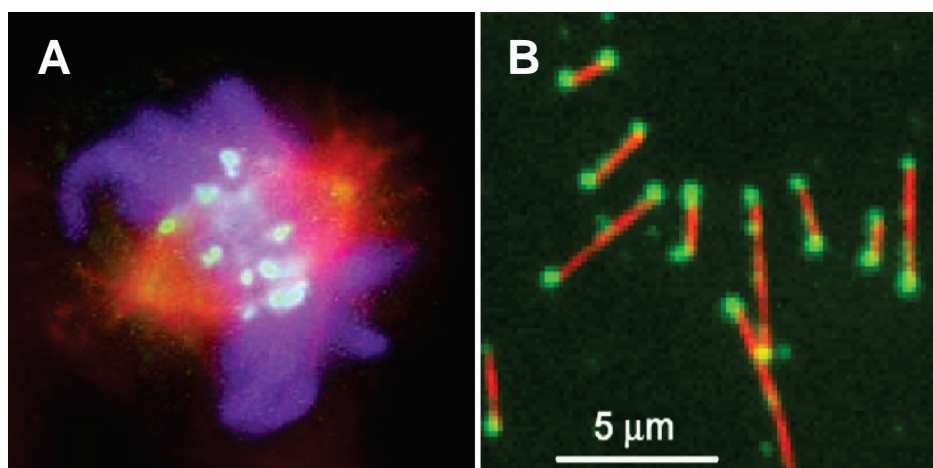


**Figure 2.10:** **A)** Localisation of MCAK proteins during mitosis. MCAK proteins are labelled green, tubulin red and DNA blue. Courtesy of L. Wordeman, Wordeman Lab, Seattle. **B)** Snapshot of MCAK motor proteins (labelled green) depolymerising stabilised microtubules (labelled red). Strong accumulation can be observed at both filament ends in contrast to the relatively weak occupation on the microtubule lattices. Courtesy of S. Diez and J. Howard, MPI for Molecular Cell Biology and Genetics, Dresden

slight discrepancy between the speeds of depolymerisation of the two ends. Here, GMPCPP-stabilised microtubules were used and the observed speeds show an increase of depolymerisation by a 100 times, compared to depolymerisation speeds of these microtubules on their own (see Fig. 2.11). Another interesting point is the difference in stimulation of ATPase activity of KIN-13 proteins and other kinesin motors. While microtubule lattices in general stimulated the ATPase of kinesin motors, Hunter et al. (2003) could show that MCAK, shows microtubule end stimulated ATPase.

#### 2.4.2. Mechanism of microtubule depolymerisation

The exact mechanism by which KIN-13 motors destabilise microtubule ends is still unclear. X-ray crystallographic studies of the core motor domain of a KIN-13 motor revealed that the microtubule-binding motor domain adopts a convex shape, in both ATP- and ADP-bound states (Ogawa et al., 2004). This specific structure would allow for a "lock-and-key" fit (Moore and Wordeman, 2004) between the motor domains and the concave shape of depolymerising tubulin dimers at microtubule ends, in accordance with observed binding of KIN-13 motors to curved protofilaments (Moore et al., 2002). It was therefore suggested, that KIN-13 motors could positively influence the depolymerisation of microtubules by strengthening the curved conformation of single protofilament ends. Although the structure of the motor domain is capable of stabilising the curved conformation of protofilaments, it was shown that the motor domain of MCAK alone is not able to depolymerise microtubules under physiological conditions, but that the so called "neck", a domain on the N-terminal side of the peptide sequence, is needed for microtubule depolymerisation activity. As the neck is positively charged, it is assumed that it interacts electrostatically with the negatively charged microtubule surface and therefore tethers the motor to the microtubule during subunit removal (Maney et al., 2001; Ovechkina et al., 2002).

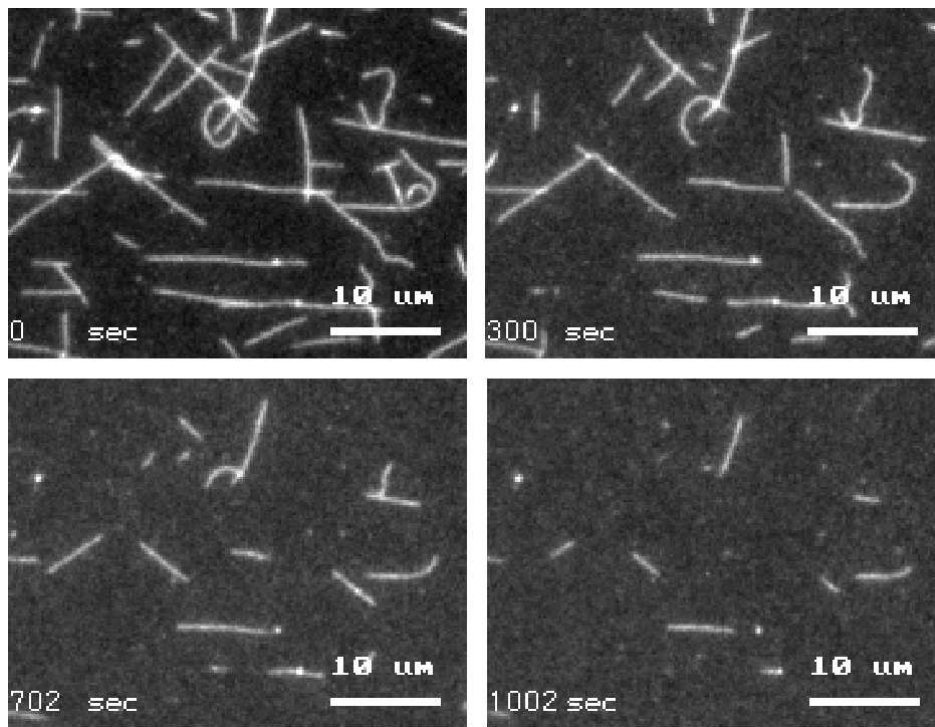


**Figure 2.11:** Snapshots of stabilised microtubules (white) which are depolymerised by MCAK molecules (not visible) at four different times. Courtesy of S. Diez and J. Howard, MPI for Molecular Cell Biology and Genetics, Dresden

Another point which remains unclear is the role of ATP hydrolysis in the removal of tubulin dimers. Desai et al. (1999) and Maney et al. (2001) showed, that incomplete depolymerisation of microtubules by MCAK molecules is possible without ATPase activity, although a 1:1 stoichiometry of motor proteins to polymerised tubulin is needed, while Hunter et al. (2003) and Niederstrasser et al. (2002) could show that fast and complete depolymerisation takes place at substoichiometry concentrations only with ATP hydrolysis. These observations led to the hypothesis that KIN-13 motors are processive in the sense that one motor is capable of removing several subunits, and that ATP hydrolysis is necessary for catalytic depolymerisation in order to free motor proteins from removed tubulin dimers. Exactly where this decoupling of motor and tubulin takes place is also unclear. Hunter et al. (2003) proposed a model for processive subunit removal in which the motor dissociates from the removed tubulin dimer while still being bound to the microtubule end, while Desai et al. (1999) suggested that this event takes place in solution.

A crucial aspect of the depolymerisation activity of KIN-13 motors in the cell is its regulation. So far two ways in which a cell might regulate the activity of KIN-13 motors are known. Aurora B kinase was shown to inhibit microtubule depolymerisation by phosphorylation of the neck region (Lan et al., 2004; Andrews et al., 2004; Ohi et al., 2004). ICIS (inner centromere KinI stimulator) seems to have the opposite effect, it was found to stimulate the activity of MCAK (Ohi et al., 2003), maybe by amplifying the connection of motors to the microtubules or by influencing the negative effect of Aurora B on MCAK (Ohi et al., 2004)

Finally one should note, that so far most experiments with depolymerising motors were performed with stabilised microtubules, either using GMPCPP or taxol. Experimental data

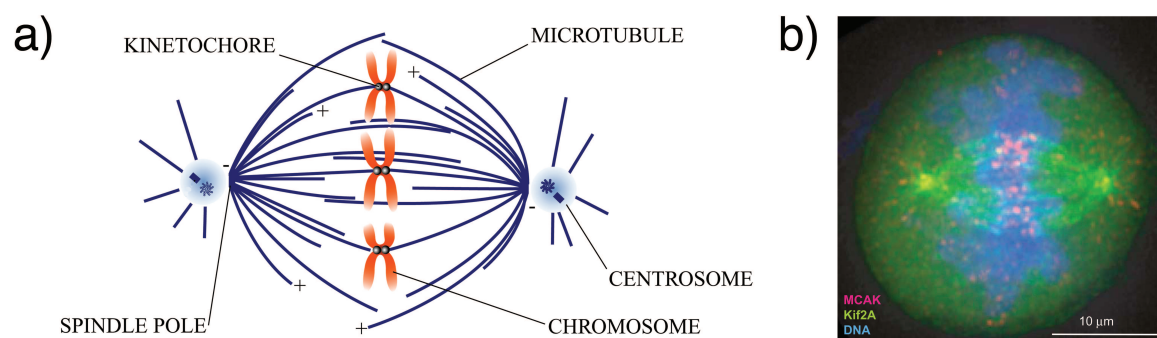


**Figure 2.12:** a) Illustration of the mitotic spindle (modified from Rogers et al. (2004), supplementary material). b) A CHO cell. DNA is labelled blue and KIN-13 motors are labelled red (MCAK) and green (Kif2A $\beta$ ) (taken from (Wordeman, 2005)).

indicates, that these methods of stabilising microtubules can lead to a change in motor-microtubule interaction, e. g. by altering a motor's processivity or by influencing the accumulation of motors at filament ends (Desai et al., 1999; Hunter et al., 2003).

### 2.4.3. Cellular functions

By interacting preferentially with microtubule ends and being capable of destabilising microtubules, KIN-13 motors are able to contribute considerably to the reordering of the microtubule network in a cell. This is highly important during cell division, where microtubules have to be reorganised in order to form the mitotic spindle and where shrinking microtubules facilitate the separation of chromosomes. Indeed it has been shown that KIN-13 motors play a important role at most stages of cell division.

While some KIN-13 proteins accumulate most strongly at centromeres and kinetochores, the site of microtubule attachment to chromosomes, during mitosis (see Fig.2.13), others are highly enriched at the centrosomes at the poles of the mitotic spindle. It is presumed that depolymerisation activity at both locations, lead to both a chromosome-to-pole movement and a poleward flux of microtubules, which is necessary for chromosome segregation (Ganem and Compton, 2004; Rogers et al., 2004; Gaetz and Kapoor, 2004), (see Fig. 2.12 and Fig. 2.13). It was also shown that some KIN-13 motors have a strong influence on the correct formation of the bipolar spindle, and that depletion of these motors leads to mono-polar spindles and abnormally long microtubules (Rogers et al., 2004; Gaetz and Kapoor, 2004; Walczak et al., 1996; Cassimeris and Morabito, 2004).

During the early stages of mitosis, microtubules growing out from the opposing poles have to capture sister chromatids and keep this bi-oriented configuration (see Fig. 2.13). As misconnections frequently occur, which would lead to the loss or gain of chromosomes in one of the daughter cells, it is important for correct separation of the genetic material that these misconnections are corrected before division takes place. Experiments with MCAK indicate, that these motors could be involved in this correction mechanism (Kline-Smith et al., 2004; Savoian et al., 2004).

Finally, KIN-13 members seem to play also an important role in brain development, where

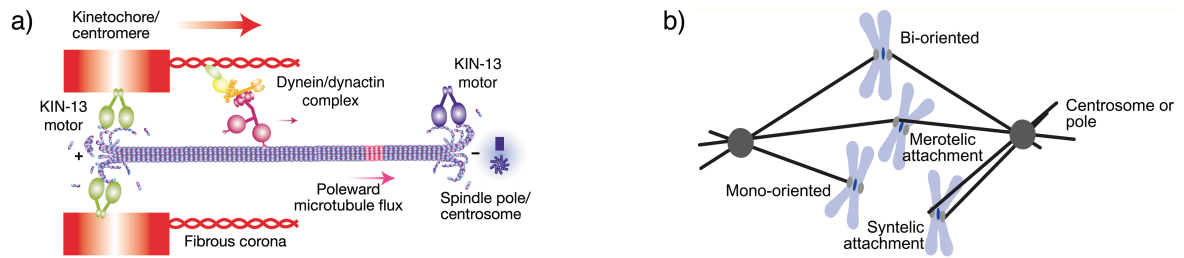


**Figure 2.13:** a) Illustration of role of members of the KIN-13 subfamily during cell division (adopted from (Rogers et al., 2004)). b) Schematic representation of possible erroneous microtubule attachments. These include one sister chromatid attached to both poles (merotelic) and both sister chromatids attached to one pole (syntelic). Members of the KIN-13 subfamily contribute to correcting these errors (adopted from (Moore and Wordeman, 2004)).

they contribute to the suppression of collateral branches (Homma et al., 2003). Unhindered growth of these branches is implicated in leading to incorrectly localised neuronal cell bodies and as a consequence to wrongly established circuitry (Wordeman, 2005).

## 2.5. Theoretical description of motor proteins

Description of motor dynamics and functions started with the works of Huxley (1957) and Hill (1974), modelling the contraction of muscles. Progress in purification of filaments and motor proteins led to new experiments, enabling the direct observation of motor dynamics along filaments *in vitro*. These experiments can be classified in two classes: "motility assays", where individual filaments are transported by many motor proteins that are bound to a surface (Kron and Spudich, 1986; Harada et al., 1987), and single molecule experiments, where the motion of motor protein-coated beads can be observed due to the interaction of motors with filaments, which are attached to a surface (Svoboda et al., 1993; Hunt et al., 1994). These experiments led to several new theoretical approaches of describing molecular motors. These can be divided into two different groups: in one group, motors are considered to be molecular complexes being able to rectify Brownian motion, leading to the observed unidirectional motion (see Julicher et al. (1997), Reimann (2002) and Hanggi et al. (2005) for reviews). Due to this approach, molecular motors are sometimes also called Brownian motors. In the other group, motor proteins can adopt different chemical and conformational states and the description of motor dynamics leads to stochastic equations for the probabilities to find motors in these states (Leibler and Huse, 1991, 1993).

### 2.5.1. Phenomenological approach

A starting point for describing molecular motors is to investigate their behaviour close to thermal equilibrium. In this case, one can apply a linear-response theory, describing the effects of small perturbations on the behaviour of a system in equilibrium (de Groot and Mazur, 1984). This description is, due to its phenomenological nature, independent of any underlying

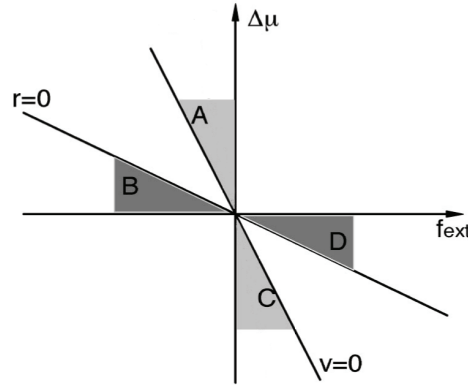


**Figure 2.14:** Illustration of the different operational regimes of an isothermal motor as a function of external force  $\mathbf{f}_{\text{ext}}$  and chemical potential difference  $\Delta\mu$ , obtained by a linear-response theory. In regime A,  $r\Delta\mu > 0$ ,  $\mathbf{f}_{\text{ext}}\mathbf{v} < 0$ , a motor generates mechanical work by hydrolysing ATP and in regime B,  $r\Delta\mu < 0$ ,  $\mathbf{f}_{\text{ext}}\mathbf{v} > 0$ , a motor produces ATP from mechanical input. Regime C,  $r\Delta\mu > 0$ ,  $\mathbf{f}_{\text{ext}}\mathbf{v} < 0$ , ADP is used to generate work and in D,  $r\Delta\mu < 0$ ,  $\mathbf{f}_{\text{ext}}\mathbf{v} > 0$ , a motor produces ADP from mechanical input (Julicher et al., 1997). Modified from (Parmeggiani et al., 1999).

microscopic details. In the case of biological motor proteins, examples of such perturbations include external forces  $\mathbf{f}_{\text{ext}}$  acting on the proteins<sup>6</sup> or the change of free energy associated with the hydrolysis of ATP molecules, measured by the chemical potential difference,  $\Delta\mu = \mu_{\text{ATP}} - \mu_{\text{ADP}} - \mu_{\text{P}}$ , of the reactants (Julicher et al., 1997; Parmeggiani et al., 1999). The effects of these perturbations, also called generalised "forces", are motion and fuel consumption of the motors, which can be described by an average velocity  $\mathbf{v}$  and a rate of hydrolysis of ATP molecules,  $r$ , also called generalised "currents". One can thus write a general description of the currents as functions of the generalised forces,

$$\mathbf{v} = \mathbf{v}(\mathbf{f}_{\text{ext}}, \Delta\mu) \quad , \quad (2.8)$$

$$r = r(\mathbf{f}_{\text{ext}}, \Delta\mu) \quad . \quad (2.9)$$

In the linear regime, where  $\Delta\mu \ll k_{\text{B}}T$  and  $|\mathbf{f}_{\text{ext}}| \ll T/\epsilon^7$ , one can expand these equations to linear order (Parmeggiani et al., 1999):

$$\mathbf{v} = \lambda_{11}\mathbf{f}_{\text{ext}} + \lambda_{12}\Delta\mu \quad (2.10)$$

$$r = \lambda_{21} \cdot \mathbf{f}_{\text{ext}} + \lambda_{22}\Delta\mu \quad . \quad (2.11)$$

Here,  $\lambda_{11}$  and  $\lambda_{22}$  describe the effect of the applied force on the velocity and the effect of the chemical difference on the consumption rate, respectively. The cross-coupling coefficients,  $\lambda_{12}$  and  $\lambda_{21}$  must be vectors due to the underlying symmetry, and they describe energy transduction. In the case of a non-polar system, e. g. a filament,  $\lambda_{21}$  has to be zero. Therefore, Eq.(2.10), shows clearly the requirements for a motor protein to generate directed motion by transforming chemical energy into mechanical energy: the system has to be out of equilibrium,

<sup>6</sup>E.g. forces due to optical or mechanical measurement instruments or due to the transport of cargo by the motor along a filament.

<sup>7</sup>Here,  $\epsilon$  is a characteristic length scale of the motor and  $T$  the equilibrium temperature. Note, that temperature gradients decay on length scales of interest in at most a few hundred nanoseconds. As typical rates between different states of a motor are in the range of milliseconds, one can consider these state to be in equilibrium at a constant temperature  $T$ .

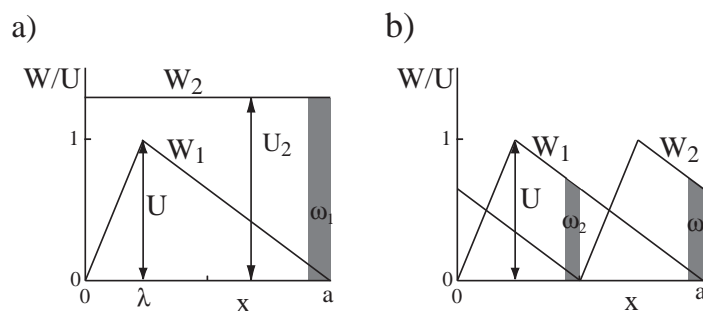


**Figure 2.15:** Two potentials  $W_1$  and  $W_2$  and transition regions (grey) are shown. In **a)**, the potential  $W_2$  is chosen to be flat, while in **b)** the potential  $W_2$  is identical to  $W_1$ , but shifted by half a period. The asymmetry of the potentials is characterised by the position  $a$  of the maximum. Transition rates between the potentials are given by  $\omega_1$  and  $\omega_2$ . Modified from (Parmeggiani et al., 1999).

$\Delta\mu \neq 0$  and the spatial symmetry has to be broken,  $\lambda_{21} \neq 0$ . From the Onsager relations one knows, that  $\lambda_{12} = \lambda_{21}$ .

Due to the second law of thermodynamics, one knows that the rate of energy dissipation,  $T\dot{S}$ , given by the performed work per unit time,  $\dot{W}$ , and the consumption of free energy,  $\dot{G}$ , must be positive. In the case of molecular motors this reads,  $T\dot{S} = \mathbf{f}_{\text{ext}}\mathbf{v} + r\Delta\mu > 0$ . As only the whole right hand side has to be positive, each individual term on the right hand side can be negative. This gives rise to eight different regimes a motor can work in (Julicher et al., 1997), see Fig. 2.14.

Biological motor proteins normally work in a regime far away from thermal equilibrium, as on average,  $\Delta\mu \approx 10k_B T$ . In order to study motors far from equilibrium, one must apply different approaches.

### 2.5.2. Isothermal ratchet models

Thermal ratchet models are used in a wide class of systems, where thermal fluctuations are rectified leading to a net current of particles. But, as already mentioned, temperature inhomogeneities decay much too fast on the length scales of interest when trying to describe molecular motors, therefore a thermal ratchet model cannot be used to describe the unidirectional motion of motors along a filament. Instead, so-called isothermal ratchets have been widely applied for describing motor dynamics. In general, a motor is placed in an interaction potential,  $W_i$ , between the motor, being in a state  $i$ , and the filament. The potential therefore reflects the underlying structure of the filament and is periodic and asymmetric. The dynamics of a motor can then be described with a Langevin equation for each state  $i$  the motor is in (Julicher et al., 1997),

$$\zeta_i \frac{dx}{dt} = -\partial_x W_i(x) + f_i(t) \quad , \quad (2.12)$$

where  $\zeta_i$  is a friction coefficient, and the fluctuating force  $f_i(t)$  has a average value  $\langle f_i(t) \rangle = 0$  and obeys the fluctuation-dissipation theorem,  $\langle f_i(t)f_j(t') \rangle = 2\eta_i k_B T \delta(t-t')$ . In order to describe the dynamics of transitions between the individual states, one can use a Fokker-Planck formalism. The number of states  $i$  depends on how many microscopic details of a

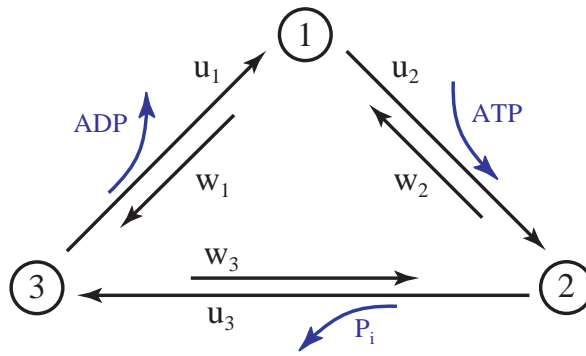


**Figure 2.16:** Illustration of a kinetic hopping scheme for a motor protein. The motor can adopt three different states, symbolising a nucleotide free conformation (1), a ATP bound conformation (2) and a ADP bound conformation (3) . Forward rates are denoted by  $u = i$ , backwards rates by  $w_i$ . Courtesy of K. Kruse

motor one wishes to include in the theoretical description. For describing individual molecular motors a two state model is often used,  $i = 1, 2$  (Magnasco, 1993; Peskin et al., 1994; Prost et al., 1994; Astumian and Bier, 1994; Aghababae et al., 1999). Introducing the probability density  $P_i(x, t)$ , to find a motor in state  $i$  at position  $x$  at time  $t$ , one can describe the dynamics with two coupled Fokker-Planck equations:

$$\partial_t P_1 + \partial_x J_1 = -\omega_1(x)P_1 + \omega_2(x)P_2 \quad , \quad (2.13)$$

$$\partial_t P_2 + \partial_x J_2 = \omega_1(x)P_1 - \omega_2(x)P_2 \quad . \quad (2.14)$$

The currents are given by,

$$J_i = \mu_i [-k_B T \partial_x P_i - P_i \partial_x W_i + P_i f_{\text{ext}}] \quad , \quad (2.15)$$

where the first term on the right hand side describes diffusion, the second the interaction with the potentials  $W_i$ , and the third takes into account an applied external force  $f_{\text{ext}}$ . The switching of the motor from one state to the other is characterised by the rates  $\omega_i(x)$ , where the spatial dependence reflects the filament symmetry (see Fig. 2.15 for examples of potentials). If no chemical energy is consumed,  $\Delta\mu = 0$ , these rates have to obey detailed balance,  $\omega_1/\omega_2 = \exp((W_1 - W_2)/k_B T)$ . One can rewrite the above equations to an effective one-dimensional equation, introducing an effective potential  $W_{\text{eff}}$ , where one can very nicely see the necessity of broken symmetry and broken detailed balance for unidirectional motion to emerge. Note that the above formalism can be generalised if a collection of motor proteins is considered instead of individual motors (see Julicher et al. (1997)).

### 2.5.3. Stochastic models on discrete lattices

A second approach to describing motor dynamics assumes the existence of several conformational states of the motor. The residence time of the motor in these states is presumed to be long in comparison to the duration of the transitions between the states. This has two consequences. Firstly each of the states can be considered to be in thermal equilibrium at a constant temperature  $T$ , and secondly one can treat the transitions as instantaneous. Transitions are considered to take place stochastically, as a motor in a solution at temperature

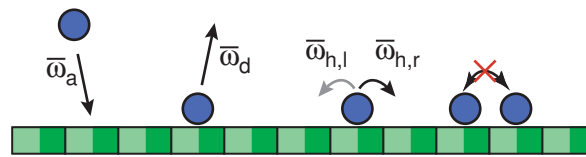


**Figure 2.17:** Illustration of stochastic lattice description of motor dynamics. Courtesy of K. Kruse

T will be subject to thermal noise (Leibler and Huse, 1991, 1993; Kolomeisky and Widom, 1998). One can therefore describe motor dynamics as a succession of stochastic transitions between these states (see Fig. 2.17). If detailed balance between these transition rates is broken, unidirectional motion can emerge. In addition to this directed motion, there will be a diffusive part, due to the stochastic switching between states.

If a whole ensemble of motor proteins is considered instead of just a single protein, one can neglect the different states and consider the motors to be in a single state only. Motors can be modelled now as identical particles, hopping stochastically on a one-dimensional lattice, symbolising the filament (Lipowsky et al., 2001; Kruse and Sekimoto, 2002; Parmeggiani et al., 2003). The asynchrony of the filament can be incorporated in this description by introducing different hopping rates of motors to adjacent sides. We will be using this approach further on in this work and refer the reader to chapter 4, for a detailed description of the microscopic details.



---

## General description of motor induced filament depolymerisation

In this chapter we discuss the dynamics of motor molecules which induce the shortening of the ends of filaments to which they bind. We present a phenomenological description that is aimed at describing the generic dynamic behaviour of these motor molecules when interacting with filaments. We neglect microscopic details of the filaments, the motor molecules and the interaction of the latter with the filaments and take into account only the most relevant macroscopic interactions between motors and filaments. Our theory is therefore not restricted to a specific class of filaments or motor proteins. We discuss necessary conditions for motors to accumulate at depolymerising ends, as observed in experiments with motors of the KIN-13 family.

### 3.1. Filament depolymerisation

The following treatment is motivated by an experiment, in which filaments are suspended in a solution in which motor proteins are present at concentration  $c$ . We assume that ATP is present at a saturating amount, so that the dynamics of motors is not constrained by it. We therefore do not explicitly take it into account. In order to describe the dynamics of motor molecules which induce the shortening of filament ends, we consider one filament end and use a semi-infinite, one-dimensional geometry. The depolymerisation activity of motors results in a movement of the filament end in space<sup>1</sup>, with a velocity  $v_d$  in a laboratory reference frame  $x'$ . For simplicity, instead of using this laboratory reference frame for our description, we use a reference frame in which the depolymerising end is located at  $x = 0$ , for all times (see Fig.3.1).

---

<sup>1</sup>Note that microtubules are normally stabilised in these experiments, preventing spontaneous depolymerisation of the filaments.

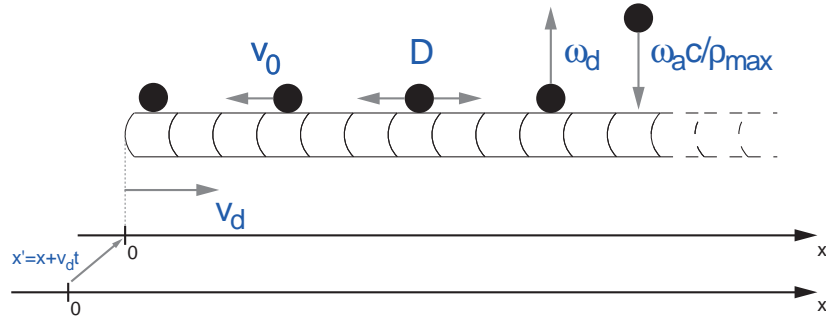


**Figure 3.1:** Illustration of the dynamic processes of motor proteins on a filament in the phenomenological description. Motors attach to the filament at rate  $\omega_a c / \rho_{\max}$  and detach with rate  $\omega_d$ . On the filament motors diffuse, characterised by the diffusion coefficient  $D$  and exhibit a directed average motion with velocity  $v_0$ . If motors at the end induce subunit removal, the filament end moves with velocity  $v_d$  in a fixed reference frame,  $x'$ . The depolymerising end is at rest for all times, in a reference frame,  $x$ , that is moving with equal velocity  $v_d$ .

### 3.1.1. Dynamics of motor densities

In the following we will denote the density of motor proteins that are bound to the filament at a distance  $x \geq 0$  from the depolymerising filament end with  $\rho(x, t)$ <sup>2</sup>. Motors present in the surrounding solution at concentration  $c$  bind to the filament with a binding rate  $\omega_a c / \rho_{\max}$ . Here  $\rho_{\max}$  is the maximum density of molecular motors, at which binding sites on the filament saturate. In the case of a microtubule with an underlying molecular length scale of  $8nm$  (given by the size of the tubulin monomers) and an average number of 13 protofilaments per microtubule,  $\rho_{\max} = 13/8nm \approx 1.63nm^{-1}$ . Motors already bound to the filament can detach with rate  $\omega_d$ . In addition, bound motors may also exhibit directed average motion towards the end of the filament with velocity  $v_m < 0$ , which in general depends on the density of motors  $\rho$  (Lipowsky et al., 2001; Kruse and Sekimoto, 2002; Parmeggiani et al., 2003; Klumpp and Lipowsky, 2004; Parmeggiani et al., 2004). Fluctuations in the velocity of the motor movement and thermal motion are described by the diffusion of the motor on the filament with a diffusion coefficient  $D$ . We can now describe the density profile along the filament by a continuity equation with additional source and sink terms, corresponding to the attachment and detachment of motor proteins. The density profile then obeys,

$$\partial_t \rho + \partial_x j = \omega_a c \left(1 - \frac{\rho}{\rho_{\max}}\right) - \omega_d \rho \quad . \quad (3.1)$$

Here, we have included hard core repulsion between motors, leading to the exclusion term  $(1 - \rho/\rho_{\max})$ . The current of motors on the filament,  $j$ , is given by

$$j = -D \partial_x \rho - v \rho \quad . \quad (3.2)$$

Here,  $v$  is the total velocity of motors on the filament with respect to the filament end, consisting of the average directed velocity  $v_m$  and the depolymerisation velocity of the filament end  $v_d$ ,

$$v = v_0 \left(1 - \frac{\rho}{\rho_{\max}}\right) + v_d \quad , \quad (3.3)$$

<sup>2</sup>In the following we will refrain from explicitly mentioning the time and space dependence of the density of bound motors and will for simplicity write  $\rho$ .

where the directed motor velocity  $v_m$  is given by the average velocity of a single motor,  $v_0$ , and the incorporation of hard core repulsion between motors,  $(1 - \rho/\rho_{\max})$ .

The depolymerisation velocity is related to the rate  $\Omega$  with which subunits are removed from the filament end by

$$v_d = \frac{\Omega a}{N} \quad , \quad (3.4)$$

where  $a$  is the size of a subunit and  $N$  is the number of protofilaments in the filament.

### 3.1.2. Motor induced filament depolymerisation

At the depolymerising end, motors can either detach, directly or by a depolymerisation event, or attach directly from the surrounding solution. We can describe the net flow of motors to the filament end with a rate  $J$  at which motors attach to the filament end. This rate  $J(\rho_0)$  is a function of the motor density  $\rho_0$  at the end and also depends on buffer conditions. In order to stay as general as possible we systematically expand  $J(\rho_0)$  in powers of  $\rho_0$ :

$$J(\rho_0) = J_0 + J_1\rho_0 + J_2\rho_0^2 + \mathcal{O}(\rho_0^3) \quad . \quad (3.5)$$

Here,  $J_0$  is the rate with which motors, additionally to the rate  $\omega_a c/\rho_{\max}$ , directly attach to the filament end. The coefficients  $J_1$  and  $J_2$  characterise how interactions between motor proteins and the filament end, e.g. the depolymerisation activity, influence the detachment rate of motors. If motors attach at the same rate to the end of the filament as to the rest of it,  $J_0 = 0$ . If in addition the direct detachment rate from the filament end is equal to the rate,  $\omega_d$ , of detachment from the bulk,  $J_1 \leq 0$ , as in this case only particles which remove subunits and leave the filament with them contribute to the current. In the case of low direct attachment of motors to the end and if  $v > 0$  (see Eq.(3.3)), motors typically detach from the end and thus  $J < 0$ .

As we are interested in motor protein induced depolymerisation, we assume that the rate of filament depolymerisation is regulated by motor proteins bound to the filament end. Therefore, the rate of subunit removal is a function  $\Omega(\rho_0)$  of the motor density at the end. Again, not taking into account any details of the underlying process of subunit removal, it is useful to express  $\Omega$  by an expansion in powers of  $\rho_0$ :

$$\Omega(\rho_0) = \Omega_0 + \Omega_1\rho_0 + \Omega_2\rho_0^2 + \mathcal{O}(\rho_0^3) \quad . \quad (3.6)$$

Here, we have introduced the expansion coefficients  $\Omega_i$ . The subunit removal rate in the absence of motor proteins  $\Omega_0$  depends on buffer conditions, for example temperature, GTP/GDP concentration and tubulin monomer concentration (Alberts et al., 2002; Lodish et al., 2003). In most experimental situations examining the influence of motor activity on the depolymerisation of filaments, the filaments are stabilised (e.g. by taxol or GTPGMP for microtubules). In these situations,  $\Omega_0 = 0$ . For motor proteins that induce filament depolymerisation, the first order expansion coefficient has positive values,  $\Omega_1 \geq 0$ . Given that the number of binding sites at the filament end is limited, the depolymerisation rate  $\Omega$  has to saturate for large motor densities, therefore typically  $\Omega_2 \leq 0$ .

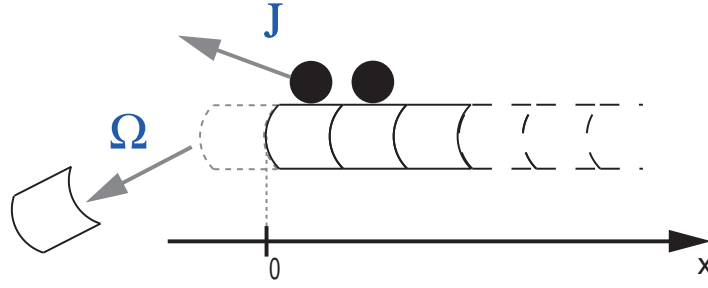


**Figure 3.2:** Illustration of the motor dynamics at the filament end. Subunits may be removed with a rate  $\Omega$  from the filament end and motors can either bind to the end or detach from it, leading to current  $J$  of motors at the end. Both quantities are functions of the bound motor density at the end (see Eq.(3.6) and (3.5))

### 3.1.3. Processive subunit removal

The removal of filament subunits by motor proteins can take place in two ways: motors may either fall off the filament with the removed subunit, or they may stay bound to the filament end after removal. The tendency of a motor to stay attached to the filament while removing a subunit can be described by its processivity. In our phenomenological description, we can define an effective processivity

$$p_{\text{eff}} = 1 - \left| \frac{J(\rho_0) - J(0)}{\Omega(\rho_0) - \Omega(0)} \right| . \quad (3.7)$$

This effective processivity differs from the processivity of an isolated motor due to collective effects resulting from interactions between motors at the end and thus depends on  $\rho_0$ . As the processivity is an intrinsic property of the motor proteins, we subtract terms of the depolymerisation rate and the particle current which are independent of the bound motor density. If  $p_{\text{eff}} \leq 0$ , motor induced depolymerisation of subunits is non-processive, corresponding to a situation where a single motor is only able to remove one subunit. Thus more motors detach from the end than subunits (in addition to motors falling off after removal, some motors may also detach directly from the filament end without removal of subunits). However, if  $0 < p_{\text{eff}} \leq 1$ , motors work processively, and one given motor will therefore be able to remove several subunits of a filament before eventually detaching from the filament. Note that the motor density at the end cannot exceed the maximal density per binding site on the filament  $\rho_0 \leq \rho_{\text{max}} = N/a$ . Thus, the effective processivity has to vanish if the density at the end reaches a critical value  $\rho_c$  with  $\rho_c \leq \rho_{\text{max}}$ . Here,  $\rho_c = \rho_{\text{max}}$ , in the case of no direct attachment of motors to or detachment from the end. It therefore follows from Eq.(3.7) that the expansion coefficients of  $J(\rho_0)$  and  $\Omega(\rho_0)$  have to fulfil the following relation:

$$\left| J_1 + J_2 \rho_{\text{max}} + \mathcal{O}(\rho_{\text{max}}^2) \right| \geq \left| \Omega_1 + \Omega_2 \rho_{\text{max}} + \mathcal{O}(\rho_{\text{max}}^2) \right| . \quad (3.8)$$

## 3.2. Steady-state solutions

Having described the dynamics of the bound motor proteins, we can now solve the equations of motion for  $\rho$ . Inserting Eqns.(3.2,3.3,3.4,3.6) in Eq.(3.1) we obtain a nonlinear parabolic

partial differential equation for  $\rho$ :

$$\partial_t \rho = D \partial_x^2 \rho + \left( v_0 \left( 1 - 2 \frac{\rho}{\rho_{\max}} \right) + v_d(\rho_0) \right) \partial_x \rho - \left( \frac{\omega_a c}{\rho_{\max}} + \omega_d \right) \rho + \omega_a c \quad . \quad (3.9)$$

Knowing that for  $x = 0$  the current on the filament, Eq.(3.2), has to equal the net rate of motors binding to or unbinding from the filament end, Eq.(3.5), we obtain a condition for the gradient of the bound motor density at  $x = 0$ :

$$\partial_x \rho_0 = -\frac{1}{D} \left( J(\rho_0) + v_0 \left( 1 - \frac{\rho_0}{\rho_{\max}} \right) \rho_0 + v_d(\rho_0) \rho_0 \right) \quad . \quad (3.10)$$

Using a semi-infinite geometry, we expect the density  $\rho$  to approach a constant value for large  $x$ . We can therefore write as the necessary second boundary equation:

$$\lim_{x \rightarrow \infty} \partial_x \rho(x) = 0 \quad . \quad (3.11)$$

In this case, one is left with the attachment-detachment dynamics of motors and as the corresponding rates obey detailed balance, the density on the filament reaches an equilibrium steady state. Considering only hard-core repulsion between the particles, the motor distribution after reaching the steady state is solely determined by the attachment and detachment rates of the motors:

$$\rho_\infty = \frac{\omega_a c \rho_{\max}}{\omega_a c + \omega_d \rho_{\max}} \quad . \quad (3.12)$$

Assuming a filament with no motors bound at  $t = 0$  (e.g. start of the experiment) we choose

$$\rho(x, 0) = 0 \quad , \quad (3.13)$$

as the initial condition.

### 3.2.1. Density profiles of motor proteins

Following experimental observations (Desai et al., 1999; Hunter et al., 2003) indicating that  $v_m \ll 1$ , we expect effects of the density dependence of the directed motor velocity,  $v_m$ , to be negligible<sup>3</sup> and we thus neglect it in the following discussion, leading to  $v_m(\rho) \rightarrow v_0$ . In this case we can analytically calculate the steady state of Eq.(3.9). Using the condition for  $x \rightarrow \infty$ , Eq. (3.11), we find the following solution:

$$\rho = \rho_\infty + (\rho_0 - \rho_\infty) e^{-x/\lambda} \quad . \quad (3.14)$$

Here,  $\lambda$  is the characteristic localisation length of motors from the end and is given by:

$$\lambda = \frac{2D}{(v_0 + v_d) + ((v_0 + v_d)^2 + 4D(\omega_a c / \rho_{\max} + \omega_d))^{1/2}} \quad . \quad (3.15)$$

---

<sup>3</sup>Note that in the case where the absolute amount of the directed motion is significant, as for kinesin motors moving processively along microtubules, the density dependence of  $v_m$  is known to lead to unexpected dynamical behaviour of motor proteins, including phase coexistence of low and high density regions of motors on the filament, which are separated by domain walls (Lipowsky et al., 2001; Parmeggiani et al., 2003; Klumpp and Lipowsky, 2004; Parmeggiani et al., 2004).

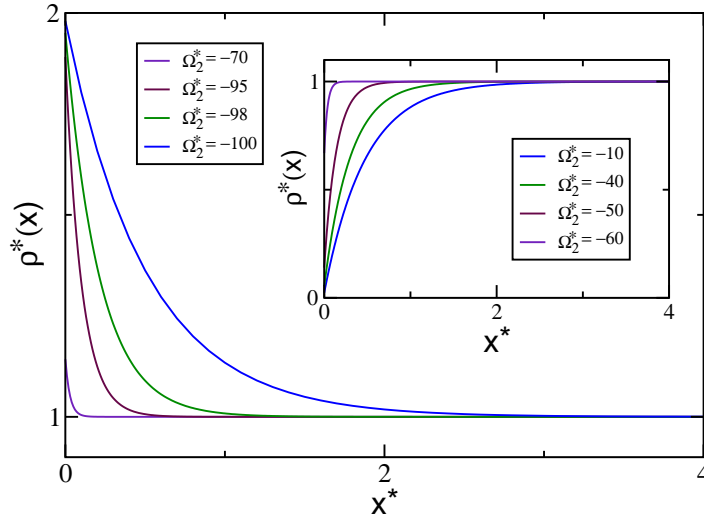


**Figure 3.3:** The motor density,  $\rho^*(x) = \rho(x)/\rho_{\max}$ , as a function of the filament extension  $x^* = x/(D/\omega_d)^{1/2}$  for different values of  $\Omega_2^* = (\Omega_2 \rho_{\max})/\sqrt{D\omega_d} = -70, -95, -98$  and  $-100$ . Parameter values are:  $c^* = (\omega_a c)/(\omega_d \rho_{\max}) = 1$ ,  $\Omega_0 = J_0 = J_2 = 0$ ,  $\Omega_1^* = \Omega_1/\sqrt{D\omega_d} = 100$ ,  $J_1^* = J_1/\sqrt{D\omega_d} = -(\Omega_1^* + \Omega_2^*)$ . Inset: Same situation, but with  $\Omega_2^* = (\Omega_2 \rho_{\max})/\sqrt{D\omega_d} = -10, -40, -50$  and  $-60$ .

The value of  $\rho_0$ , has to be determined selfconsistently, using the remaining boundary condition at  $x = 0$ , Eq.(3.10). Inserting Eq.(3.14) in Eq.(3.10) would, due to the expansions of Eqns.(3.6) and (3.5), lead to a polynomial of infinite order in  $\rho_0$ . In the following, we will restrict ourselves to terms up to second order in the expansions of Eqns.(3.5) and (3.6):

$$J(\rho_0) \approx J_0 + J_1 \rho_0 + J_2 \rho_0^2, \quad (3.16)$$

$$\Omega(\rho_0) \approx \Omega_0 + \Omega_1 \rho_0 + \Omega_2 \rho_0^2, \quad (3.17)$$

leading to a polynomial of fifth order,

$$\Theta_5 \rho_0^5 + \Theta_4 \rho_0^4 + \Theta_3 \rho_0^3 + \Theta_2 \rho_0^2 + \Theta_1 \rho_0 + \Theta_0 = 0, \quad (3.18)$$

which can readily be solved numerically in order to determine the value of  $\rho_0$  (see Appendix for explicit calculation of the polynomial coefficients,  $\Theta_i$ ). With the calculation of  $\rho_0$ , the steady state solution is fully determined, and we can now examine the stability of the obtained steady states.

### 3.2.2. Stability of solutions

In order to determine the stability of the above derived solutions, we will examine their evolution in time after an applied perturbation.

#### Linear stability analysis

For this purpose, we expand  $\rho$  around the steady-state. Assuming that the perturbations of the steady-state are small, it is sufficient to consider the expansion only up to the linear

order term,  $\rho(x, t) = \rho_s(x) + \rho_1(x, t)$ . With  $\rho_1(x, t) = \tilde{q}(x)e^{\zeta t}$ , where in general  $\zeta \in \mathbb{C}$ , we can write:

$$\rho(x, t) = \rho_s(x) + \tilde{q}(x)e^{\zeta t} \quad (3.19)$$

The solutions start to become unstable if the highest value of  $Re[\zeta]$  changes sign from negative, where perturbations decay in time, to positive values. Inserting the above equation in Eq.(3.9), considering only terms up to linear order in  $\tilde{q}$  and using that  $\rho_s$  is a solution of the steady-state of Eq.(3.9) we obtain:

$$D\partial_x^2 q + (v_0 + v_d)\partial_x q - \left( \frac{\omega_a c}{\rho_{\max}} + \omega_d + \zeta \right) q = \frac{(\rho_s(0) - \rho_\infty)(\Omega_1 + 2\Omega_2\rho_s(0))}{\lambda\rho_{\max}} e^{-x/\lambda} \quad (3.20)$$

Here,  $q = \tilde{q}/\tilde{q}(0)$  and  $\lambda$  is defined by Eq.(3.15). In order to be able to solve this equation, we also have to insert Eq.(3.19) in the Eq.(3.10) and Eq.(3.11), giving us two boundary conditions for the perturbation amplitude:

$$D\partial_x q_0 = - \left( \frac{\Omega_0}{\rho_{\max}} + J_1 \right) - 2 \left( \frac{\Omega_1}{\rho_{\max}} + J_2 \right) \rho_s(0) - \frac{3\Omega_2}{\rho_{\max}} \rho_s(0)^2 \quad , \quad (3.21)$$

and

$$q_\infty = 0 \quad . \quad (3.22)$$

From the substitution used above,  $q = \tilde{q}/\tilde{q}(0)$ , we obtain an additional condition,

$$q(0) = 1 \quad . \quad (3.23)$$

We find the following solution to Eq.(3.20),

$$q = A_+ e^{-x/k_+} + A_- e^{-x/k_-} + B e^{-x/\lambda} \quad . \quad (3.24)$$

Here,

$$k_\pm = \frac{2D}{(v_0 + v_d) \pm \sqrt{(v_0 + v_d)^2 + 4D \left( \frac{\omega_a c}{\rho_{\max}} + \omega_d + \zeta \right)}} \quad , \quad (3.25)$$

and

$$B = - \frac{(\rho_{s,0} - \rho_\infty)(\Omega_1 + \Omega_2\rho_{s,0})}{\zeta\lambda\rho_{\max}} \quad . \quad (3.26)$$

Using the boundary conditions, Eq.(3.21) and Eq.(3.23) we can determine  $A_+$  and  $A_-$ , which can be written as (see appendix for determination of coefficients,  $\gamma_i$ ):

$$A_\pm = \Gamma_0 \pm \Gamma_1 \zeta^{-1/2} + \Gamma_2 \zeta^{-1} \pm \Gamma_3 \zeta^{-3/2} \quad . \quad (3.27)$$

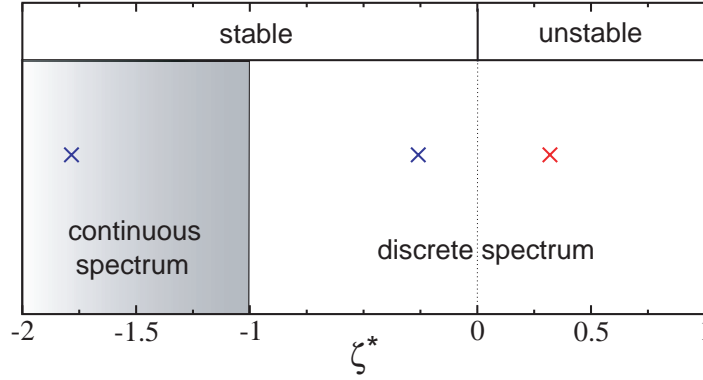


**Figure 3.4:** Illustration of the possible eigenvalue spectrum. One always gets a continuous spectrum in the stable regime, with  $\zeta < \zeta_c = -(\omega_a c / \rho_{\max} + \omega_d)$ . Depending on the chosen parameters, one can additionally get a discrete eigenvalue spectrum, with the possibility of positive eigenvalues, leading to unstable solutions. Possible discrete values are given by solutions to Eq.(3.28). The shown three eigenvalues,  $\zeta^* = \zeta / \omega_d$ , were obtained for:  $c^* = (\omega_a c) / (\omega_d \rho_{\max}) = 0.0038$ ,  $\Omega_2^* = (\Omega_2 \rho_{\max}) / (\sqrt{D \omega_d}) = -\Omega_1^* = -(\Omega_1) / (\sqrt{D \omega_d}) = 100$ ,  $J_2 = J_1 = J_0 = \Omega_0 = 0$ .

### Spectrum of eigenvalues

We can now use Eq.(3.22) to determine the spectrum of eigenvalues  $\zeta$ , and especially the conditions, for which solutions are stable or unstable. From Eq.(3.24), one sees that in order to fulfil Eq.(3.22),  $Re[k_+]$  and  $Re[k_-]$  both have to be positive if  $A_{\pm} \neq 0$ . For  $\zeta \in \mathbb{R}$ , it follows directly from Eq.(3.25), that for  $\zeta < \zeta_c$  with  $\zeta_c = -(\omega_a c / \rho_{\max} + \omega_d)$ ,  $Re[k_{\pm}] > 0$ <sup>4</sup>. In this case Eq.(3.24), fulfils the above boundary conditions for all values of  $\zeta \in ]-\infty, -(\omega_a c / \rho_{\max} + \omega_d)[$ , and we get a continuous spectrum of eigenvalues  $\zeta$ .

For values of  $\zeta > \zeta_c$ , the real part of  $k_+$  continues to have positive values, while  $Re[k_-]$  becomes negative. In order for the boundary condition for  $x \rightarrow \infty$ , Eq.(3.22), to be fulfilled in this situation,  $A_- \stackrel{!}{=} 0$ . Due to this condition, the spectrum, of  $\zeta$  switches at  $\zeta_c$  from a continuous spectrum to a discrete spectrum (see Fig.(3.4)), given by the solutions to:

$$\Gamma_0^2 \zeta^3 + (2\Gamma_0 \Gamma_2 - \Gamma_1) \zeta^2 + (\Gamma_2^3 - 2\Gamma_1 \Gamma_3) \zeta - \Gamma_3^2 = 0 \quad (3.28)$$

## 3.3. Dynamic accumulation of motor proteins

### 3.3.1. Mechanisms of motor accumulation at filament ends

Having calculated the steady-state of Eq.(3.9) and its stability, we can now investigate the behaviour of the system. Here we are interested in the conditions under which motors can accumulate at the end of a filament which they depolymerise. One can immediately think of two different mechanisms by which accumulation of motors at the end can occur:

First, motors can accumulate by directly binding to the filament end if they have a higher affinity to the end than to the subunits along the filament. This effect will dominate if the

<sup>4</sup>See Appendix for derivation of  $\zeta_c$  if  $\zeta \in \mathbb{C}$ .

total velocity of motor proteins on the filament  $v = v_0 + v_d$  is small,  $v^2 \ll 4D(\omega_a c / \rho_{\max} + \omega_d)$ . In this case, the localisation length is given by the diffusion length, during the attachment time

$$\lambda \simeq \sqrt{D/(\omega_a c + \omega_d)} \quad . \quad (3.29)$$

A second mechanism of attachment is given by transport of motors to the end with an average speed  $v_0$ . This will dominate for  $|v_0| \gg v_d$  and  $v_0^2 \gg 4D(\omega_a c / \rho_{\max} + \omega_d)$ . The localisation length in this case reads:

$$\lambda \simeq \frac{D}{v_0} \quad . \quad (3.30)$$

The first mechanism can lead to accumulation at both ends of a filament of finite length, while the second will lead to accumulation of motors at one end only.

While these mechanisms quite obviously lead to accumulation, in the following we now examine a third possibility of motors accumulating at a filament end. In this case, motors that bind along the filament are captured by the shortening end. This mechanism will dominate for  $v_d \gg |v_0|$  and  $v_d^2 \gg 4D(\omega_a c / \rho_{\max} + \omega_d)$ . The localisation length here is given by

$$\lambda \simeq \frac{D}{v_d} \quad . \quad (3.31)$$

As with direct attachment of motors to the end, this mechanism can lead to accumulation of motor proteins at both ends of a filament.

In order to distinguish clearly between the different mechanisms, we consider the case where  $v_d \gg |v_0|$  and the spontaneous velocity of  $v_0$  can be neglected. This is in accordance with experimental observations of motors of the Kin-13 subfamily, showing that  $v_d \gg |v_0|$  (Desai et al., 1999; Hunter et al., 2003). Additionally we assume that attachment to and detachment from the filament end occur at the same rates as in the bulk, thus  $J_0 = 0$  and  $J_1 \leq 0$  (compare p. 31).

From Eq.(3.10) we can calculate the borderline between accumulation and depletion of motor proteins at the end as a function of the expansion parameters  $\Omega_i$  and  $J_i$ . Along the borderline motors are homogeneously distributed on the filament,  $\rho(0) = \rho_\infty$  and the expansion coefficients have to fulfil the following relation:

$$\frac{\Omega_2}{\rho_{\max}} \rho_\infty^3 + \left( \frac{\Omega_1}{\rho_{\max}} + J_2 \right) \rho_\infty^2 + \left( \frac{\Omega_0}{\rho_{\max}} + J_1 \right) \rho_\infty + J_0 = 0 \quad . \quad (3.32)$$

### 3.3.2. Influence of collective effects

#### Linear theory of depolymerisation

We will first examine the effects of motor induced depolymerisation in the case where one can neglect interactions between motor proteins at the end. To a good approximation, this will be the case if the concentration of proteins in the surrounding solution, or the attachment rate of motors to the filament, are very low. We therefore restrict the expansion of  $J(\rho_0)$  and  $\Omega(\rho_0)$  to linear order terms:

$$\begin{aligned} J(\rho_0) &\simeq J_1 \rho(0) \quad , \\ \Omega(\rho_0) &\simeq \Omega_1 \rho(0) \quad . \end{aligned} \quad (3.33)$$

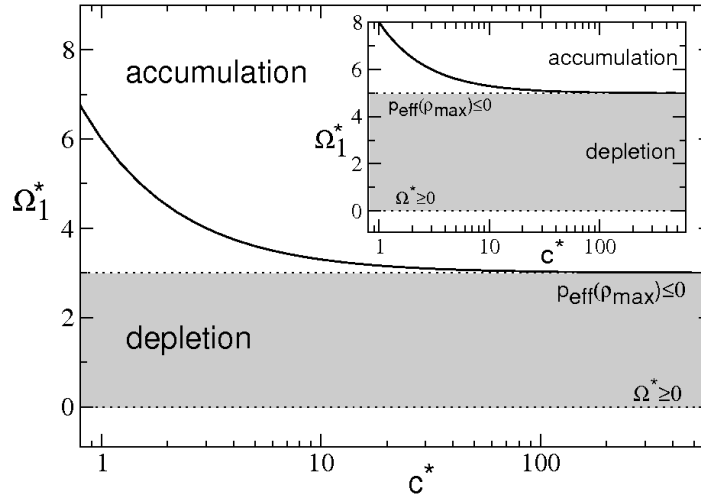


**Figure 3.5:** Regimes of accumulation and depletion of motors at the shrinking filament end as a function of the coefficient  $\Omega_1^* = \Omega_1/\sqrt{D\omega_d}$  and the bulk motor concentration  $c^* = (\omega_a c)/(\omega_d \rho_{\max})$  for  $J_1^* = J_1/\sqrt{D\omega_d} = -3$  and  $J_0 = \Omega_0 = J_2 = \Omega_2 = 0$ . Accumulation occurs above the solid line, depletion occurs below. The grey area indicates the region of physical interest. Above this area,  $p_{\text{eff}}(\rho_{\max}) \geq 0$  which is forbidden by steric exclusion of particles (see Eq.(3.8)). Below this area the depolymerisation rate  $\Omega$  becomes negative, signifying motor induced polymerisation of filaments. Inset: the same situation as above, but with  $J_2^* = (J_2 \rho_{\max})/\sqrt{D\omega_d} = -2$ .

Here we have neglected  $J_0$  because of the reasons mentioned above and  $\Omega_0$  because we are here interested only in motor-induced depolymerisation. We thus neglect spontaneous depolymerisation of the filament, described by  $\Omega_0$ . In order for motor induced depolymerisation to occur, we require  $\Omega_1 \geq 0$ , as otherwise  $\Omega(\rho_0) < 0$ , corresponding to motor induced polymerisation. By concentrating on the case where no direct attachment and detachment of motors at the end is taking place, the current  $J(\rho_0)$  is simply given by motors depolymerising subunits and falling of the filament with them, leading to  $J(\rho_0) < 0$ . From Eq.(3.8) we can then immediately see, that

$$\Omega_1 \leq -J_1 \quad , \quad (3.34)$$

has to hold. Inserting the above relation, in Eq.(3.32) we get

$$\Omega_1 \left( \frac{\rho_\infty}{\rho_{\max}} - 1 \right) = 0 \quad . \quad (3.35)$$

In the case of motor activity,  $\Omega_1 \neq 0$ , we see that  $\rho_\infty \stackrel{!}{=} \rho_{\max}$ , in order to have a homogeneously covered filament. As in this case the maximal amount of motors is already attached to the filament, no additional accumulation can occur at the end. From Eq.(3.7) one sees that as long as Eq.(3.34) holds, the effective processivity,  $p_{\text{eff}} \leq 0$ , irrespective of the explicit value of  $\Omega_1$ .

### Nonlinear theory of depolymerisation

Having seen that without motor-motor interaction at the end, no dynamic accumulation is possible, we will now focus on the effects of these interactions. Therefore we now also

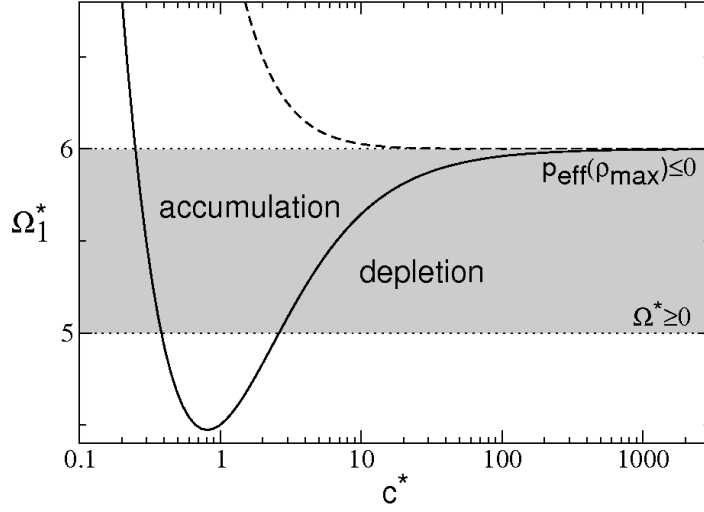


**Figure 3.6:** Regimes of accumulation and depletion of motors at the shrinking filament end in the case of a nonlinear depolymerisation rate are shown as a function of the coefficient  $\Omega_1^* = \Omega_1/\sqrt{D\omega_d}$  and the bulk motor concentration  $c^* = (\omega_a c)/(\omega_d \rho_{\max})$  for  $J_1^* = J_1/\sqrt{D\omega_d} = -1$ ,  $\Omega_2^* = (\Omega_2 \rho_{\max})/\sqrt{D\omega_d} = -5$  and  $J_0 = \Omega_0 = J_2 = 0$ . The dashed line shows the borderline between accumulation and depletion for  $J_1^* = \Omega_2^* = -3$ . In this case no accumulation can occur. Note that in this case, the lower boundary of the region of physical interest is shifted to  $\Omega_1^* = 1$ , not shown in this graph.

consider terms of quadratic order in  $\rho_0$  in the expansions of Eq.(3.6) and Eq.(3.5). We separately examine the influence of  $J_2$  and  $\Omega_2$  on the accumulation of motors at the end.

**Nonlinear edge current:** Here we assume nonlinear effects in the depolymerisation rate to be negligible,  $|\Omega_2| \ll 1$ , and therefore neglect nonlinear terms in  $\Omega(\rho_0)$ .

$$\begin{aligned} J(\rho_0) &\simeq J_1 \rho(0) + J_2 \rho(0)^2 \quad , \\ \Omega(\rho_0) &\simeq \Omega_1 \rho(0) \quad . \end{aligned} \quad (3.36)$$

Consulting again Eq.(3.8), we see that the relation the expansion coefficients have to fulfil in this situation is  $|J_1 + J_2 \rho_{\max}| \geq |\Omega_1|$ . Requiring again that  $J(\rho_0) \leq 0$  and  $\Omega_1 \geq 0$ , we obtain

$$\Omega_1 \leq -J_1 - J_2 \rho_{\max} \quad . \quad (3.37)$$

The critical value  $\Omega_1^a$ , leading to an homogeneous distribution of motors on the filament, follows from Eq.(3.32) to be

$$\Omega_1^a = -J_1 \frac{\rho_{\max}}{\rho_\infty} - J_2 \rho_{\max} \quad . \quad (3.38)$$

For values of  $\Omega_1$  larger than  $\Omega_1^a$ , particles accumulate at the end. Comparing Eq.(3.38) with Eq.(3.37), one sees immediately that no accumulation at the filament end is possible, instead the end will be depleted of motors for all values of  $J_1$  and  $J_2$ . The depletion of motors at the end is only overcome for high motor concentrations, where  $\rho_\infty \rightarrow \rho_{\max}$ , and thus the whole filament is covered with the maximum number of proteins (see Fig.(3.5)).

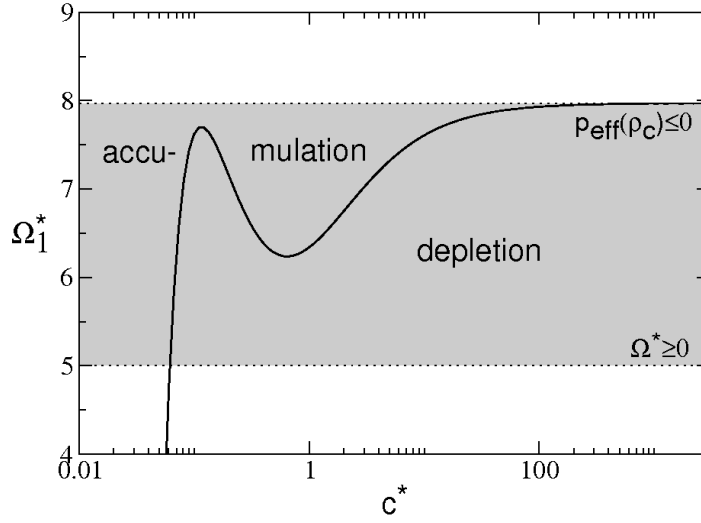


**Figure 3.7:** Accumulation and depletion of proteins at the depolymerising filament end as a function of the coefficient  $\Omega_1^* = \Omega_1/\sqrt{D\omega_d}$  and the bulk motor concentration  $c^* = (\omega_a c)/(\omega_d \rho_{\max})$ . Parameter values are:  $J_0^* = J_0/(\rho_{\max}\sqrt{D\omega_d}) = 0.05$ ,  $J_1^* = J_1/\sqrt{D\omega_d} = -1.02$ ,  $J_2^* = J_2/\sqrt{D\omega_d}$  and  $\Omega_2^* = (\Omega_2\rho_{\max})/\sqrt{D\omega_d} = -5$ . The upper boundary of the physically interesting area, shaded grey, is given by  $p_{\text{eff}}(\rho_c) \leq 0$  with  $\rho_c \leq \rho_{\max}$ .

**Nonlinear depolymerisation rate:** We expand  $J(\rho_0)$  and  $\Omega(\rho_0)$  in the following way:

$$\begin{aligned} J(\rho_0) &\simeq J_1\rho(0) \quad , \\ \Omega(\rho_0) &\simeq \Omega_1\rho(0) + \Omega_2\rho(0)^2 \quad . \end{aligned} \quad (3.39)$$

Because of effects of steric exclusion, taken into account by Eq.(3.8), the coefficients have to fulfil in this situation,

$$\Omega_1 \leq -J_1 - \Omega_2\rho_{\max} \quad . \quad (3.40)$$

Note, that we expect the depolymerisation rate to saturate with increasing protein density at the filament end and we therefore, in addition to  $\Omega(\rho_0) \geq 0$ , require  $\Omega_2 < 0$ , with  $|\Omega_2| \leq \Omega_1$ . For the critical value of  $\Omega_1$  we get here

$$\Omega_1^a = -J_1 \frac{\rho_{\max}}{\rho_{\infty}} - \Omega_2\rho_{\infty} \quad . \quad (3.41)$$

The effect of the nonlinear term in  $\Omega(\rho_0)$  can be seen in Fig.(3.6). In contrast to the cases considered before, a regime of accumulation can now also exist. Interestingly, the possibility of a minimum in Eq.(3.41) at  $c = (\sqrt{\Omega_2/(J_1\rho_{\max})} - 1)^{-1}$  can lead to a reentrant behaviour in the motor accumulation as a function of increasing bulk motor concentration for a certain regime of parameters (see Fig.(3.6)).

Note that additionally taking into account quadratic order terms in  $J(\rho_0)$  will additionally shift the borderline of accumulation in Fig.(3.6) to higher or smaller values of  $\Omega_1$ , depending on the sign of  $J_2$ . At the same time, the upper limit of the physical interesting region, given by  $p_{\text{eff}}(\rho_{\max}) \leq 0$ , will be shifted by the same amount while the lower boundary, given by  $\Omega(\rho_0) \geq 0$ , will stay unchanged. This can lead to an area of depletion for small values of  $\Omega_1$ , irrespective of the motor concentration.

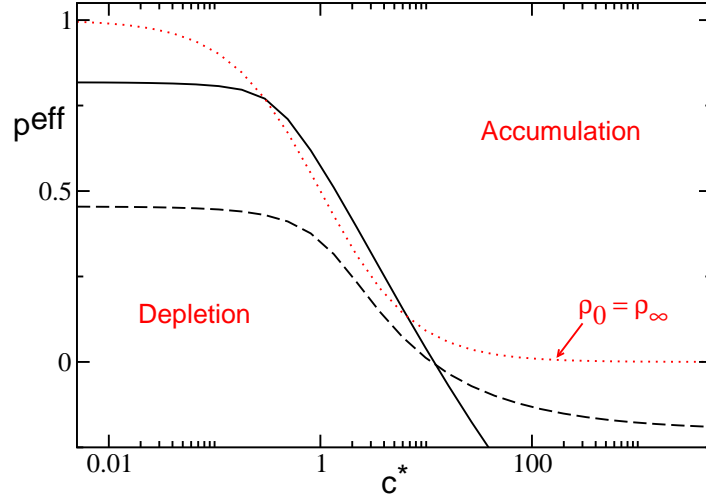


**Figure 3.8:** The effective processivity is shown for  $J_1^* = -1$ ,  $\Omega_1^* = 5$  and  $\Omega_2^* = -5$  (solid line) and  $J_1^* = -3$ ,  $\Omega_1^* = 5$  and  $\Omega_2^* = -3$  (dashed line), corresponding to those used in Fig.3.6.  $J_0^* = \Omega_0^* = J_2^* = 0$  in both cases. The limit values for  $c \rightarrow 0$  and  $c \rightarrow \infty$  are given for the solid (dashed) line by  $1 - |J_1^*/\Omega_1^*| \approx 0.81(0.45)$  and  $1 - |(J_1^* + J_2^*)/(\Omega_1^* + \Omega_2^*)| = -1(-0.5)$  respectively (see text). The red dotted line marks the critical effective processivity needed to get a homogenous distribution of motor on the filament. Below it, processivity is not high enough to lead to accumulation of motors, while above it motor processivity leads to accumulation at the ends.

Here we have focused on the case where no direct attachment of proteins to the filament end is taking place. In the case of  $J_0 \neq 0$ , we find additional regimes of accumulation in the situations considered above (see Fig.(3.7)).

### 3.3.3. Role of processivity

From the discussion above, we have seen that motors can dynamically ( $J_0 = 0$ ) accumulate at filament ends and that nonlinear terms in the depolymerisation rate are essential for this accumulation. In order to examine the interplay between the nonlinear terms in the current and in the depolymerisation rate, which is responsible for accumulation or depletion, we will discuss the effective processivity, defined in Eq.(3.7). The effective processivity as a function of the bulk motor concentration is plotted in Fig.3.8 for parameter values matching those used for Fig.(3.6) (solid and dashed line) and compared to the value of the effective processivity in the case of an homogenous motor distribution on the filament (red dotted line). The effective processivity in the case of an homogenous distribution where  $\rho(0) = \rho_\infty$  can be calculated by solving Eq.(3.32) for  $\Omega_1$ ,

$$\Omega_1^a = - \left( \Omega_2 \rho_\infty + J_2 \rho_{\max} + \frac{\Omega_0 + J_1 \rho_{\max}}{\rho_\infty} - \frac{J_0 \rho_{\max}}{\rho_\infty^2} \right) , \quad (3.42)$$

and inserting the solution into Eq.(3.7), leading to:

$$p_{\text{eff}}^a = 1 - \left| \frac{J_1 \rho_\infty + J_2 \rho_\infty^2}{-(J_1 \rho_{\max} + J_2 \rho_{\max} \rho_\infty)} \right| \quad (3.43)$$

Here we have used again  $\Omega_0 = J_0 = 0$ . In the limit of small motor concentrations,  $c \rightarrow 0$ , implying also  $\rho_\infty \rightarrow 0$ , motors have to become highly processive in order for accumulation to

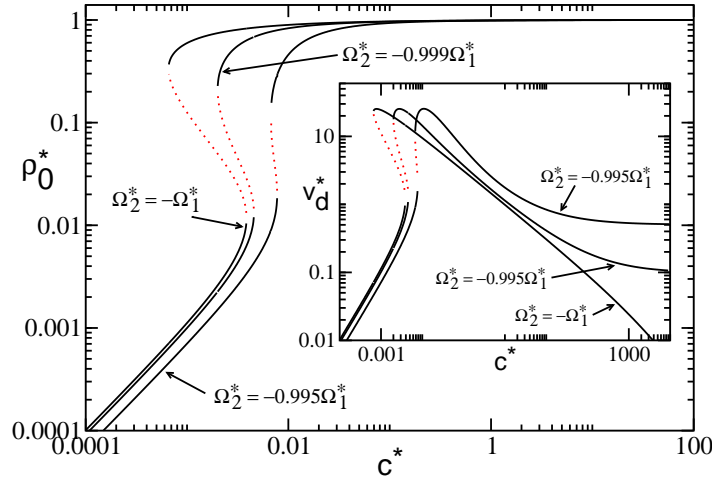


**Figure 3.9:** The motor density at the filament end  $\rho_0^* = \rho_0/\rho_{\max}$  as a function of the bulk motor concentration  $c^* = (\omega_a c)/(\omega_d \rho_{\max})$  for different values of the nonlinear expansion coefficient  $\Omega_2^* = (\Omega_2 \rho_{\max})/(\sqrt{D\omega_d})$ .  $\Omega_1^* = (\Omega_1)/(\sqrt{D\omega_d}) = 100$ ,  $J_2^* = (J_2 \rho_{\max})/(\sqrt{D\omega_d}) = 0$ . Due to Eq.(3.8),  $J_1^* = -\Omega_1^* - \Omega_2^*$ . Stable solutions are plotted with solid black lines, unstable ones with dashed red lines. Inset: The depolymerisation velocity  $v_d^* = v_d/\sqrt{D\omega_d}$  as a function of the bulk motor concentration  $c^*$  for the same situations.

occur at the end. Thus  $p_{\text{eff}}^a \rightarrow 1$ . For  $c \rightarrow \infty$ , implying  $\rho_\infty \rightarrow \rho_{\max}$ , however, the processivity has to vanish  $p_{\text{eff}}^a \leq 0$  as in this case the whole filament will be covered with proteins and therefore motors cannot stay attached after subunit removal. Following the solid line in Fig.3.8, one sees that the average processivity of individual motor proteins, given by the limit of  $c \rightarrow 0$  of Eq.(3.7),

$$p_{\text{eff}}^a|_{c \rightarrow 0} = 1 - \left| \frac{J_1}{\Omega_1} \right| \quad (3.44)$$

is not high enough to lead to accumulation. For increasing motor density the effective processivity crosses the critical effective processivity twice, giving rise to the observed regime of accumulation in Fig.3.6. For very high motor concentrations,  $c \rightarrow \infty$ , the processivity saturates at

$$p_{\text{eff}}^a|_{c \rightarrow \infty} = 1 - \left| \frac{J_1 + J_2 \rho_{\max}}{\Omega_1 + \Omega_2 \rho_{\max}} \right| \quad (3.45)$$

In the case of the dashed line, the effective processivity always stays below the critical value, thus leading to the observed depletion of motor proteins for all values of  $c$  (see Fig.3.6).

Therefore the processivity of each single motor protein is not the critical condition for accumulation to occur, rather how the processivity of many motors accumulating at the end, described by the effective processivity, behaves for increasing motor concentrations.

### 3.4. Instabilities due to collective effects

Previously, we have seen that collective effects of motor proteins at filament ends can lead to accumulation. Let us now discuss the situation, where collective effects lead to multiple

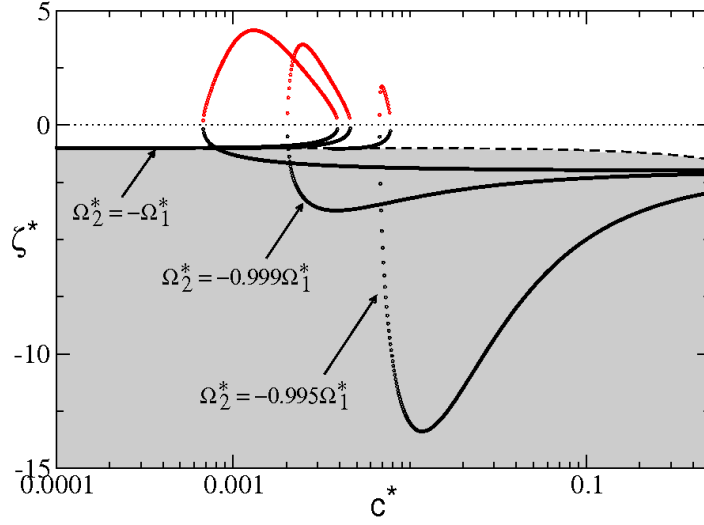


**Figure 3.10:** Spectrum of the eigenvalue  $\zeta^* = \zeta/\omega_d$  as a function of the motor concentration  $c^* = (\omega_a c)/(\omega_d \rho_{\max})$  for  $\Omega_2^* = (\Omega_2 \rho_{\max})/(\sqrt{D\omega_d}) = -\Omega_1^* = -(\Omega_1)/(\sqrt{D\omega_d})$ ,  $\Omega_2^* = -0.999\Omega_1^*$  and  $\Omega_2^* = -0.995\Omega_1^*$ .  $\Omega_1^* = 100$ ,  $J_2^* = (J_2 \rho_{\max})/(\sqrt{D\omega_d}) = 0$ . Due to Eq.(3.8),  $J_1^* = -\Omega_1^* - \Omega_2^*$ . For each parameter set a continuum of stable eigenvalues exists (shaded area). In addition, discrete eigenvalues can exist, shown here as individual points. Discrete eigenvalues can cross from the stable,  $\zeta < 0$  (black points) to the unstable,  $\zeta > 0$ , regime (red points).

steady state solutions for a given set of parameters. Multiple steady state solutions are encountered when collective effects are strong, i. e. for high effective processivities. In order for the effective processivity to be close to unity, the current of particles at the end has to be close to zero, as approximately all subunit-removing motors stay on the filament. From Eq.(3.8) we see that in this case the magnitude of the nonlinear expansion coefficient,  $|\Omega_2|$ , has to have approximately the magnitude of the linear expansion coefficient,  $|\Omega_2| \approx |\Omega_1|$ . Due to the premise of  $\Omega(\rho_0) \geq 0$  for all values of  $\rho_0$  and the assumption that the depolymerisation velocity has to saturate for high motor concentrations due to the finite number of binding sites available at filament ends, the value of the nonlinear term is limited by  $-\Omega_1 \leq \Omega_2 \leq 0$ . Figure 3.9 displays the motor density at the filament end and the depolymerisation velocity as a function of the bulk motor concentration  $c$ . Three cases are shown, differing in the magnitude of the nonlinear term in the depolymerisation rate,  $\Omega_2 \rho_{\max} = -\Omega_1$ ,  $\Omega_2 \rho_{\max} = -0.999\Omega_1$  and  $\Omega_2 \rho_{\max} = -0.995\Omega_1$ . The motor density saturates for large concentrations,  $\rho_0 \rightarrow \rho_{\max}$ , while it increases linearly for small motor concentrations. Increasing the bulk motor concentration further, a dynamic instability appears where two stable states with different  $\rho_0$  coexist within a range of the bulk concentration  $c$ . A third unstable steady state is indicated with the red dotted line. Note that as the nonlinear expansion coefficient of the depolymerisation rate, which describes collective effects of motors at the end, is reduced, the instability gets less pronounced (see also Fig.3.10). Lowering the value of  $|\Omega_2|$  further leads to the disappearance of the dynamic instability. Interestingly, the corresponding depolymerisation velocities  $v_d$ , shown in the inset of Fig.3.9, exhibit a maximum as a function of the motor concentration for strong motor interactions and then saturate for higher  $c$ . In the case of strongest interactions,  $\Omega_2 \rho_{\max} = -\Omega_1$ , the depolymerisation velocity even vanishes for large  $c$ , as in this case  $\rho_0 \rightarrow \rho_{\max}$  and,

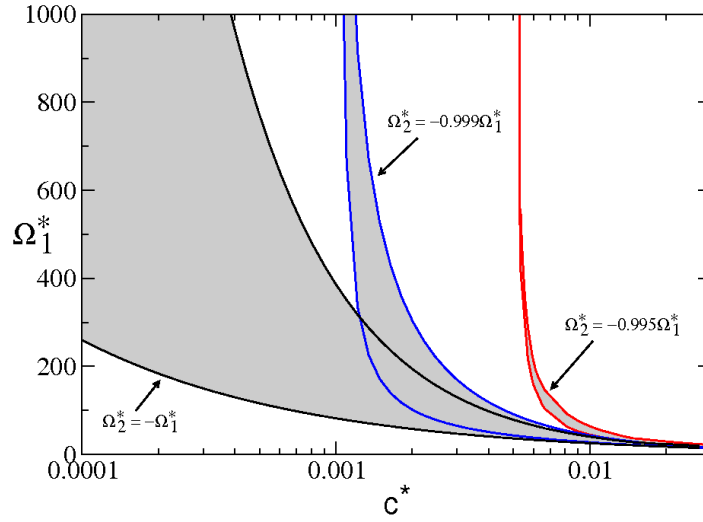


**Figure 3.11:** Regimes of multiple steady state solutions as a function of  $\Omega_1^* = (\Omega_1)/(\sqrt{D\omega_d})$  and  $c^* = (\omega_a c)/(\omega_d \rho_{\max})$  for different values of  $\Omega_2^* = (\Omega_2 \rho_{\max})/(\sqrt{D\omega_d}) = -\Omega_1^*, -0.999\Omega_1^*, -0.995\Omega_1^*$ .  $J_2^* = (J_2 \rho_{\max})/(\sqrt{D\omega_d}) = 0$  and  $J_1^* = -\Omega_1^* - \Omega_2^*$ . For each parameter set of the shaded area, two stable steady state solutions and one unstable solution exist.

$$v_d = \Omega_1 \rho_{\max} + \Omega_2 \rho_{\max}^2 = -\Omega_2 \rho_{\max}^2 + \Omega_2 \rho_{\max}^2 \quad . \quad (3.46)$$

Note that for lower values of  $|\Omega_2|$ , the maximum vanishes and velocities saturate for high  $c$  after a linear increase.

In order to examine the stability of the solutions, we use the linear stability analysis introduced in section 3.2. In Fig.3.10 the eigenvalue spectrum for the three different values of  $\Omega_2$  discussed above are shown. As discussed in section 3.2, one gets a region of continuous eigenvalues (shaded area) in the stable regime. The borderline is defined by  $\zeta = -(\omega_a c/\rho_{\max} + \omega_d)$ . In addition to this continuum, discrete eigenvalues exist in the cases considered here (dotted lines). In Fig.3.10 only the biggest discrete eigenvalue for each parameter set is displayed and for intermediate concentrations these cross over from the stable,  $\zeta < 0$ , to the unstable regime,  $\zeta > 0$ . Note, that for higher concentrations, no discrete values can be found and all solutions are stable as the highest eigenvalue is given by the borderline of the continuum.

Next we examine the occurrence of multiple solutions as the two nonlinear expansion coefficients,  $J_2$  and  $\Omega_2$  are varied. As already stated, a high effective processivity is needed for multiple solutions. In Fig.3.11 the regions of multiple solutions (shaded areas) are shown in dependence of the linear expansion coefficient of the depolymerisation rate and the motor concentration again for  $\Omega_2 \rho_{\max} = -\Omega_1$ ,  $\Omega_2 \rho_{\max} = -0.999\Omega_1$  and  $\Omega_2 \rho_{\max} = -0.995\Omega_1$ . We see that multiple solutions, and therefore dynamic instabilities, only occur if  $\Omega_1$  and thus subunit removal is large enough. As expected, the shaded area decreases for decreasing values of the nonlinear expansion coefficient and finally vanishes totally. At the same time, the area of coexistence is shifted towards higher motor concentrations. As dynamic instability is a result of two competing events, namely processive subunit removal and the hardcore

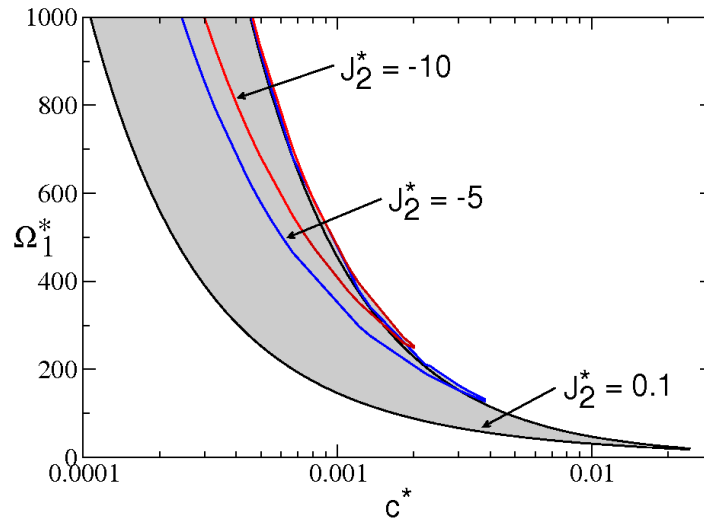


**Figure 3.12:** Regimes of multiple steady state solutions as a function of  $\Omega_1^* = (\Omega_1)/(\sqrt{D\omega_d})$  and  $c^* = (\omega_a c)/(\omega_d \rho_{\max})$  for different values of  $J_2^* = (J_2 \rho_{\max})/(\sqrt{D\omega_d}) = 0.1, -5, -10$ .  $J_1^* = (J_1)/(\sqrt{D\omega_d}) = -0.1$  and  $\Omega_2^* = -\Omega_1^* = -100$ . For each parameter set of the shaded area, two stable steady state solutions and one unstable solution exist.

exclusion of motors at the filament end, it is consistent, that for less processivity, higher motor concentrations are needed for the instability to occur.

In order to investigate the influence of  $J_2$  on the region of multiple solutions and therefore on the occurrence of the dynamic instability, we fix  $\Omega_2 \rho_{\max} = -\Omega_1$  and increase  $|J_2|$ . In Fig.3.12 the regions of coexisting solutions are shown for different values of  $J_2$ . Interactions between motors at the end are expected to be strongest in the case of  $J_2 \rho_{\max} = J_1$ , as the current of motors leaving the filament end after subunit removal is smallest for this parameter. Accordingly the area of coexistence is largest for this case and decreases for increasing  $|J_2|$ .

### 3.5. Summary

We have developed a generic theory of motor-induced filament depolymerisation. This description is valid irrespective of details of the mechanism of motor-induced subunit removal and of the structure of the depolymerising filament end. It is therefore not restricted to motors of the KIN-13 family which interact with microtubules but applies in general to associated proteins which regulate the dynamics of filament ends. Our phenomenological description reveals that motors can accumulate dynamically at the filament ends even if their binding affinity to the ends is not larger than in the bulk. In this process, motors which bind along the filament are subsequently captured by the retracting filament ends. We have shown that a positive effective processivity,  $p_{\text{eff}}$ , of subunit removal is essential to achieve dynamic accumulation of motors at the filament end. This effective processivity is a collective effect and results from steric exclusion of motors bound near the end.



---

## Microscopic mechanisms and fluctuations

In this chapter we present a discrete stochastic model for motor displacements along filaments. In order to obtain a picture of the microscopic events which influence the effective processivity as a result of crowding, we extend discrete stochastic models to capture subunit removal at the ends. Although providing a more detailed and physical picture of motor dynamics and cooperativity of motors bound at the end of a filament, this more microscopic description is still generic in the sense that specific details of the individual motor proteins or the filament are not included.

### 4.1. Lattice description of motor dynamics

In the following we will consider a semi-infinite lattice with equally spaced binding sites (with lattice constant  $a$ ), representing the filament. Binding sites will be indexed by  $i = 1, 2, 3, \dots \infty$ . Motor proteins are represented as identical particles, moving stochastically on the lattice. Each binding site can only be occupied by one single particle and its occupation number  $n_i$  is therefore either equal to zero (empty) or equal to one (occupied). Note that filaments like microtubules and actin filaments, which are composed of globular subunits, naturally exhibit such a lattice structure. In addition, "decoration" experiments with microtubules have shown that each tubulin dimer can only be occupied by one kinesin motor domain (Song and Mandelkow, 1993). Description of particle dynamics will be placed in a moving reference frame, such that site  $i = 1$  denotes the binding site at the filament end for all times.

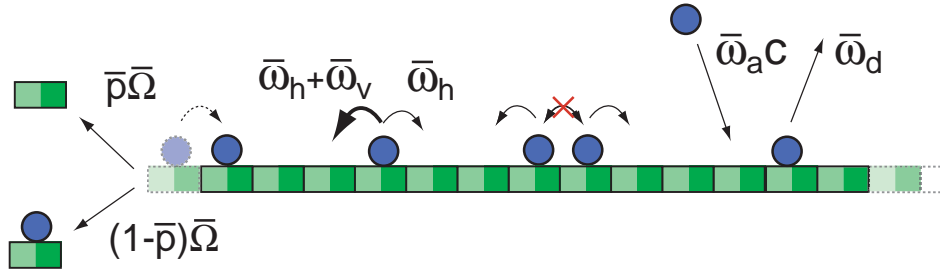


**Figure 4.1:** Schematic representation of a discrete description of motor-induced filament depolymerisation. Motors can occupy discrete lattice sites. Unbound motors occupy empty sites with rate  $\bar{\omega}_a c$ . They detach from the lattice with rate  $\bar{\omega}_d$  and hop to free neighbouring sites with rate  $\bar{\omega}_h$ . A biased motion can be incorporated by a higher hopping rate to one side of the lattice,  $\bar{\omega}_h + \bar{\omega}_v$  than to the other. At the filament end an occupied subunit is removed with rate  $\bar{\Omega}$ . The particle detaches from the filament with the removed subunit with probability  $1 - \bar{p}$ , while it stays bound to the new filament end with probability  $\bar{p}$ , if the adjacent site is empty.

#### 4.1.1. Microscopic interactions

An unoccupied site on the lattice can be filled with rate  $\bar{\omega}_a c$ . Here,  $c$  is the concentration of particles in the space surrounding the lattice, which can be seen as a reservoir of particles. We will assume a uniform distribution of particles in the reservoir and identical binding sites, leading to a space independent attachment rate. An occupied binding site can be freed with a rate  $\bar{\omega}_d$ . Particles that are bound to the lattice can hop stochastically to unoccupied adjacent sites with equal rate  $\bar{\omega}_h$ . Directed motion of motor proteins due to the underlying polarity of the filament, can be incorporated by introducing an additional rate,  $\bar{\omega}_v$ , with which motors hop in one direction, leading to  $\bar{\omega}_{h,l} = \bar{\omega}_h + \bar{\omega}_v$ .

At the filament end, attachment and detachment rates will in general be different from those in the bulk of the filament. Consequently we introduce separate attachment and detachment rates to the first binding site,  $i = 1$ , which we denote by  $\bar{\Omega}_a$  and  $\bar{\Omega}_d$  respectively. Additionally, if a particle is bound to the first binding site, it can remove the first subunit from the filament with rate  $\bar{\Omega}$ . In order to include processivity in the model, we have to distinguish between two different ways in which subunit removal can occur. First, a particle removing the first subunit can stay bound to the new filament end after subunit removal. We will denote the probability for this to occur with  $\bar{p}$ . Second, a particle can detach from the filament together with the removed subunit with probability  $1 - \bar{p}$ . Note that the processivity described above by the probability  $\bar{p}$  to remain attached after subunit removal is an intrinsic property of each single motor protein. It describes the catalytic subunit removal, if only one particle is present. In order to avoid confusion with the effective processivity, defined in Eq.(3.7), which describes collective processivity of many motors, we will denote  $\bar{p}$  as the microscopic processivity of motor proteins. If  $\bar{p} > 0$ , a single particle is processive and can repeatedly remove subunits from the end without falling off. This processive removal of subunits requires the simultaneous interaction of a motor with the end and the adjacent subunit. This process will thus be influenced by other particles bound near to the filament end. In particular, if site  $i = 2$  is occupied while the end subunit is removed, the new end site is already occupied and the particle cannot stay attached to the filament. In the following we will discuss two cases, showing different behaviour in the situation of crowding of particles

at the filament end.

#### 4.1.2. Influence of crowding

##### Collective effects influencing the depolymerisation rate - Model A

Here we consider the case, where motor proteins at the filament end,  $n_1 = 1$ , have to interact with the adjacent binding site,  $i = 2$ , prior to subunit removal in order to be able to work processively. This interaction will in general be obstructed by an occupied neighbouring binding site and a processive protein will, in this model, remain on the first subunit without cutting if the next subunit is occupied. The processivity of the particle stays unaltered in this case. Consequently, the probability per unit time to processively remove a subunit at the end is given in this model by  $\bar{p}\bar{\Omega}(1 - n_2)$ . Non-processive subunit removal is possible without interaction with neighbouring binding sites and will take place with probability  $(1 - \bar{p})\bar{\Omega}$ . This model, from now on referred to as model A, is thus characterised by

$$\begin{aligned}\bar{p}^A &= \bar{p} \quad , \\ \bar{\Omega}^A &= \bar{\Omega}(1 - \bar{p}n_2) \quad .\end{aligned}\tag{4.1}$$

Here,  $\bar{\Omega}^A$  is the total probability per unit time to remove a subunit from the filament end and  $\bar{p}^A$  is the collective microscopic processivity. Crowding at the end obviously obstructs cutting and reduces the rate of subunit removal (see Fig. 4.2).

##### Collective effects influencing the processivity - Model B

In the case considered here, processive subunit removal is possible without prior interactions with the adjacent binding site. Processive proteins at the first binding site will remove subunits and then immediately rebind to the new first binding site of the filament. In the case of the second binding site being occupied before subunit removal, the protein on the former first binding site will not be able to rebind to the new filament end after cutting. An occupied second binding site thus does not obstruct subunit removal, but rather reduces the processivity of proteins. Processive cutting happens in this situation, with probability  $\bar{p}\bar{\Omega}(1 - n_2)$ , and non-processive subunit removal takes place with probability  $(1 - \bar{p}(1 - n_2))\bar{\Omega}$ . Again, we can characterise this model, in the following called model B, by the total probability per unit time to remove a subunit from the filament end and the collective microscopic processivity:

$$\begin{aligned}\bar{p}^B &= \bar{p}(1 - n_2) \quad , \\ \bar{\Omega}^B &= \bar{\Omega} \quad .\end{aligned}\tag{4.2}$$

In contrast to model A, particles in this model will always remove a subunit with rate  $\bar{\Omega}$ , independent of the occupation of neighbouring sites. Due to the hardcore repulsion between particles, the only way for this to happen, is to reduce the processivity if neighbouring sites are occupied. Note, that for  $\bar{p} = 0$  or  $n_2 = 0$  both models coincide, as in this case no interaction between particles at the filament end will occur (see Fig. 4.2).

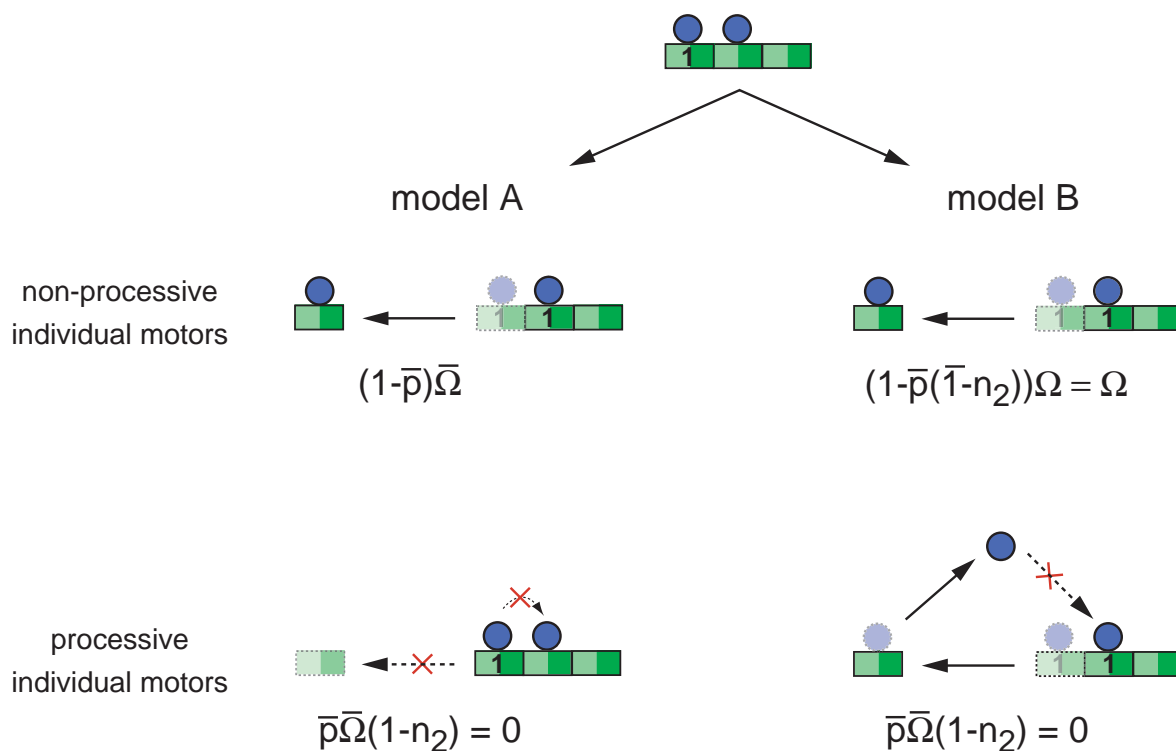


**Figure 4.2:** Schematic representation of two different scenarios of subunit removal in the case of particle crowding at the filament end, illustrated through occupation of the first two binding sites. **Model A:** Processive subunit removal requires interaction with the second binding site. This interaction will be hindered by a particle occupying the second site and as a consequence, subunit removal will be prevented,  $\bar{p}\bar{\Omega}(1-n_2) = 0$ . Non-processive subunit removal is not affected by an occupied second binding site and occurs with rate  $(1-\bar{p})\bar{\Omega}$ . The total rate of subunit removal in this model is therefore given by,  $\bar{\Omega}(1-\bar{p}n_2)$ , and depends on the occupation of the second binding site. **Model B:** Subunit removal occurs independently of the second binding site for non-processive as well as for processive removal. Processive particles rebind immediately after subunit removal to the new first binding site. While removal is independent of the second binding site, rebinding can only take place if the second binding site (the future first binding site) is unoccupied. If this is not the case particles cannot rebind and in spite of being individually processive, effectively non-processive subunit removal has been performed. The total rate of subunit removal is therefore given in this model by,  $\bar{\Omega}$ .

## 4.2. Master equation approach

The state of the lattice system at a given time is characterised by the configuration of particles on the lattice,  $\mathbf{n} = \{n_1, n_2, n_3, \dots\}$ . The time evolution of the probability,  $\mathbf{P}(\mathbf{n}, t)$ , to find a particular configuration  $\mathbf{n}$  of particles on the lattice at time  $t$  can be described by a master equation:

$$\partial_t \mathbf{P}(\mathbf{n}, t) = \sum_{\mathbf{n}' \neq \mathbf{n}} [\omega_{\mathbf{n}\mathbf{n}'} \mathbf{P}(\mathbf{n}', t) - \omega_{\mathbf{n}'\mathbf{n}} \mathbf{P}(\mathbf{n}, t)] \quad , \quad (4.3)$$

where  $\omega_{\mathbf{n}'\mathbf{n}} \geq 0$  is the transition rate from configuration  $\mathbf{n}$  to  $\mathbf{n}'$  (Van Kampen, 2001). Taking into account only the dynamic interactions introduced above and using that  $P(n_i) = \sum_{\substack{n_j=0,1 \\ j \neq i}} P(n_1, \dots, n_i, \dots)$ , we can write for the time evolution of the probability to find a particle at site  $i \geq 2$ :

$$\begin{aligned} \partial_t P(n_i) &= \bar{\omega}_h (P(n_{i-1} = 1, n_i = 0) + P(n_i = 0, n_{i+1} = 1) \\ &\quad - P(n_{i-1} = 0, n_i = 1) - P(n_i = 1, n_{i+1} = 0)) \\ &\quad - \bar{\omega}_v (P(n_i = 0, n_{i+1} = 1) - P(n_i = 1, n_{i-1} = 0)) \\ &\quad + \bar{p}\bar{\Omega} (P(n_1 = 1, n_2 = 0, n_{i+1} = 1) - P(n_1 = 1, n_2 = 0, n_i = 1)) \\ &\quad + (1 - \bar{p})\bar{\Omega} (P(n_1 = 1, n_{i+1} = 1) - P(n_1 = 1, n_i = 1)) \\ &\quad + \bar{\omega}_a P(n_i = 0) - \bar{\omega}_d P(n_i = 1) \quad , \end{aligned} \quad (4.4)$$

and at the first binding site,  $i = 1$ :

$$\begin{aligned} \partial_t P(n_1) &= \bar{\omega}_h (P(n_1 = 0, n_2 = 1) - P(n_1 = 1, n_2 = 0)) \\ &\quad + \bar{\omega}_v P(n_1 = 0, n_2 = 1) \\ &\quad + (1 - \bar{p})\bar{\Omega} (P(n_1 = 1, n_{i+1} = 1) - P(n_1 = 1, n_i = 1)) \\ &\quad + \bar{\Omega}_a P(n_i = 0) - \bar{\Omega}_d P(n_i = 1) \quad . \end{aligned} \quad (4.5)$$

Instead of using these master equations directly, we will in the following use average occupation numbers defined by,

$$\langle n_i \rangle = \sum_{n_i=0}^1 n_i P(n_i) = P(n_i = 1) \quad , \quad (4.6)$$

which are governed by the same dynamics as the probabilities  $P(n_i)$  (see Appendix for derivation). The time dependence of lattice occupation of an binding site  $i \geq 2$  is generally given by:

$$\frac{d}{dt} \langle n_i \rangle = \langle j_{i-1} \rangle - \langle j_i \rangle + \langle l_i \rangle \quad (4.7)$$

Here,  $\langle j_{i-1} \rangle$  and  $\langle j_i \rangle$  are the net currents of particles per unit time from binding site  $i - 1$  to binding site  $i$  and from site  $i$  to  $i + 1$  respectively. The term  $\langle l_i \rangle$  takes into account changes confined to binding site  $i$ . With the dynamic rules introduced in section 4.2, one can derive the following expression for the currents,

$$\begin{aligned} \langle j_i \rangle &= \bar{\omega}_h \langle n_i (1 - n_{i+1}) - n_{i+1} (1 - n_i) \rangle \\ &\quad - \bar{\omega}_v \langle n_{i+1} (1 - n_i) \rangle \\ &\quad - \langle \bar{\Omega}^{A,B} n_1 n_{i+1} \rangle \quad , \end{aligned} \quad (4.8)$$

where  $\langle j_{i-1} \rangle$  is given by replacing  $i \rightarrow (i-1)$  in the above expression. Here,  $\bar{\Omega}^{A,B}$ , is defined by Eq.(4.1) if model A is to be discussed, and by Eq.(4.2) in the case of model B. Interactions confined to the  $i$ th binding site read:

$$l_i = \bar{\omega}_a \langle 1 - n_i \rangle - \bar{\omega}_d \langle n_i \rangle . \quad (4.9)$$

The dynamics of particles in the bulk are thus completely described by:

$$\begin{aligned} \frac{d}{dt} \langle n_i \rangle &= \bar{\omega}_h (\langle n_{i+1} \rangle - 2 \langle n_i \rangle + \langle n_{i-1} \rangle) \\ &+ \bar{\omega}_v (\langle n_{i+1} (1 - n_i) \rangle - \langle n_i (1 - n_{i-1}) \rangle) \\ &+ \bar{\omega}_a c \langle 1 - n_i \rangle - \bar{\omega}_d \langle n_i \rangle \\ &+ \langle \bar{\Omega}^{A,B} n_1 (n_{i+1} - n_i) \rangle . \end{aligned} \quad (4.10)$$

Note, that the dynamic equation derived here by looking at particle currents is concordant with Eq.(B.6), which is derived directly from the master equation, Eq.(4.4).

The current between the first and the second binding site,  $\langle j_1 \rangle$ , is given by

$$\begin{aligned} \langle j_1 \rangle &= \bar{\omega}_h \langle n_1 (1 - n_2) - n_2 (1 - n_1) \rangle \\ &- \bar{\omega}_v \langle n_2 (1 - n_1) \rangle \\ &- (1 - \bar{p}) \bar{\Omega} \langle n_1 n_2 \rangle , \end{aligned} \quad (4.11)$$

and the local terms read,

$$l_1 = -(1 - \bar{p}) \bar{\Omega} \langle n_1 \rangle + \bar{\Omega}_a \langle 1 - n_1 \rangle - \bar{\Omega}_d \langle n_1 \rangle . \quad (4.12)$$

One can see, that only non-processive particles can contribute to the current between binding site 2 and 1. Therefore, Eq.(4.11) holds for both model A and model B, as these two models show different behaviours only in the case of collective processive subunit removal. In addition to the depolymerisation term in the current, we also have to take depolymerisation into account through a local term, stemming from the fact that non-processive depolymerisation can occur in both models, independently of the occupation of the adjacent binding site.

The complete description of particle dynamics at the first binding site is thus given by,

$$\begin{aligned} \frac{d}{dt} \langle n_1 \rangle &= -\langle j_1 \rangle + \langle l_1 \rangle \\ &= \bar{\omega}_h \langle n_2 - n_1 \rangle \\ &+ \bar{\omega}_v \langle n_2 - n_1 \rangle \\ &+ \bar{\Omega}_a c \langle 1 - n_1 \rangle - \bar{\Omega}_d \langle n_1 \rangle \\ &- (1 - \bar{p}) \bar{\Omega} \langle n_1 (1 - n_2) \rangle , \end{aligned} \quad (4.13)$$

which is in agreement with the dynamic equation, Eq.(B.8), derived from the master equation, Eq.(4.5).

### 4.3. Mean-field approximation

#### 4.3.1. Continuum limit and mean-field approximation

The dynamic behaviour of motor proteins on large length scales, compared to the lattice spacing  $a$ , can conveniently be described by a continuum approximation. Expecting, that

the lattice structure in this case does not affect our results in a crucial way, we introduce a continuous density of bound motors at a distance  $x \geq 0$  from the depolymerising filament end,  $\rho(x)$ , by defining:

$$\langle n_i \rangle = \int_{(i-1/2)a}^{(i+1/2)a} \rho(x) dx \approx a\rho(x) \quad . \quad (4.14)$$

Here we have assumed that the density of motors is homogenous over distances comparable to the discrete lattice constant  $a$ . In this approximation, we can write for the average occupation of site  $i \pm 1$

$$\langle n_{i\pm 1} \rangle = a\rho(x) \pm a^2 \frac{\partial \rho(x)}{\partial x} + \frac{a^3}{2} \frac{\partial^2 \rho(x)}{\partial x^2} \dots \quad . \quad (4.15)$$

Here, we generally expand up to first order, except in the cases where this is zero and we have to take into account the second order term.

In order to obtain an analytically tractable system we have to introduce another approximation. From Eq.(4.10) and (4.13), one sees that the time evolution of the average occupation of the  $i$ th site depends on two-point correlation functions like  $\langle n_i n_{i\pm 1} \rangle$ . One can without difficulty derive evolution equations for these correlation functions (Derrida and Evans, 1997), but sees, that these then depend on three-point correlations such as  $\langle n_i n_{i+1} n_{i+2} \rangle$ , which again depend on higher correlations. One therefore would have to solve all correlations simultaneously in order to solve the time evolution of  $n_i$  exactly. As this involves an infinite hierarchy of equations, the problem is generally unsolvable, except for relatively simple systems like for example the TASEP (totally asymmetric simple exclusion process) (Schuetz, 2001; Derrida and Evans, 1997). As our system is more complicated, we will introduce a mean field approximation to solve this problem. This approximation consists in the following replacement of two point correlation functions:

$$\langle n_i n_{i\pm 1} \rangle \approx \langle n_i \rangle \langle n_{i\pm 1} \rangle \quad . \quad (4.16)$$

In the discrete description of the preceding section, we derived two different relations for the dynamic description of particles in the bulk and on the first binding site. In the case of describing dynamics on length scale larger than the lattice spacing, the differentiation between individual binding sites is inconsistent. In order to be consistent, Eq.(4.10) must equal Eq.(4.13) in the case of  $i = 1$ . This requirement defines a boundary condition at  $x = 0$  for the continuum mean-field description, as we now have to define an average edge current,  $\langle j_0 \rangle$  in order for Eq.(4.10) to take the form of Eq.(4.13). From Eq.(4.8-4.9) and Eq.(4.11, 4.12) we find

$$\langle j_0^A \rangle = (\bar{\Omega}_a - \bar{\omega}_a)(1 - n_1) - (\bar{\Omega}_d - \bar{\omega}_d)\langle n_1 \rangle - (1 - \bar{p})\bar{\Omega}\langle n_1 \rangle \quad , \quad (4.17)$$

for model A, and

$$\langle j_0^B \rangle = (\bar{\Omega}_a - \bar{\omega}_a)\langle 1 - n_1 \rangle - (\bar{\Omega}_d - \bar{\omega}_d)\langle n_1 \rangle - (1 - \bar{p})\bar{\Omega}\langle n_1 \rangle - \bar{p}\bar{\Omega}\langle n_1 n_2 \rangle \quad , \quad (4.18)$$

for model B (see Fig.4.3 and 4.4).

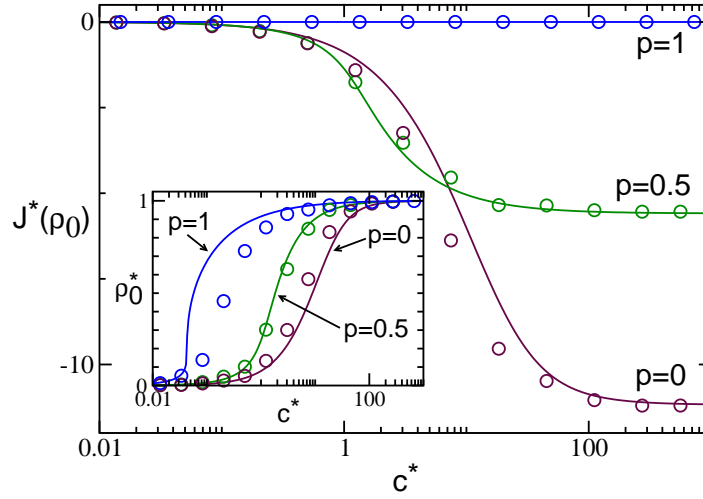


**Figure 4.3:** The edge current,  $J^*(\rho_0) = J/(\bar{\omega}_h \bar{\omega}_d)^{1/2}$ , as a function of the bulk motor concentration  $c^* = \bar{\omega}_a c / \bar{\omega}_d$  obtained in stochastic simulations of model A for different values of the processivity  $\bar{p} = 0, 0.5$  and 1 (symbols). For comparison the corresponding solutions of the phenomenological equations are displayed (lines). Inset: The motor density at the end  $\rho_0^* = \rho_0 / \rho_{\max}$  as a function of  $c^*$  for the same situations. Parameters are  $\bar{\omega}_a = \bar{\Omega}_a$ ,  $\bar{\omega}_d = \bar{\Omega}_d = 0.008 \bar{\omega}_h$  and  $\bar{\Omega} = \bar{\omega}_h$ .

Applying now the continuum limit of Eq.(4.14) and the mean-field approximation of Eq.(4.16) to Eq.(4.10) and Eq.(4.17, 4.18), we can derive the following equations,

$$\begin{aligned} \partial_t \rho &= a^2 \bar{\omega}_h \partial_x^2 \rho + (a \omega_v (1 - 2a\rho) + (a^2 \bar{\Omega} \rho_0 - a^3 \bar{p} \bar{\Omega} \rho_0^2)) \partial_x \rho \\ &\quad + \frac{\bar{\omega}_a c}{a} (1 - a\rho) - \bar{\omega}_d \rho \quad , \end{aligned} \quad (4.19)$$

$$J^A(\rho_0) = (\bar{\Omega}_a - \bar{\omega}_a) (1 - a\rho_0) - (\bar{\Omega}_d - \bar{\omega}_d) \rho_0 - (1 - \bar{p}) \bar{\Omega} \rho_0 \quad , \quad (4.20)$$

for model A, and

$$\begin{aligned} \partial_t \rho &= a^2 \bar{\omega}_h \partial_x^2 \rho + (a \omega_v (1 - 2a\rho) + (a^2 \bar{\Omega} \rho_0)) \partial_x \rho \\ &\quad + \frac{\bar{\omega}_a c}{a} (1 - a\rho) - \bar{\omega}_d \rho \quad , \end{aligned} \quad (4.21)$$

$$J^B(\rho_0) = (\bar{\Omega}_a - \bar{\omega}_a) (1 - a\rho_0) - (\bar{\Omega}_d - \bar{\omega}_d) \rho_0 - (1 - \bar{p}) \bar{\Omega} \rho_0 - \bar{p} \bar{\Omega} \rho_0^2 \quad , \quad (4.22)$$

for model B.

### 4.3.2. Connection to generic description

We can now introduce macroscopic parameters as in the generic description of chapter 3 where each macroscopic parameter is defined by the underlying microscopic interactions of model A or model B. For both models, we find the following relations for the diffusion coefficient, the average directed speed of a motor on the filament, the macroscopic attachment rate and

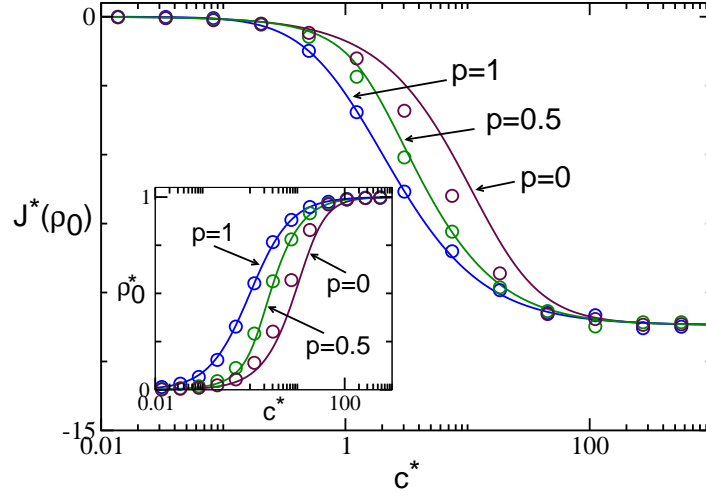


**Figure 4.4:** The edge current,  $J^*(\rho_0) = J/(\bar{\omega}_h \bar{\omega}_d)^{1/2}$ , as a function of the bulk motor concentration  $c^* = \bar{\omega}_a c / \bar{\omega}_d$  obtained in stochastic simulations of model B for different values of the processivity  $\bar{p} = 0, 0.5$  and 1 (symbols). For comparison the corresponding solutions of the phenomenological equations are displayed (lines). Inset: The motor density at the end  $\rho_0^* = \rho_0 / \rho_{\max}$  as a function of  $c^*$  for the same situations. Parameters are  $\bar{\omega}_a = \bar{\Omega}_a$ ,  $\bar{\omega}_d = \bar{\Omega}_d = 0.008 \bar{\omega}_h$  and  $\bar{\Omega} = \bar{\omega}_h$ .

the macroscopic detachment rate:

$$D = a^2 \bar{\omega}_h \quad , \quad (4.23)$$

$$v_0 = a \bar{\omega}_v \quad , \quad (4.24)$$

$$\omega_a c = \bar{\omega}_a c / a \quad , \quad (4.25)$$

$$\omega_d = \bar{\omega}_d \quad . \quad (4.26)$$

The maximal density of motors for which binding sites saturate is  $\rho_{\max} = 1/a$ <sup>1</sup>. The constant and linear expansion coefficients of the depolymerisation rate and the edge current are also the same for both models and are given by:

$$J_0 = \bar{\Omega}_a - \bar{\omega}_a \quad , \quad (4.27)$$

$$J_1 = -((\bar{\Omega}_a - \bar{\omega}_a) + (\bar{\Omega}_d - \bar{\omega}_d) + (1 - \bar{p})\bar{\Omega}) \quad , \quad (4.28)$$

$$\Omega_0 = 0 \quad , \quad (4.29)$$

$$\Omega_1 = a^2 \bar{\Omega} \quad . \quad (4.30)$$

One can see, that in the continuum description only the additional attachment rate to and detachment rate from the filament end appear. Therefore, if attachment and detachment rates to and from the filament end do not differ from the rest of the filament,  $J_0 = 0$  and  $J_1 = -(1 - \bar{p})\bar{\Omega}$ . The nonlinear coefficients which describe collective effects of motors at the filament end, are model dependent and are given in model A by:

$$J_2 = 0 \quad (4.31)$$

$$\Omega_2 = -a^3 \bar{p} \bar{\Omega} \quad , \quad (4.32)$$

<sup>1</sup>Note that the definition of the maximal density is in general  $\rho_{\max} = N/a$ , where  $N$  is the number of protofilaments.

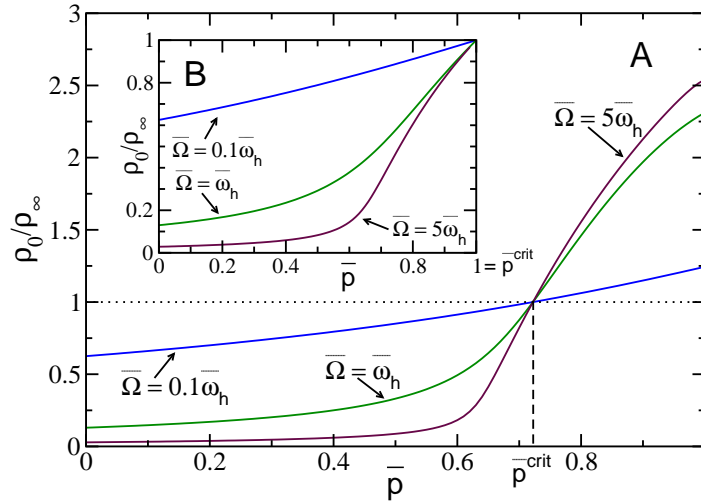


**Figure 4.5:** The accumulation of motors obtained in model A, characterised by the ratio  $\rho_0/\rho_\infty$  of motor density at the end and far from the end is shown as a function of the microscopic processivity  $\bar{p}$  for different values of the depolymerisation rate  $\bar{\Omega}$ . The critical value of the processivity for which accumulation occurs is emphasised. Inset: The same situations for model B. Parameters are  $\bar{\omega}_a c^* = \bar{\Omega}_a c^* = 0.005\bar{\omega}_h$ ,  $\bar{\omega}_d = \bar{\Omega}_d = 0.008\bar{\omega}_h$ .

and in model B by:

$$J_2 = -a^3 \bar{p} \bar{\Omega} \quad (4.33)$$

$$\Omega_2 = 0 \quad (4.34)$$

The above relations again clearly show the differences between model A and model B. In model A, the nonlinear coefficient of the current vanishes, demonstrating that crowding of motors at the filament end does not influence the number of motors leaving the filament. The processivity of motors is therefore unaltered by crowding in this model. The nonlinear coefficient of the depolymerisation rate is negative, thus reducing the rate of cutting if crowding occurs. In contrast, in model B, the depolymerisation rate is unaltered by crowding of motors at the end,  $\Omega_2 = 0$ , but the number of motors leaving the filament increases as crowding occurs, due to the negative value of  $J_2$ <sup>2</sup>. Thus, the processivity is reduced in this model. Inserting the macroscopic parameters defined in Eq.(4.23)-(4.34) into Eq.(4.19)-(4.22), we are able to recover exactly Eq.(3.9) from the generic description.

#### 4.4. Depolymerisation mechanisms influencing accumulation

Recovering the same equations as in the generic description by taking the continuum mean field limit of the discrete equations of model A and model B, allows us to apply the results of our discussion of the generic model to the mean field approximation of model A and model B. From the results obtained in section 3.3, we expect the differences in the depolymerisation mechanisms of model A and model B to have a crucial influence on the accumulation of

<sup>2</sup>The current is defined to be positive for motors attaching to the filament end from the surrounding solution and negative if particles detach from the end.

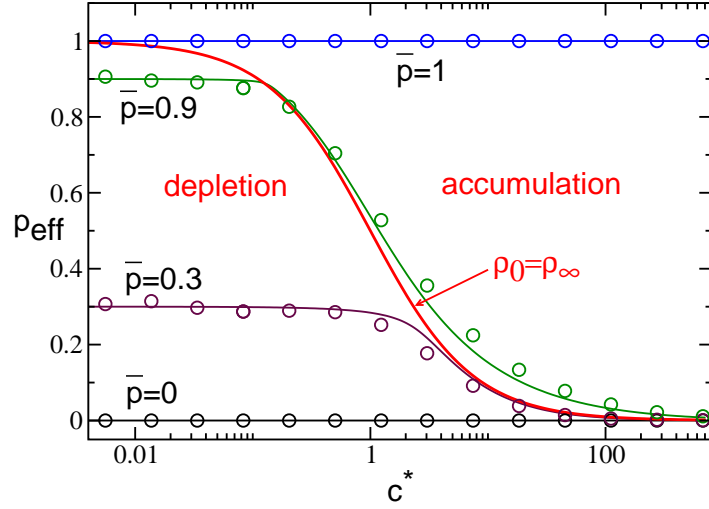


**Figure 4.6:** The effective processivity as a function of the bulk motor concentration  $c^* = \bar{\omega}_a c / \bar{\omega}_d$  obtained in simulations of model A for different values of the processivity  $\bar{p} = 0, 0.3, 0.9$  and  $1$  (symbols). For comparison the corresponding solutions of the phenomenological equations are displayed (lines). The red line symbolises the effective processivity necessary for a homogeneous motor distribution along the filament. Below this line depletion occurs, above accumulation. Parameter values are  $\bar{\omega}_a = \bar{\Omega}_a$ ,  $\bar{\omega}_d = \bar{\Omega}_d = 0.008\bar{\omega}_h$  and  $\bar{\Omega} = 2\bar{\omega}_h$ .

motor proteins at the filament end: while accumulation should be possible in model A, no accumulation should be observable in model B. In order to show this, we will in the following use Eq.(3.32), which defines the borderline between accumulation and depletion, and replace the expansion coefficients of the generic theory,  $\Omega_i$  and  $J_i$ , by their microscopic definitions, Eq.(4.27)-(4.34).

#### 4.4.1. Crowding hindering depolymerisation

The criterion for an homogenous motor distribution in model A reads:

$$-\bar{p}\bar{\Omega}\frac{\rho_\infty^3}{\rho_{\max}^3} + \bar{\Omega}\frac{\rho_\infty^2}{\rho_{\max}^2} - ((\bar{\Omega}_a - \bar{\omega}_a)c + (\bar{\Omega}_d - \bar{\omega}_d) + (1 - \bar{p})\bar{\Omega})\frac{\rho_\infty}{\rho_{\max}} + (\bar{\Omega}_a - \bar{\omega}_a)c = 0 \quad (4.35)$$

Here, we have used that for one protofilament  $\rho_{\max} = 1/a$  and  $\Omega_0 = 0$ . As we are interested in dynamic accumulation due to motor-induced depolymerisation, we will assume that the attachment and detachment rate to and from the end, do not differ from the rest of the filament and therefore  $J_0 = \bar{\Omega}_a - \bar{\omega}_a = 0$  and  $J_1 = -a(1 - \bar{p})\bar{\Omega}$ . The above equation then reduces to:

$$-\bar{p}\bar{\Omega}\frac{\rho_\infty^2}{\rho_{\max}^2} + \bar{\Omega}\frac{\rho_\infty}{\rho_{\max}} - (1 - \bar{p})\bar{\Omega} = 0 \quad (4.36)$$

From our generic analysis, we know that processivity plays a crucial role in accumulation. We can now define a critical microscopic processivity  $\bar{p}_{\text{crit}}$ , for which an homogenous distribution

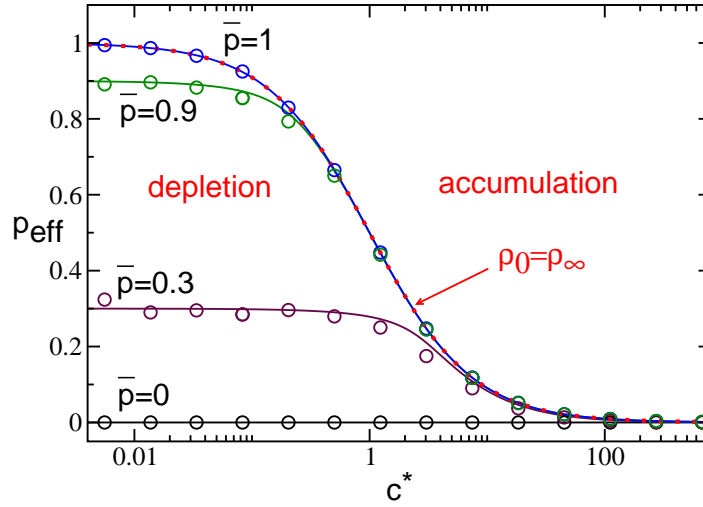


**Figure 4.7:** The effective processivity as a function of the bulk motor concentration  $c^* = \bar{\omega}_a c / \bar{\omega}_d$  obtained in simulations of model B for different values of the processivity  $\bar{p} = 0, 0.3, 0.9$  and  $1$  (symbols). For comparison the corresponding solutions of the phenomenological equations are displayed (lines). The red line symbolises the effective processivity necessary for a homogeneous motor distribution along the filament. Below this line depletion occurs, above accumulation. Parameter values are  $\bar{\omega}_a = \bar{\Omega}_a$ ,  $\bar{\omega}_d = \bar{\Omega}_d = 0.008\bar{\omega}_h$  and  $\bar{\Omega} = 2\bar{\omega}_h$ .

is reached on the filament. From the above equation we get,

$$\bar{p}_{\text{crit}}^A = \frac{1 - \frac{\rho_\infty}{\rho_{\text{max}}}}{1 - \frac{\rho_\infty^2}{\rho_{\text{max}}^2}} = \frac{\bar{\omega}_a c + \bar{\omega}_d}{2\bar{\omega}_a c + \bar{\omega}_d} \quad , \quad (4.37)$$

where we have used  $\rho_\infty = (\rho_{\text{max}}\bar{\omega}_a c) / (\bar{\omega}_a c + \bar{\omega}_d)$ . Surprisingly, the critical processivity does not depend on the depolymerisation rate  $\bar{\Omega}$ , but is solely determined by the attachment and detachment rate to and respectively from the filament<sup>3</sup> (see Fig.4.5) and varies from  $\bar{p}_{\text{crit}} = 1$  if  $\bar{\omega}_a c \rightarrow 0$  to  $\bar{p}_{\text{crit}} = 0.5$  if  $\bar{\omega}_a c \rightarrow \infty$ .

#### 4.4.2. Crowding reducing processivity

In model B we obtain the following criterion for an homogenous motor distribution from Eq.(3.32),

$$(\bar{\Omega} - \bar{p}\bar{\Omega}) \frac{\rho_\infty}{\rho_{\text{max}}} - (1 - \bar{p})\bar{\Omega} = 0 \quad , \quad (4.38)$$

where we have already used  $J_0 = 0$  and  $J_1 = -a(1 - \bar{p})\bar{\Omega}$ . The critical microscopic processivity thus reads in this model:

$$\bar{p}_{\text{crit}}^B = 1 \quad . \quad (4.39)$$

We therefore obtain an homogenous distribution, independent of depolymerisation rate and attachment or detachment rates, only for  $\bar{p} = 1$ . As  $\bar{p} = 1$  is also the maximal value possible,

<sup>3</sup>Note, that this is not the case if attachment and detachment rates at the filament edge differ from those to and respectively from the rest of the filament.

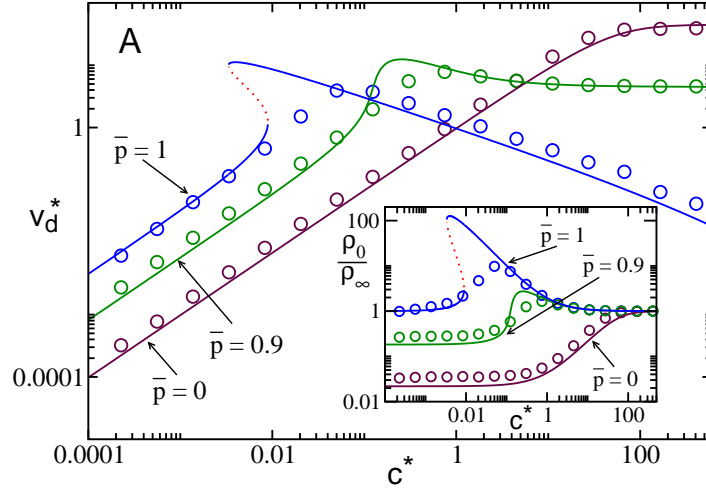


**Figure 4.8:** The velocity  $v_d^* = v_d/a(\bar{\omega}_h\bar{\omega}_d)^{1/2}$  of depolymerisation as a function of the bulk motor concentration  $c^* = \bar{\omega}_a c/\bar{\omega}_d$  obtained in simulations of model A for different values of the processivity  $\bar{p} = 0, 0.9$  and  $1$  (symbols). For comparison, the corresponding solutions of the phenomenological equations are displayed (lines). For  $\bar{p} = 1$  a dynamic instability occurs, where two stable states with different  $v_d$  coexist within a range of  $c^*$  values (red dotted line shows instable state). Inset: The accumulation of motors, characterised by the ratio  $\rho_0/\rho_\infty$  of motor density at the end and far from the end is shown as a function of  $c^*$  for the same situations. Parameter values are  $\bar{\omega}_a = \bar{\Omega}_a, \bar{\omega}_d = \bar{\Omega}_d = 0.008 \bar{\omega}_h$  and  $\bar{\Omega} = 4 \bar{\omega}_h$ .

no accumulation is possible within this model<sup>4</sup>.

With the value of  $\bar{p}_{\text{crit}}$  we have determined the microscopic processivity, i. e. the average processivity of each single motor protein, which is necessary to reach an homogeneous distribution on the filament. In order to investigate the way in which many proteins, that interact as in model A or B, behave collectively, we can see how the effective processivity, Eq.(3.7), evolves as a function of the bulk motor concentration. Replacing the macroscopic parameters by their microscopic definitions, we obtain:

$$p_{\text{eff}}^{\text{A}} = \frac{\bar{p}(\rho_{\text{max}} - \rho_0)}{\rho_{\text{max}} - \bar{p}\rho_0}, \quad (4.40)$$

$$p_{\text{eff}}^{\text{B}} = \bar{p} \left( 1 - \frac{\rho_0}{\rho_{\text{max}}} \right). \quad (4.41)$$

The behaviour is illustrated in Fig.4.6 and 4.7. The red line shows the effective processivity that is necessary for an homogeneous motor distribution on the filament as a function of the bulk motor concentration. For  $c \rightarrow 0$ , one obtains the average microscopic processivity,  $\bar{p}$ , of a single protein. Consistent with our results for the critical microscopic processivity, one sees that in model A (Fig.4.6), the effective processivity can become large enough for accumulation to occur (crossing the red borderline), if the microscopic processivity is large enough. In contrast, in model B (Fig.4.7), the effective processivity coincides exactly with the red borderline for the maximal value of the microscopic processivity,  $\bar{p} = 1$  and proceeds below it for lower microscopic processivities.

<sup>4</sup>Note that this holds only if  $J_0 = 0$ . If the affinity to the end is high, accumulation is also possible in model B.

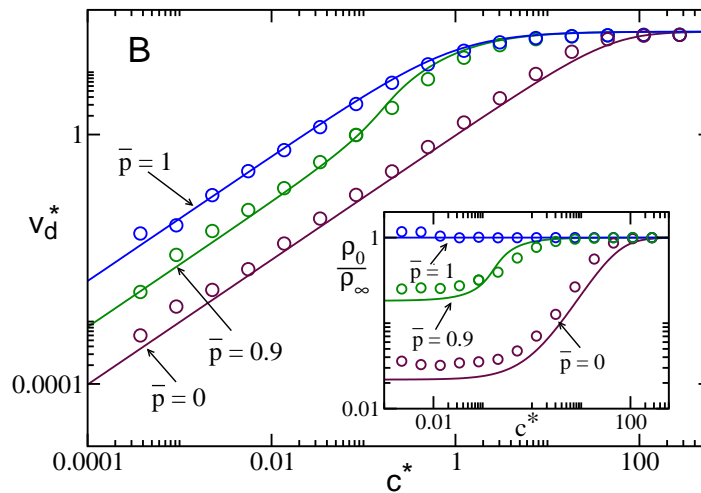


**Figure 4.9:** The velocity  $v_d^* = v_d/a(\bar{\omega}_h\bar{\omega}_d)^{1/2}$  of depolymerisation as a function of the bulk motor concentration  $c^* = \bar{\omega}_a c/\bar{\omega}_d$  obtained in simulations of model B for different values of the processivity  $\bar{p} = 0, 0.9$  and  $1$  (symbols). For comparison, the corresponding solutions of the phenomenological equations are displayed (lines). Inset: The accumulation of motors, characterised by the ratio  $\rho_0/\rho_\infty$  of motor density at the end and far from the end is shown as a function of  $c^*$  for the same situations. Parameter values are  $\bar{\omega}_a = \bar{\Omega}_a, \bar{\omega}_d = \bar{\Omega}_d = 0.008 \bar{\omega}_h$  and  $\bar{\Omega} = 4 \bar{\omega}_h$ .

## 4.5. Effects of fluctuations

In Fig.4.8 and 4.9 the depolymerisation velocity  $v_d$  obtained in mean-field theory corresponding to model A and model B respectively is displayed as a function of the bulk monomer concentration  $c$  for different values of the processivity  $\bar{p}$ . For comparison, results obtained from stochastic computer simulations are shown. In general, the velocity saturates at  $v_d(\rho_{\max})$  for large values of  $c$ , while it increases linearly for small  $c$ . We find that mean-field theory and stochastic simulations in general agree quantitatively. Note that we do not have to use effective parameters in the mean-field theory in order for this good agreement of stochastic simulations and mean-field theory to occur. As elucidated in chapter 3, a dynamic instability can be found for large enough values of  $\bar{p}$  in the mean-field approximation of model A. As this instability present in the mean-field theory (see Fig.4.8) is concealed in simulations by fluctuations, the vicinity of this dynamic instability is an exception to the generally good agreement, with results obtained in simulations and obtained in mean-field theory deviating from each other.

## 4.6. Summary

We have introduced a discrete stochastic model describing subunit removal by motor proteins. In this description a single protofilament was represented by an one-dimensional lattice. We focused on two different scenarios of subunit removal, model A and model B, providing a physical picture of the cooperativity and processivity of motors bound to the end of a single protofilament. In model A, interactions between motors crowding at the filament end lead to obstruction of subunit removal, while the processivity of motor proteins stays unaltered.

In model B, these interactions do not affect subunit removal, but influence the processivity of motors. In the case where motors do not have a higher binding affinity to the end than to the rest of the filament, dynamic accumulation at the end can only occur in model A, while subunit removal in model B leads to depletion of motors at the end. Applying a continuum mean-field approximation to the evolution equation of binding site occupation, we obtained differential equations and boundary conditions identical to expressions of the generic description in chapter 3. In the corresponding mean-field theory of model A a dynamic instability occurs for large enough processivities, an effect that is concealed due to fluctuations in stochastic simulations of the discrete description.



---

## Effects of multiple protofilaments

In this chapter we discuss how multiple protofilaments influence subunit removal and motor dynamics in general. For this, we extend the discrete stochastic description of chapter 4 to two dimensions and introduce additional motor-filament interactions, allowing motor proteins to interact also with adjacent protofilaments. In addition we discuss how the structure of the edge, formed by the ends of multiple protofilaments, evolves due to motor induced subunit removal.

### 5.1. Coupling of sublattices by motor dynamics

A microtubule consisting of  $Y$  protofilaments is represented by a lattice of  $Y$  one-dimensional semi-infinite sublattices. Adjacent sublattices are shifted with respect to each other by  $\delta \in [0, a[$  where  $a$  is the length of a site, corresponding to one subunit or tubulin dimer<sup>1</sup>. Sites along a sublattice are labeled by  $i = 1, 2, \dots$ , where for each protofilament or sublattice  $i = 1$  labels the leftmost site for all times. Sublattice 1 is adjacent to sublattice  $Y$ , reflecting the cylindrical structure of a microtubule (see Fig.5.1). The shift between these two sublattices is  $(Y - 1)\delta$ , which in general is not an integer multiple of  $\delta$  and thus forms a seam. The occupation number of a lattice site  $(i, j)$  with  $j = 1, \dots, Y$  is  $n_{i,j}$ , which is 0 for an empty site and 1 for an occupied site. Due to differences in subunit removal on different sublattices, neighbouring subunits on adjacent sublattices in general do not have coincident labelling and a particle moving to adjacent sublattices will thus not only change its  $y$ -coordinate,  $j \rightarrow j \pm 1$ , but in general also its  $x$ -coordinate,  $i \rightarrow l$ , (see Appendix for determination of  $l$ ).

Analogous to the discrete description of one protofilament in chapter 4, we introduce the following interactions of particles with one sublattice: bound particles can hop to unoccupied binding sites to the left and right with hopping rate  $\bar{\omega}_{h,x}$ . Biased motion can be incorporated by introducing an additional hopping rate towards one filament end,  $\bar{\omega}_v$ . Particles can attach to and detach from the filament with rates  $\bar{\omega}_a$  and  $\bar{\omega}_d$  respectively and again, we will treat

---

<sup>1</sup>In general this offset is around  $0.9nm$  (Howard, 2001).

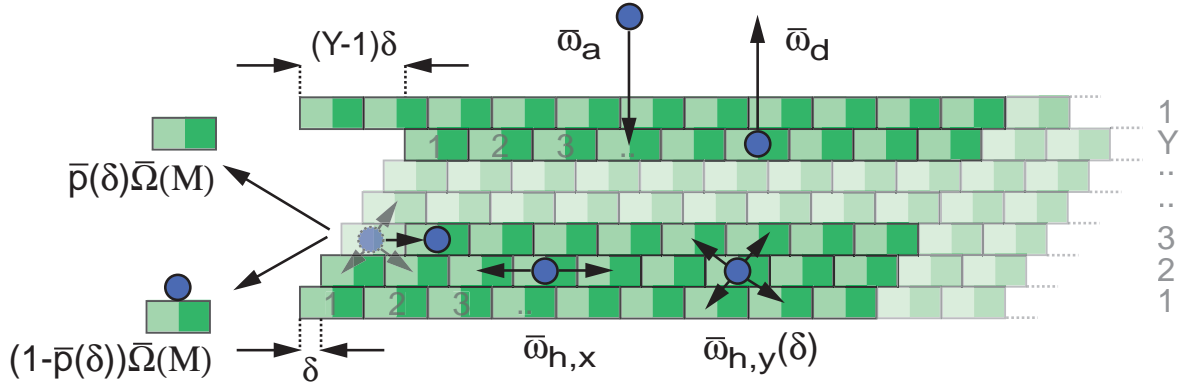


**Figure 5.1:** Illustration of the two-dimensional lattice model with  $Y$  protofilaments. Each protofilament, labelled  $j = 1, 2, 3, \dots, Y$ , has a semi-infinite linear geometry with regularly spaced binding sites  $i = 1, 2, 3, \dots$ . Adjacent protofilaments are shifted in respect to each other by a distance  $\delta$ . In order to resemble the cylindrical geometry of a microtubule, protofilaments are repeated periodically after  $Y$  protofilaments. The offset between each protofilament leads to a different shifting between the  $Y$ th and the 1st protofilament, depending on the offset  $\delta$  and the number of protofilaments,  $Y$ . Motor proteins, pictured as identical particles, can attach to and detach from the lattice with the rate  $\bar{\omega}_a$  and  $\bar{\omega}_d$  respectively. At the first binding site rates may differ and are denoted by  $\bar{\Omega}_a$  and  $\bar{\Omega}_d$ . Bound motors can hop in both directions on one protofilament with rate  $\bar{\omega}_{h,x}$  and can hop between binding sites on adjacent protofilaments with rate  $\bar{\omega}_{h,y}(\delta)$ , which depends on the distance between binding sites, and is therefore a function of the offset  $\delta$ . At the first binding site, motors can remove the first subunit with a rate  $\bar{\Omega}$ , either non-processively with probability  $(1 - \bar{p}(\delta))$  or processively with probability  $\bar{p}_y(\delta)$ . Processive motors can rebind, in addition to the protofilament,  $j$ , a subunit was removed from, also on the neighbouring protofilaments,  $j \pm 1$ . The probability of rebinding on adjacent protofilaments depends on the distance between the binding sites and is a function of the offset,  $\delta$ .

the first binding site separately and define extra attachment and detachment rates,  $\bar{\Omega}_a$  and  $\bar{\Omega}_d$ .

In addition to the above interactions of particles with one single sublattice, particles can also interact with adjacent sublattices: particles bound on a sublattice can hop on the two flanking sublattices with equal rate  $\bar{\omega}_{h,y} = \bar{\omega}_{h,j\pm 1}^l(\delta) + \bar{\omega}_{h,j\pm 1}^r(\delta)$ , where  $\bar{\omega}_{h,j\pm 1}^l(\delta)$  and  $\bar{\omega}_{h,j\pm 1}^r(\delta)$  are hopping rates to left and right neighbouring binding sites on the adjacent sublattices. Here we assume, that the hopping rate between binding sites on adjacent sublattices is influenced by the distance between them, which in general depends on the offset between sublattices,  $\delta$ . We presume a linear dependence on  $\delta$  and define the hopping rates from site  $(i, j)$  to left and right binding sites on the  $(j \pm 1)$ th sublattice in the following way:

$$\bar{\omega}_{h,j+1}^l = \bar{\omega}_{h,j-1}^r = \bar{\omega}_{h,y} \delta / a \quad , \quad (5.1)$$

$$\bar{\omega}_{h,j+1}^r = \bar{\omega}_{h,j-1}^l = \bar{\omega}_{h,y} (1 - \delta / a) \quad . \quad (5.2)$$

Here we have used, that due to the lattice symmetry hopping rates to upper and lower neighbouring sublattices have to be the same in diagonal direction. Note, that due to the different offset between the  $Y$ th and 1st sublattice, hopping rates between these two sublattices in general differ from those between other sublattices (see Fig. 5.2 and Appendix).

The removal of subunits can also be influenced by neighbouring sublattices. In the following we will assume, that the rate of subunit removal will decrease with the number of neighbouring subunits. Here we assume the depolymerisation rate to depend exponentially on the

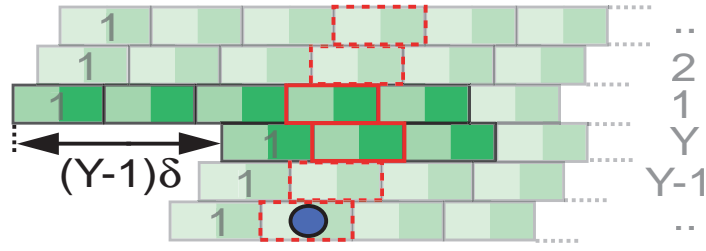


**Figure 5.2:** Illustration of the seam between the  $Y$ th and the 1st protofilament. The shift between adjacent protofilaments,  $\delta$ , and the periodic alignment of the protofilaments, will in general lead to an offset between the subunits of the  $Y$ th and the 1st protofilament that is different from the offset of subunits between the other protofilaments. This difference in the offset, breaks the symmetry of the lattice and is reflected in differences in the respective hopping rates between protofilaments. This symmetry-breaking can provoke directed motion of motors between protofilaments (see section 5.4). The shortest distances between binding sites provide a path which leads to higher hopping rates (emphasised by red borders).

number of neighbouring subunits,

$$\bar{\Omega}_j(M) = \bar{\Omega} e^{-\frac{\alpha M_j}{k_B T}} \quad . \quad (5.3)$$

where  $M_j$  is the number of neighbouring subunits of the first subunit of the  $j$ th protofilament and  $\alpha$  a parameter characterising the strength of the subunit-subunit interaction<sup>2</sup>.

In addition to effects on the depolymerisation rate, the processivity will also be influenced by the presence of neighbouring sublattices. Processive motor proteins can now not only rebind to the next binding site on the sublattice from which they removed a subunit with probability  $\bar{p}_x$ , but can alternatively rebind to binding sites on the adjacent sublattices with probability  $\bar{p}_y$ . The probability to rebind to binding sites on flanking sublattices will depend on the distance to these sites, determined by the offset between sublattices  $\delta$ . We define the probabilities for a particle to rebind to binding sites on adjacent sublattices by:

$$\bar{p}_{y,j+1}^l = \bar{p}_{y,j-1}^r = \frac{1}{2} \bar{p}_y \delta / a \quad , \quad (5.4)$$

$$\bar{p}_{y,j+1}^r = \bar{p}_{y,j-1}^l = \frac{1}{2} \bar{p}_y (1 - \delta / a) \quad . \quad (5.5)$$

where we have again used the symmetry of the lattice. Note that the probabilities of rebinding at the seam between the 1st and  $y$ th sublattices are in general different (see Appendix). The total probability to stay bound on the lattice after subunit removal is thus given by,

$$\begin{aligned} \bar{p} &= \bar{p}_x + \bar{p}_y \\ &= \bar{p}_x + \bar{p}_{y,j+1}^l + \bar{p}_{y,j+1}^r + \bar{p}_{y,j-1}^l + \bar{p}_{y,j-1}^r \quad . \end{aligned} \quad (5.6)$$

In chapter 4 we introduced two different kind of destabilising mechanisms. In model B subunit removal was independent of the second binding site on the filament, while in model A

<sup>2</sup>The rate of subunit removal could in principle not only depend on the number of neighbouring subunits, but also on the number of motor proteins at the end. Such cooperative effects between motor proteins, enhancing the rate of subunit removal can be incorporated here assuming  $\alpha$  to be a function of the number of occupied neighbouring binding sites.

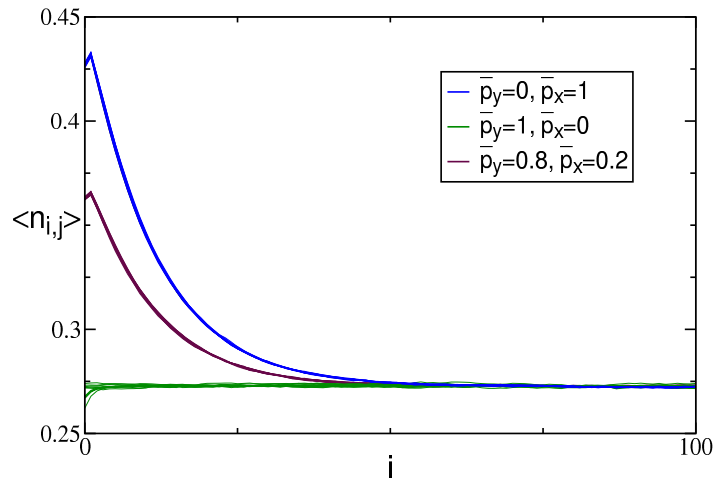


**Figure 5.3:** The average occupation  $\langle n_{i,j} \rangle$  as a function of the binding sites  $i$  for an alignment of 13 protofilaments in the case of strictly processive subunit removal, obtained in model A. Three different apportionments of the probability to stay bound to the filament after subunit removal,  $\bar{p}(\delta) = \bar{p}_x + \bar{p}_y(\delta) = 1$ , are shown:  $\bar{p}_x = 0$  and  $\bar{p}_y(\delta) = 1$ ,  $\bar{p}_x = 0.2$  and  $\bar{p}_y(\delta) = 0.8$ , and  $\bar{p}_x = 1$  and  $\bar{p}_y(\delta) = 0$ . Parameter values are:  $\bar{\omega}_{h,y}(\delta) = 0.5\bar{\omega}_{h,x}$ ,  $\bar{\omega}_{a,c} = \bar{\Omega}_{a,c} = 0.003\bar{\omega}_{h,x}$ ,  $\bar{\omega}_d = \bar{\Omega}_d = 0.008\bar{\omega}_{h,x}$ ,  $\bar{\Omega} = 4\bar{\omega}_{h,x}$ ,  $\delta/a = 0.2$  and  $\alpha = 1$

a free second binding site was necessary for subunit removal (see page 49). We can directly adopt both models for the case of multiple protofilaments, where now the interaction of motor proteins at the ends of protofilaments with each neighbouring binding site is subject to the rules of model A or model B.

Analogous to the case of one protofilament, we can describe the dynamics of motor proteins on the two-dimensional lattice, subject to the microscopic interactions described above, completely by a master equation. Due to the lengthy format of the explicit master equation, we refer the reader to the appendix, where the complete master equations can be found for model A and model B.

## 5.2. Effects on accumulation

We will start our discussion of the multi-protofilament model by looking at the conditions for accumulation of motors at the depolymerising filament end. It was already demonstrated in chapter 4, that the critical condition for accumulation on one individual protofilament is a sufficiently high processivity,  $\bar{p}$ . Due to the possibility of removing a subunit and rebinding to an adjacent protofilament, processive motors now have an additional degree of freedom when removing a subunit. In the following discussion we will thus concentrate on the interplay between the probability to stay attached to the sublattice a subunit was removed from,  $\bar{p}_x$ , and the probability to rebind on an adjacent sublattice, described by the inter-protofilament processivity,  $\bar{p}_y(\delta)$ . As also previously described, motors are able to accumulate only if the processivity is not altered by collective effects due to crowding of particles. This behaviour is described in model A and we will restrict the following analysis to this model.

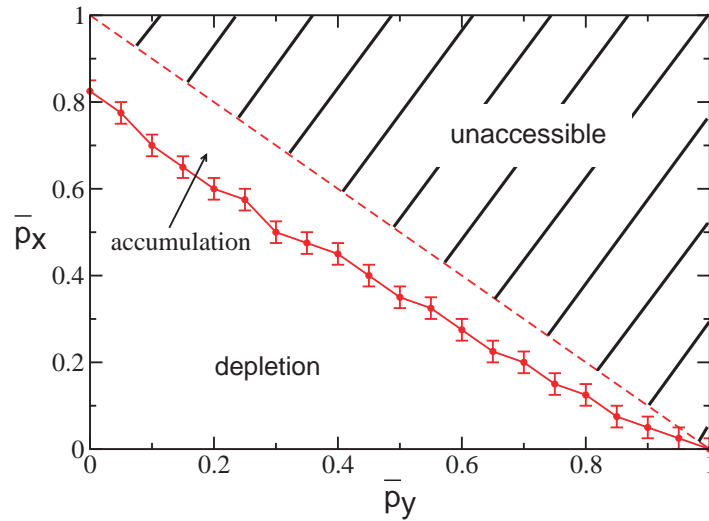


**Figure 5.4:** Regimes of accumulation and depletion as a function of the probability to stay attached to the protofilament a subunit was removed from,  $\bar{p}_x$ , and the probability to rebind on an adjacent protofilament,  $\bar{p}_y$ . The red borderline was obtained for an alignment of 13 protofilaments. The accessible regime is limited by the constraint  $\bar{p}_x + \bar{p}_y \leq 1$ , illustrated by the red dashed line. Along this line motors remove subunits processively. Parameter values are:  $\bar{\omega}_{h,y} = 0.5\bar{\omega}_{h,x}$ ,  $\bar{\omega}_{a,c} = \bar{\Omega}_a c = 0.003\bar{\omega}_{h,x}$ ,  $\bar{\omega}_d = \bar{\Omega}_d = 0.008\bar{\omega}_{h,x}$ ,  $\bar{\Omega} = 4\bar{\omega}_{h,x}$ ,  $\delta/a = 0.2$  and  $\alpha = 1.5$

### 5.2.1. Effects of inter-sublattice processivity

Let us discuss the case of strictly processive particles first. In this case,  $\bar{p}(\delta) = \bar{p}_x + \bar{p}_y(\delta) = 1$  and no motor will leave the lattice after subunit removal, but it can still interchange sublattices, depending on the ratio of  $\bar{p}_x$  and  $\bar{p}_y(\delta)$ . In Fig. 5.3 the average motor occupation of the  $i$ th-binding site of the  $j$ th sublattice is plotted as a function of the binding site  $i$  for three different ratios of the probability to rebind on the filament,  $\bar{p}(\delta) = 1$ . As expected from the discussion of individual protofilaments in chapter 4, one can observe strong accumulation at the filament end in the case of motors not interchanging sublattices,  $\bar{p}_x = 1$  and  $\bar{p}_y(\delta) = 0$ . Lowering the probability to stay attached to the sublattice from which a subunit was removed and increasing the probability to change sublattices proportionately, thus keeping the sum of both constant at unity, leads to a reduction of accumulation at the filament end. This reduction of accumulation can occur, because although motors do not leave the microtubule after subunit removal, they do leave the depolymerised sublattice and rebind to adjacent sublattices. Thus, this process resembles non-processive subunit removal on the sublattice a subunit was removed from and consequently reduces the motor density on this sublattice (just as already observed for an individual sublattice in chapter 4). The consequent rebinding of the motor protein on an adjacent sublattice resembles normal diffusion of particles between different sublattices and cannot therefore lead to accumulation on the respective sublattice. For the case where motors always rebind on adjacent sublattices,  $\bar{p}_x = 0$  and  $\bar{p}_y(\delta) = 1$ , the accumulation vanishes completely and we find sublattices with an homogeneous motor distribution and sublattices with depletion of motors at the filament end (see Fig. 5.3 green curves). This division is a result of the specific depolymerisation mechanism in model A: density fluctuations will provoke different depolymerisation velocities of the sublattices, leading

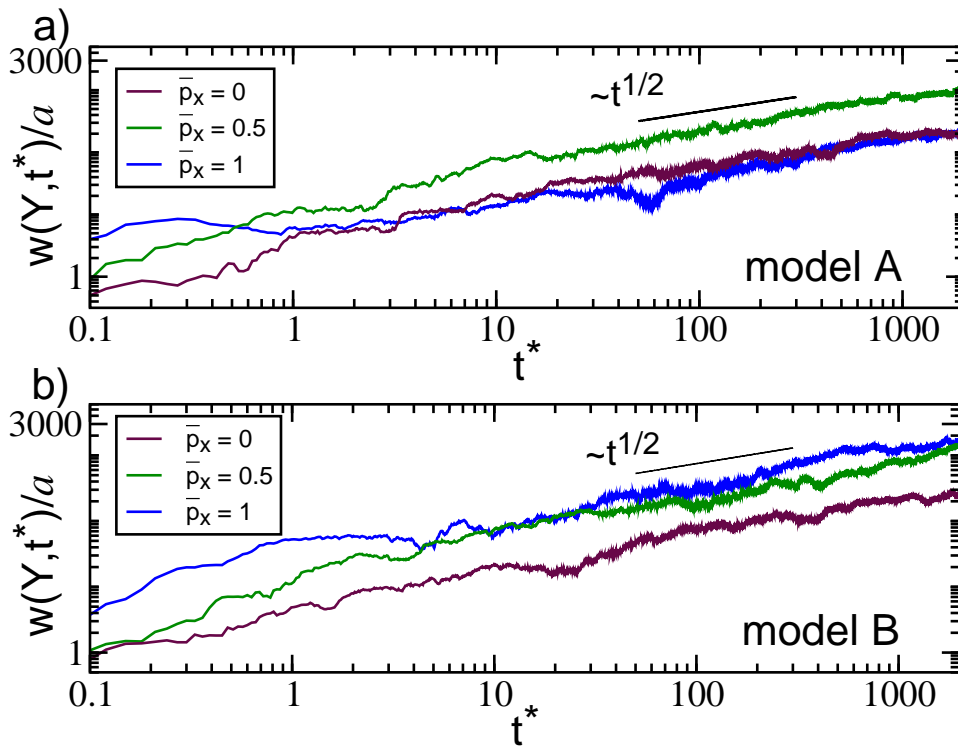


**Figure 5.5:** Time evolution of the edge width of an alignment of 12 uncoupled sublattices is shown as a function of time,  $t^* = t\bar{\omega}_d$ , for different values of the processivity  $\bar{p}_x = 1, 0.5$  and  $0$  for model A and model B. The scaling behaviour of the width is indicated by the black line. Parameter values are:  $\bar{p}_y = 0$ ,  $\bar{\omega}_{h,y}(\delta) = 0$ ,  $\bar{\omega}_a c = \bar{\Omega}_a c = 0.01\bar{\omega}_{h,x}$ ,  $\bar{\omega}_d = \bar{\Omega}_d = 0.008\bar{\omega}_{h,x}$ ,  $\bar{\Omega} = 4\bar{\omega}_{h,x}$ ,  $\delta/a = 0.5$  and  $\alpha = 0$

to protrusions of single sublattices. As soon as the edge of a sublattice protrudes by more than one subunit relative to the adjacent sublattices, depolymerisation of this sublattice will stop. This is due to the fact that in the case of  $\bar{p}_y(\delta) = 1$ , motors can only remove a subunit if a free binding site is in reach on one of the neighbouring sublattices. As soon as no subunit removal is taking place, motors will, because of diffusion, distribute equally along the protofilament leading to the observed homogeneous distribution on some sublattices. On the sublattice whose end subunit is neighbored by adjacent sublattices, the mechanism explained above leads to the observed depletion. The consequences of this different motor behaviour for the edge structure of the whole lattice will be addressed in the next section.

### 5.2.2. Regimes of accumulation

In the case of motor proteins removing subunits in a manner which is not strictly processive, we expect accumulation or depletion to depend on an interplay of the probability to stay on the protofilament a subunit was removed from,  $\bar{p}_x$ , and the probability to interchange protofilaments after subunit removal,  $\bar{p}_y(\delta)$ . This interplay is shown in Fig. 5.4, where the regimes of accumulation and depletion are shown as a function of the two probabilities,  $\bar{p}_x$ , and  $\bar{p}_y(\delta)$ . The accessible regime is limited by the constraint  $\bar{p} \leq 1$ , symbolised by the red dashed line. Along this line, strictly processive subunit removal is taking place, and below it non-processive depolymerisation is occurring.

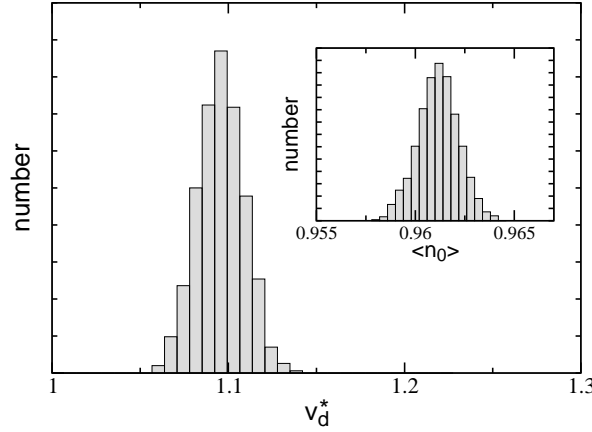


**Figure 5.6:** Histogram of the depolymerisation velocity,  $v_d^* = v_d/a(\bar{\omega}_{h,x}\bar{\omega}_d)^{1/2}$ , in model A in the case of uncoupled protofilaments. Inset: Histogram of the average occupation of the first binding site. Parameter values are:  $\bar{p}_x = 1$ ,  $\bar{p}_y = 0$ ,  $\bar{\omega}_{h,y}(\delta) = 0$ ,  $\bar{\omega}_{ac} = \bar{\Omega}_a c = 0.01\bar{\omega}_{h,x}$ ,  $\bar{\omega}_d = \bar{\Omega}_d = 0.008\bar{\omega}_{h,x}$ ,  $\bar{\Omega} = 4\bar{\omega}_{h,x}$ ,  $\delta/a = 0.5$  and  $\alpha = 0$

### 5.3. Edge structure of multiple sublattices

Next, we want to examine how different microscopic interactions, coupling adjacent protofilaments can affect the structure of the edge of the lattice, where depolymerisation is taking place. Starting with a smooth edge of a microtubule at the beginning of any motor-filament interactions (as illustrated in Fig. 5.1), subunit removal will, depending on motor dynamics and on the coupling of sublattices, influence the texture of this structure. We can imagine the depolymerisation process as an inverse growth process of an interface consisting of individual columns and therefore apply directly the concepts already known from surface growth models. We can define a mean distance by which a filament has been shortened at time  $t$  through subunit removal by

$$\bar{x}(t) \equiv \frac{1}{Y} \sum_{j=1}^Y x_j(t) \quad . \quad (5.7)$$

Here,  $Y$  is the total number of protofilaments and  $x_j(t)$  the length by which the  $j$ th sublattice has been shortened, which is given by the length of one subunit and the number of removed subunits at time  $t$ ,  $x_j(t) = a m_j(t)$ . With this, we can define the width of the edge characterising the roughness of it by (Barabasi and Stanley, 1995):

$$w(Y, t)^2 = \frac{1}{Y} \sum_{j=1}^Y (x_j(t) - \bar{x}(t))^2 \quad . \quad (5.8)$$

After reaching a steady-state density distribution of motors on the filament, we expect the width, depending on the details of subunit removal, either to increase as a power of time,

$$w(Y, t) \sim t^\beta \quad , \quad (5.9)$$

where  $\beta$  is called the *growth exponent*, or to saturate at a value  $w_{\text{sat}}$  (Barabasi and Stanley, 1995).

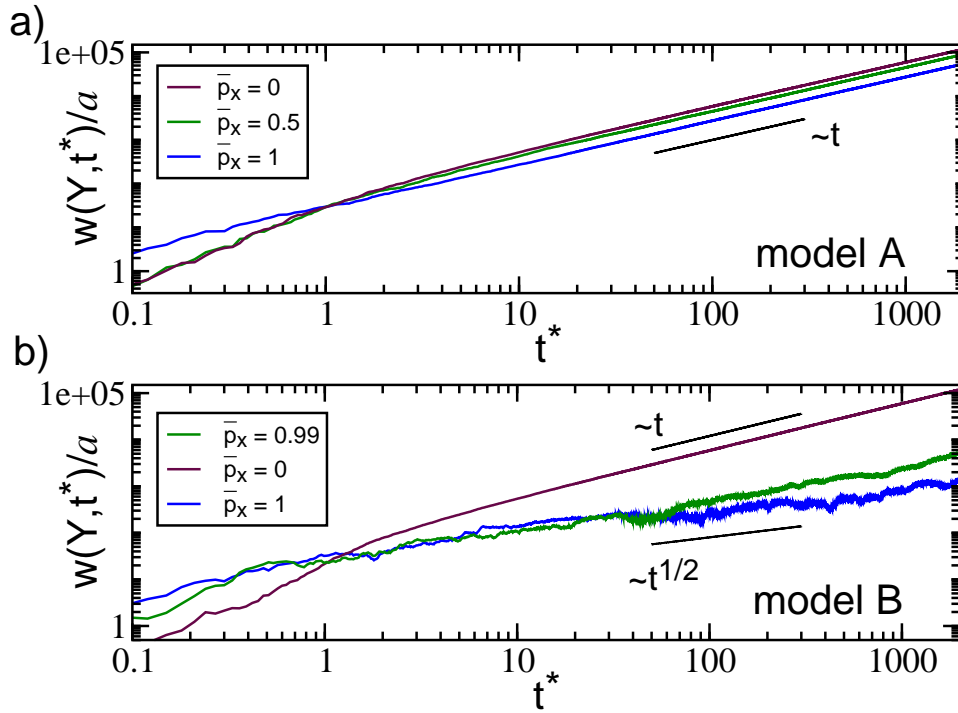


**Figure 5.7:** The width of the edge of an alignment consisting of 12 protofilaments, coupled only by interprotofilament diffusion, is shown as a function of time,  $t^* = t\bar{\omega}_d$ , for different values of the processivity,  $\bar{p}_x$ , in model A and model B. The growth exponent  $\beta$  is indicated (compare Eq.(5.9)). Parameter values are:  $\bar{p}_y = 0$ ,  $\bar{\omega}_{h,y}(\delta) = 0.5\bar{\omega}_{h,x}$ ,  $\bar{\omega}_a c = \bar{\Omega}_a c = 0.01\bar{\omega}_{h,x}$ ,  $\bar{\omega}_d = \bar{\Omega}_d = 0.008\bar{\omega}_{h,x}$ ,  $\bar{\Omega} = 4\bar{\omega}_{h,x}$ ,  $\delta/a = 0.5$  and  $\alpha = 0$ .

As a first step, we are interested in how the width of the microtubule edge is affected by subunit removal in time. We will distinguish between the influence of the diffusion between sublattices,  $\bar{\omega}_{h,y}$ , the strength of the sublattice coupling, described by the parameter  $\alpha$ , and the influence of the inter-protofilament processivity,  $\bar{p}_y(\delta)$  on the roughness of the edge. As collective effects, influencing subunit removal, will have a strong effect on the evolution of structure of the edge, we will distinguish henceforth between model A and model B (compare chapter 4, p. 49).

### 5.3.1. Uncoupled sublattices

We will begin by discussing the structure of the edge of the lattice for the case where motor dynamics on individual sublattices is unaffected by the presence of neighbouring sublattices. In this case, diffusion between sublattices,  $\bar{\omega}_{h,y}$ , the probability of rebinding to adjacent sublattices after subunit removal,  $\bar{p}_y$ , and coupling of adjacent subunits,  $\alpha$ , are equal to zero and one has  $Y$  individual sublattices, as described in chapter 4.

In Fig. 5.5 the width is displayed as a function of time for different values of the processivity,  $\bar{p}_x$ , obtained in model A and model B. One can see, that in both model A and model B the width is not saturating, but grows indefinitely with time. This behaviour is understandable, as saturation of growing interfaces is caused by correlations between the individual columns, which do not exist in the case considered here. Instead the average occupation of the first binding site on each sublattice,  $\langle n_{0,j} \rangle$ , and consequently the average depolymerisation velocity,

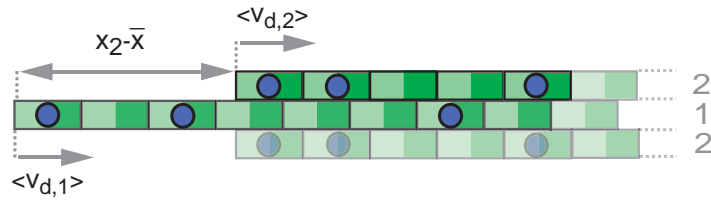


**Figure 5.8:** Illustration of two sublattices and the effect of different average depolymerisation velocities of each sublattice. One can define an effective velocity by,  $v_{\text{eff}} = \langle v_{d,2} \rangle - \langle v_{d,1} \rangle$ , leading to an average distance  $\langle x_{\text{eff}} \rangle$  between the ends of the sublattices. For an homogeneous motor distribution on each sublattice,  $\langle v_{d,2} \rangle = \langle v_{d,1} \rangle$ , and  $\langle x_{\text{eff}} \rangle = 0$ , thus the width of the edge is determined by fluctuations in subunit removal, leading in general to a growth of the width proportional to the square root of time. For different motor distributions on the sublattices, the width behaves in time according to  $w(Y, t)^2 \sim D_{\text{eff}} t + v_{\text{eff}}^2 t^2$ .

$\langle v_d \rangle$ , have to be the same on each sublattice (see Fig. 5.6).

Looking at how the growth of the width scales with time, we find growth exponents  $\beta \approx 0.5$  (see Fig. 5.5). As all sublattices show the same average depolymerisation velocity, the structure of the edge is determined by fluctuations of the subunit removal which can be described by an effective diffusion coefficient for the end of each sublattice. The behaviour of the width of uncoupled sublattices in time can therefore be written as

$$w(Y, t)^2 \sim D_{\text{eff}} t \quad . \quad (5.10)$$

This behaviour is in good accordance with standard growth models without correlations between the individual growing columns, for example in the random deposition model, where  $\beta = 0.5$  (see appendix).

### 5.3.2. Coupled sublattices

One possible way to couple sublattices by motor dynamics is to consider diffusion of motors perpendicular to the axes of the sublattices,  $\bar{\omega}_{h,y} \neq 0$ . Looking at how the width of the lattice edge is evolving in time with motors additionally diffusing between sublattices, one finds a major difference compared to uncoupled sublattices. In Fig. 5.7, the width is displayed for model A and model B as a function of time for different values of the processivity. Determining the growth parameter,  $\beta$ , one finds that the width of the lattice edge grows approximately linearly in time,  $\beta \approx 1$ , in model A (see Fig. 5.7 a)). In model B, strictly processive motors,  $\bar{p}_x = 1$ , cause an approximately square-root behaviour of the time evolution of the width,  $\beta \approx 0.5$ , like in the case of uncoupled sublattices. For non-processive subunit removal, the growth of the width scales approximately linear with time and one can observe a cross-over regime in the case of  $\bar{p}_x = 0.99$  from  $\beta \approx 0.5$  to  $\beta \approx 1$  (see Fig. 5.7 b)).

In order to understand how diffusion of motors among sublattices can influence the scaling behaviour of the width and why differences occur between model A and model B, we will, for clarity, look in the following discussion at the case of two aligned sublattices,  $Y = 2$ , (see Fig. 5.8).

After motor proteins have reached the end of each sublattice and subunit removal has started, fluctuations in the occupation of the first binding side will lead to slightly different depolymerisation velocities between the two sublattices. If this difference in the depolymerisation

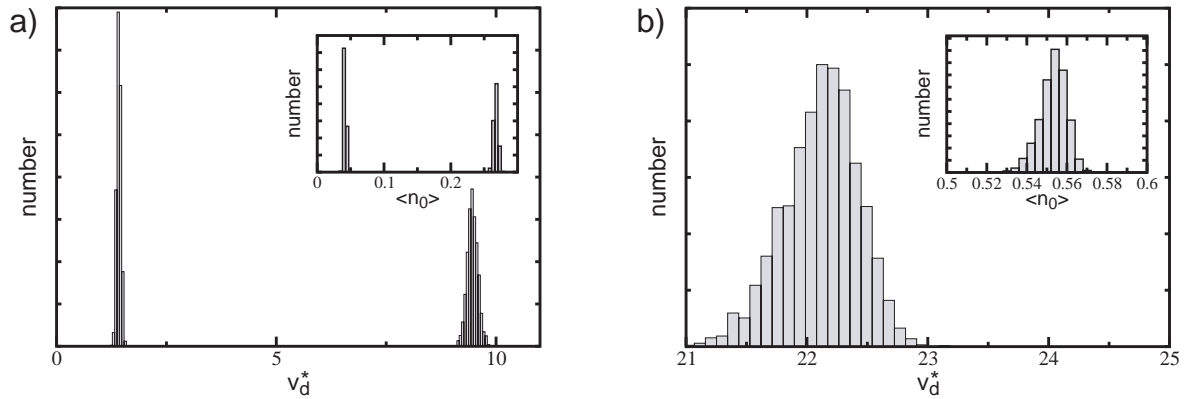


**Figure 5.9:** Comparison of histograms of the depolymerisation velocities and the occupation of the first binding side (insets) for the situation of linear growth of the width, **a)**, and for a square-root behaviour in time, **b)**. Histograms were obtained in model B with  $\bar{p}_x = 0$  in a) and  $\bar{p}_x = 1$  in b). Parameter values are:  $\bar{p}_y = 0$ ,  $\bar{\omega}_{h,y}(\delta) = 0$ ,  $\bar{\omega}_a c = \bar{\Omega}_a c = 0.01\bar{\omega}_{h,x}$ ,  $\bar{\omega}_d = \bar{\Omega}_d = 0.008\bar{\omega}_{h,x}$ ,  $\bar{\Omega} = 4\bar{\omega}_{h,x}$ ,  $\delta/a = 0.5$  and  $\alpha = 0$

velocity persists long enough, one of the sublattices' ends will start to protrude, leaving the end subunits of this sublattice isolated from the neighbouring sublattice (see Fig. 5.8). In this case, diffusion between sublattices cannot take place at the end subunits and motors will start to show the same dynamic behaviour at the protruding end as observed on uncoupled sublattices; depending on the value of the processivity,  $\bar{p}_x$ , motors start to accumulate or deplete at the end. If the protrusion is long enough, the motor density on this sublattice will either decay, in the case of accumulation at the end, or increase, in the case of depletion at the end, to the equilibrium bulk value  $\langle n_\infty \rangle$ , as in the case of an individual lattice.

Motors at the other end, which is still neighboured by bulk subunits of the adjacent sublattice, will also accumulate or deplete depending on  $\bar{p}_x$ . This will in general lead to a density gradient between these end subunits and the bulk subunits on the neighbouring sublattice. Diffusion between the sublattices will reduce such a gradient, therefore leading to less accumulation or depletion at the end which has fallen back, in comparison to the protruding end. This mechanism therefore leads to two distinct stationary motor distributions at the end of the two sublattices and consequently to two distinct depolymerisation velocities (see Fig. 5.9 a)). The structure of the end of the lattice is therefore no longer solely determined by fluctuations, as was the case for uncoupled sublattices, but we now have to take into account the effect of the different depolymerisation velocities. This difference allows the two ends to permanently drift apart, leading to the linear scaling behaviour of the width (see Fig. 5.10 a)). We can describe the behaviour of the width in these cases by,

$$w(Y, t)^2 \sim D_{\text{eff}}t + v_{\text{eff}}^2 t^2 \quad , \quad (5.11)$$

where the effective velocity,  $v_{\text{eff}}^2$ , is given by the difference between the average depolymerisation velocity,  $\bar{v}_d$ , and the fastest depolymerisation velocity of one of the sublattices.

With this, we can now also explain the observed differences between model A and model B in Fig. 5.7 and also the change from square-root to linear scaling in model B when the processivity is decreased. In order for distinct depolymerisation velocities to occur on the sublattices, motors either have to accumulate or deplete at the ends, as only in this case a

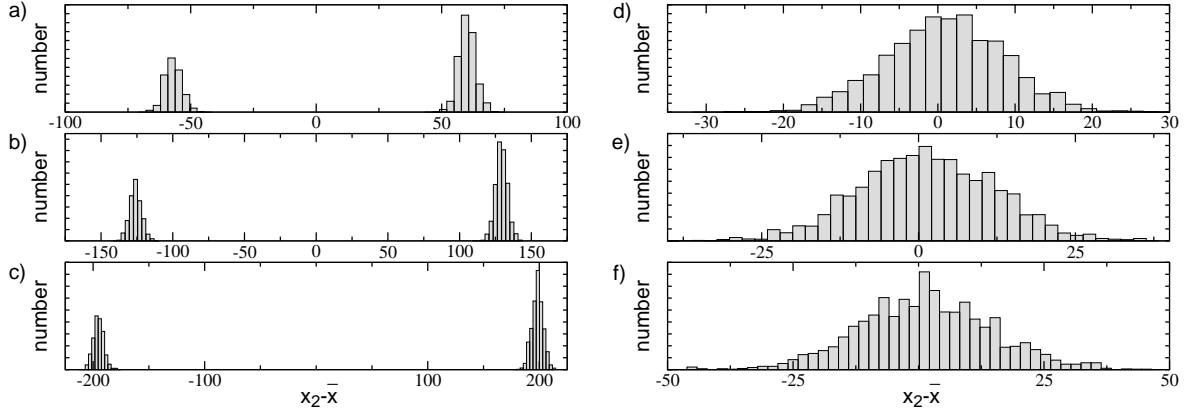


**Figure 5.10:** **a)-c)** Histograms of the difference  $x_2 - \bar{x}$  (compare Eq. (5.7)) in model B are shown for different times,  $t^* = t\bar{\omega}_d = 13(a)$ ,  $26(b)$  and  $40(c)$  in the case where the width grows linearly with time. Parameter values are:  $\bar{p}_x = 0$ ,  $\bar{p}_y = 0$ ,  $\bar{\omega}_{h,y}(\delta) = 0.5\bar{\omega}_{h,x}$ ,  $\bar{\omega}_a c = \bar{\Omega}_a c = 0.01\bar{\omega}_{h,x}$ ,  $\bar{\omega}_d = \bar{\Omega}_d = 0.008\bar{\omega}_{h,x}$ ,  $\bar{\Omega} = 4\bar{\omega}_{h,x}$ ,  $\delta/a = 0.5$  and  $\alpha = 0$ . For comparison, histograms of the difference  $x_2 - \bar{x}$  are shown, **d)-f)**, in the case where the width grows with the square-root of time. Parameter values are:  $\bar{p}_x = 1$ ,  $\bar{p}_y = 0$ ,  $\bar{\omega}_{h,y}(\delta) = 0.5\bar{\omega}_{h,x}$ ,  $\bar{\omega}_a c = \bar{\Omega}_a c = 0.01\bar{\omega}_{h,x}$ ,  $\bar{\omega}_d = \bar{\Omega}_d = 0.008\bar{\omega}_{h,x}$ ,  $\bar{\Omega} = 4\bar{\omega}_{h,x}$ ,  $\delta/a = 0.5$  and  $\alpha = 0$ .

density gradient can exist between the adjacent sublattices, leading ultimately to two stationary motor densities at the end of the sublattices. In model A, all three values of the processivity,  $\bar{p}_x$ , shown in Fig. 5.7 lead to either accumulation or depletion, consequently to different stationary depolymerisation velocities of the sublattices and therefore to the linear growth of the width. From the discussion in chapter 4 we know, that in model B subunit removal by motors always leads to depletion at the end of the lattice except for the case of  $\bar{p}_x = 1$ , where one finds an homogeneous motor distribution along the lattice. In this case the motor distribution is not affected if one sublattice protrudes due to fluctuations. Consequently all sublattices show the same average depolymerisation velocity (see Fig. 5.9) and therefore,  $v_{\text{eff}} = 0$ , leading to the observed square-root behaviour of the width (see Fig. 5.7 and Fig. 5.10). Note that the width can also show a square-root behaviour in model A, if  $\bar{p}_x = \bar{p}_{\text{crit}}$ , for which a homogeneous motor distribution occurs in model A (compare chapter 4). Reducing the processivity in model B even just slightly, leads to a linear behaviour because of the mechanism explained above. For values of the processivity,  $\bar{p}_x \approx 1$ , the effective velocity is going to be small, leading to a longer crossover-time,

$$t_{\text{cross}} = \frac{D_{\text{eff}}}{v_{\text{eff}}^2} . \quad (5.12)$$

This crossover can be observed in Fig. 5.7b) for  $\bar{p}_x = 0.99$ .

Note that the arguments given here for two sublattices also hold for multiple sublattices.

### Effects of inter-sublattice processivity

The behaviour of motor proteins at the end of sublattices, i. e. whether accumulation or depletion occurs, can also be influenced by the probability of rebinding on adjacent sublattices after subunit removal,  $\bar{p}_y$ . We therefore expect the growth of the width to show the same

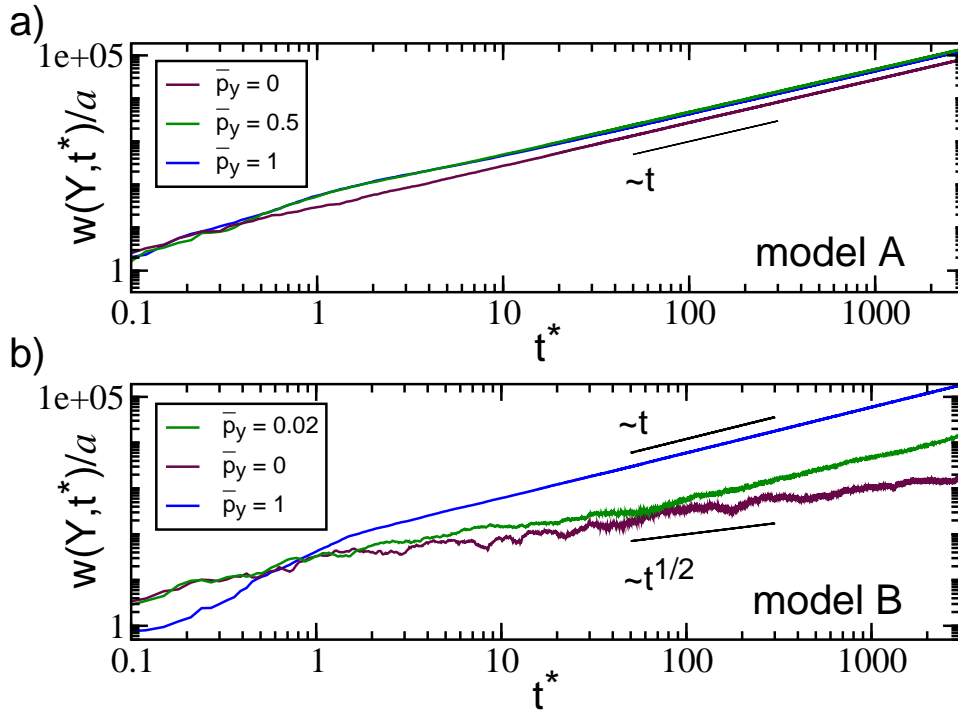


**Figure 5.11:** The width of the edge of an alignment consisting of 12 protofilaments is shown as a function of time,  $t^* = t\bar{\omega}_d$ , for two different values of the inter-protofilament processivity,  $\bar{p}_y$  for model A and model B. The growth exponent  $\beta$  is indicated (compare Eq.(5.9)). Parameter values are:  $\bar{p}_x = 1 - \bar{p}_y$ ,  $\bar{\omega}_{h,y}(\delta) = 0.5\bar{\omega}_{h,x}$ ,  $\bar{\omega}_{a,c} = \bar{\Omega}_{a,c} = 0.01\bar{\omega}_{h,x}$ ,  $\bar{\omega}_d = \bar{\Omega}_d = 0.008\bar{\omega}_{h,x}$ ,  $\bar{\Omega} = 4\bar{\omega}_{h,x}$ ,  $\delta/a = 0.5$ ,  $\alpha = 0$ .

behaviour for varying  $\bar{p}_y$  as for varying  $\bar{p}_x$ . In Fig. 5.11 the time evolution of the width is shown for different values of  $\bar{p}_y$  for model A and model B. As expected, we find in model A for all considered ratios of,  $\bar{p} = \bar{p}_x + \bar{p}_y = 1$ , a linear growth behaviour of the width, as in all three cases motors either accumulate or deplete at the ends. In model B we find that the growth exponent changes from  $\beta \approx 0.5$  in the case of  $\bar{p}_x = 1$  and  $\bar{p}_y = 0$ , where a homogeneous motor distribution occurs, to  $\beta \approx 1$  in the case of  $\bar{p}_y = 1$  and  $\bar{p}_x = 0$ , where motors deplete at the end. Again, one can observe a crossover in the case where only weak depletion at the ends occurs,  $\bar{p}_y = 0.02$  and  $\bar{p}_x = 0.08$ .

### Effects of subunit-subunit coupling

We have seen that sublattices coupled by motor dynamics can show a stronger fraying of the edge than in the case of uncoupled sublattices. These results were obtained for alignments of sublattices, with no binding between the different subunits of adjacent sublattices,  $\alpha = 0$ . We expect the fraying to decrease when introducing a coupling,  $\alpha \neq 0$ , between sublattices, as in this case the probability to remove an isolated end subunit is higher than to remove a subunit surrounded by subunits on adjacent sublattices (see Eq. 5.3), hindering the protrusion of individual sublattices. This effect can be seen in Fig. 5.12, where the time evolution of the width is shown in the case of processive subunit removal,  $\bar{p}_x = 1$ , in model A and model B. As expected, the growth of the width is reduced with increasing coupling, until finally the width saturates for even stronger coupling, in both models.

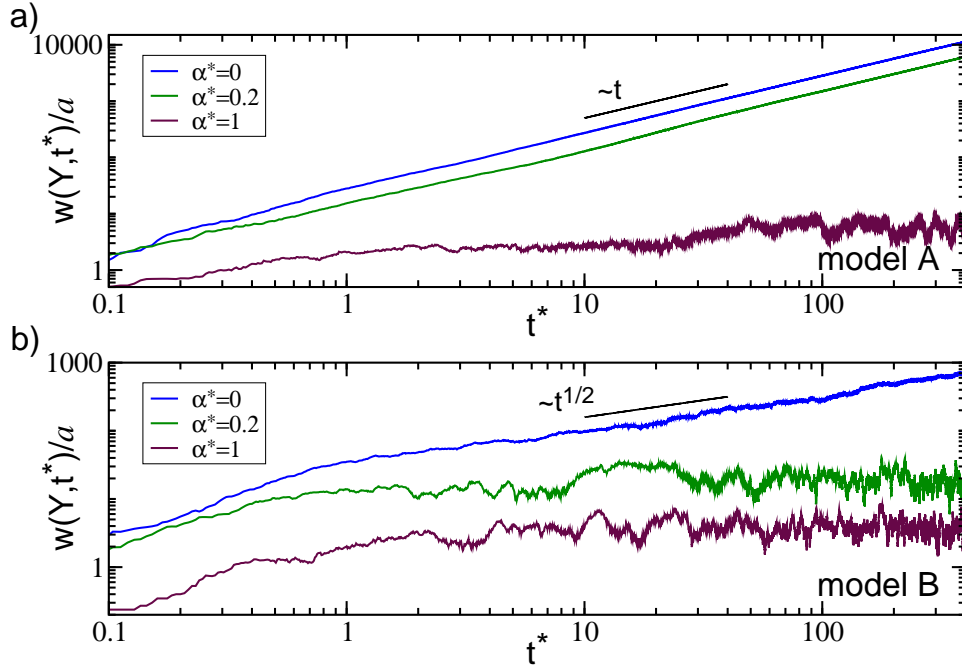


**Figure 5.12:** The width of the edge of an alignment consisting of 50 protofilaments is shown as a function of time,  $t^* = t\bar{\omega}_d$ , for three different values of the subunit-subunit coupling,  $\alpha^* = \alpha/k_B T = 0, 0.2$  and 1 of adjacent protofilaments for model A and model B. The growth exponent  $\beta$  is indicated (compare Eq.(5.9)). Parameter values are:  $\bar{p}_x = 1$ ,  $\bar{p}_y = 0$ ,  $\bar{\omega}_{h,y}(\delta) = 0.5\bar{\omega}_{h,x}$ ,  $\bar{\omega}_a c = \bar{\Omega}_a c = 0.01\bar{\omega}_{h,x}$ ,  $\bar{\omega}_d = \bar{\Omega}_d = 0.008\bar{\omega}_{h,x}$ ,  $\bar{\Omega} = 4\bar{\omega}_{h,x}$ ,  $\delta/a = 0.2$ .

## 5.4. Ring currents of motors

In section 2.5 we have seen that two conditions have to be fulfilled in order for motor proteins to perform directed motion on microtubules: spatial symmetry has to be broken and the system has to be out of equilibrium, e. g. detailed balance of transition rates between different states of the motor has to be violated. As elucidated earlier, the spatial symmetry in  $y$ -direction of the two dimensional lattice is generally broken at the seam between the first and the last protofilament of the alignment. In addition, detailed balance is broken, if subunit removal at the filament end is taking place. We therefore expect motor proteins to exhibit a current in  $y$ -direction, circular around the microtubule, if these two conditions are fulfilled.

The symmetry will be broken at the seam if the offset between the  $Y$ th and the 1st protofilaments differs from the offset between the rest of the protofilaments (see Fig. 5.2). Whether the offset at the seam is different, depends on the number of protofilaments and the original offset between protofilaments. The offset at the seam is given by:

$$\delta_{\text{seam}} = [(Y - 1)\delta + 1] - (Y - 1)\delta \quad , \quad (5.13)$$

where the Gauss brackets,  $[(Y - 1)\delta/a]$ , denote the largest integer less than or equal to  $(Y - 1)\delta/a$ .

Broken spatial symmetry leads to different hopping rates,  $\bar{\omega}_{h,y}(\delta)$ , between the  $Y$ th and the 1st protofilament than between other protofilaments (compare Eq. (5.1,5.2) and Eq. (C.10, C.11)). In addition, probabilities of rebinding on adjacent protofilaments,  $\bar{p}_y(\delta)$ , if a subunit

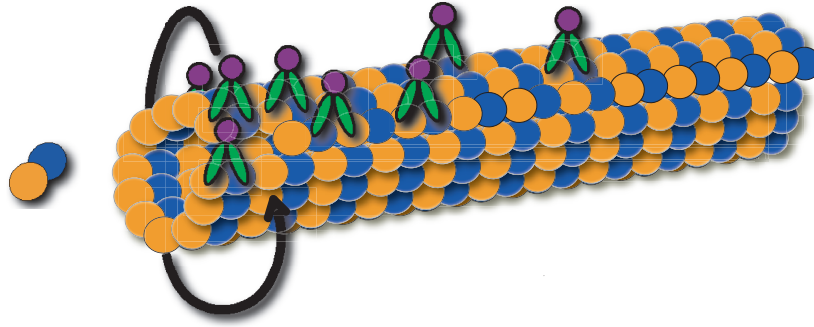


**Figure 5.13:** Illustration of motor current between protofilaments. The symmetry of the microtubule lattice can be broken at the seam of the  $Y$ th and the 1st protofilament. This broken symmetry induces a current of motor proteins around the microtubule, if in addition detailed balance is broken due to subunit removal. Whether the symmetry is broken at the seam depends on the number of protofilaments,  $Y$ , and the shift between each protofilament,  $\delta$ .

is removed from the  $Y$ th or the 1st protofilament are different than for subunit removal on other protofilaments (compare Eq. (5.4,5.5) and Eq. (C.12,C.13)).

The effect of this symmetry breaking, an induced current of motors in  $y$ -direction, can be seen in Fig. 5.14. Here, the current is shown for the case of an alignment of 13 protofilaments as a function of the offset,  $\delta$ , for non-processive subunit removal,  $\bar{p}_x = \bar{p}_y = 0$ , and processive subunit removal with  $\bar{p}_x = 1$ ,  $\bar{p}_y = 0$  and  $\bar{p}_x = 0.2$ ,  $\bar{p}_y = 0.8$ . We see that the current is most pronounced in the case of processive subunit removal with a high probability of motors rebinding on adjacent protofilaments,  $\bar{p}_y = 0.8$ . The magnitude of the current reduces in the case where motors rebind on the same protofilament a subunit was removed from and in the case of non-processive depolymerisation but is still clearly distinguishable from the case of no depolymerisation taking place,  $\bar{\Omega} = 0$ . The offset for which the current vanishes in all three cases,  $\delta/a \approx 0.46$ , leads to a symmetric lattice, where the offset between the  $Y$ th and the 1st protofilament is identical to the offset between the other protofilaments (compare Eq.(5.13).

## 5.5. Mean-field description with effective parameters

In section 4.3, we have demonstrated, how the discrete stochastic description of motor dynamics on one protofilament can be approximated by a continuous mean-field theory. This approximation was shown to be in very good agreement with the results obtained from simulations of the discrete stochastic model (see section 4.5). In this section we want to discuss to what degree we can use the continuous mean-field theory from chapter 4 to approximate the two-dimensional discrete stochastic description introduced in this chapter. For this purpose we introduce effective one-dimensional parameters, in order to mimic motor dynamics in two dimensions.

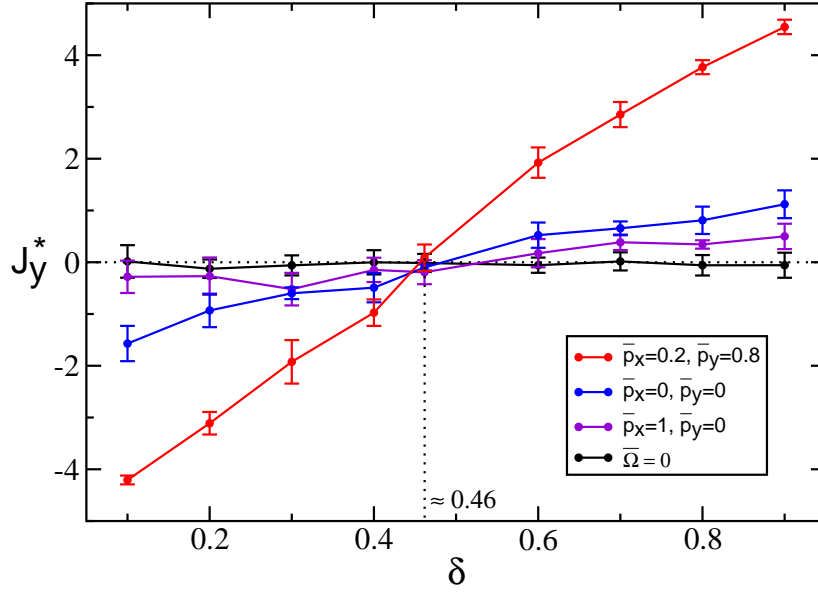


**Figure 5.14:** The ring current of motors,  $J_y^* = J_y/\bar{\omega}_d$  is shown as a function of the protofilament offset,  $\delta/a$ , for three different processivities,  $\bar{p}_x = 0.2, \bar{p}_y = 0.8$  (red dots),  $\bar{p}_x = 0, \bar{p}_y = 0$  (blue dots) and  $\bar{p}_x = 1, \bar{p}_y = 0$  (violet dots) and for diffusion without subunit removal,  $\bar{\Omega} = 0$  (black dots). Each dot symbolises the average value of five different simulations of motor dynamics on an alignment of 13 protofilaments in model A. Error bars symbolise standard deviation. Parameter values are:  $\bar{\omega}_{h,y}(\delta) = 0.5\bar{\omega}_{h,x}$ ,  $\bar{\omega}_{ac} = \bar{\Omega}_{ac} = 0.003\bar{\omega}_{h,x}$ ,  $\bar{\omega}_d = \bar{\Omega}_d = 0.008\bar{\omega}_{h,x}$ ,  $\bar{\Omega} = 8\bar{\omega}_{h,x}$ , and  $\alpha = 1$ .

### Average motor density of many protofilaments

In order to be able to compare the one-dimensional mean-field theory with the discrete stochastic simulation of  $Y$  protofilaments, we define average occupation numbers characterising the motor occupation on the protofilament alignment:

$$\langle n_{i+k_j} \rangle = \frac{1}{N_i} \sum_1^Y \langle n_{i+k_j,j} \rangle \quad , \quad (5.14)$$

with  $i = 1, 2, \dots$ , and  $k_j = m_j - \text{Min}\{m_j\}$  being the difference of removed subunits between the  $j$ th protofilament and the protofilament with the least removed subunits of all.  $N_i$  characterises the number of subunits on different protofilaments at the same position  $i$  (see Fig. 5.15). In the case of strong fraying, the combination of bulk subunits and end subunits, having in general distinct average motor occupations, will lead to a strong deviation from a smooth exponential density profile, due to the averaging procedure of Eq. 5.14. We thus expect the continuous mean-field approximation to be valid only if protrusions of individual protofilaments of the alignment do not differ by more than a few subunits. The characterisation of the two-dimensional discrete model with a one-dimensional continuous mean-field approximation is therefore limited to the cases where the width of the edge is saturating at small subunit values.



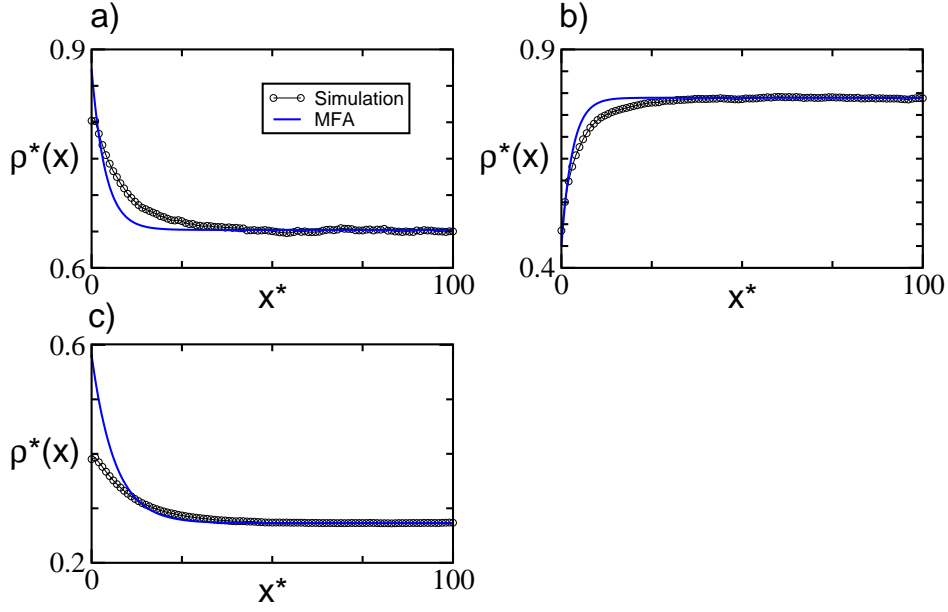


**Figure 5.16:** Comparison of density profiles obtained from simulation of motor dynamics on an alignment of 13 protofilaments (circles) and from a continuous one-dimensional mean-field approximation with effective parameters (blue line). **a)**  $\bar{p}_x = 1$ ,  $\bar{p}_y = 0$  and  $c^* = \bar{\omega}_a c = \bar{\Omega}_a c = 0.015\bar{\omega}_{h,x}$ . Rescaled parameters are:  $\bar{\Omega}^s = 0.08\bar{\Omega}$  with  $\bar{\Omega} = 4\bar{\omega}_{h,x}$  and  $\bar{\omega}_{h,x}^s = 0.47\bar{\omega}_{h,x}$ . **b)**  $\bar{p}_x = 0$ ,  $\bar{p}_y = 0$  and  $c^* = \bar{\omega}_a c = \bar{\Omega}_a c = 0.03\bar{\omega}_{h,x}$ . Rescaled parameters are:  $\bar{\Omega}^s = 0.09\bar{\Omega}$  with  $\bar{\Omega} = 8\bar{\omega}_{h,x}$  and  $\bar{\omega}_{h,x}^s = 2.03\bar{\omega}_{h,x}$ . **c)**  $\bar{p}_x = 0.5$ ,  $\bar{p}_y = 0.5$  and  $c^* = \bar{\omega}_a c = \bar{\Omega}_a c = 0.003\bar{\omega}_{h,x}$ . Rescaled parameters are:  $\bar{\Omega}^s = 0.09\bar{\Omega}$  with  $\bar{\Omega} = 4\bar{\omega}_{h,x}$  and  $\bar{\omega}_{h,x}^s = 0.14\bar{\omega}_{h,x}$ . Parameters in all three cases are:  $\bar{\omega}_{h,y} = 0.5\bar{\omega}_{h,x}$ ,  $\bar{\omega}_d = \bar{\Omega}_d = 0.008\bar{\omega}_{h,x}$ ,  $\delta/a = 0.2$ ,  $\alpha = 1$ .

rescaling of the depolymerisation rate is only due to the subunit-subunit binding, leading to a variation of subunit removal rate in dependence of the number of neighbouring subunits (see Eq. (5.3), in the simulation). The rescaled depolymerisation rate in the mean-field approximation is thus an average of the variable values of the depolymerisation rate in the simulation. For non-processive motors,  $\bar{p}_x = \bar{p}_y = 0$  (Fig. 5.16 b)), results from the mean-field approximation are in even better agreement with results obtained from simulations, than in the case of processive motors. This is understandable, as in the case of non-processive motors, collective effects between motors on the first and the second binding site do not play any role. These interactions between two single binding sites are not captured very well by a continuous mean-field approximation, leading to stronger deviations in the case of processive motors, where these interactions play a crucial role.

In Fig. 5.16 c), the case of processive motors with equal probabilities of rebinding on adjacent or the same protofilament,  $\bar{p}_x = 0.5, \bar{p}_y = 0.5$  is shown. Here, we can observe a strong deviation between the motor density at the edge obtained in mean-field theory and simulation. As explained in section 5.2, subunit removal and rebinding on adjacent protofilaments leads to a diminishing of accumulation. This effect cannot be captured by the one-dimensional mean-field approximation, where one can only distinguish between processive or non-processive subunit removal, and not between rebinding on the same or adjacent protofilaments.

## 5.6. Summary

We introduced a two-dimensional discrete description of motor-induced subunit removal. With this description we were able to investigate how multiple protofilaments influence motor dynamics and subunit removal on a filament. Rebinding to adjacent protofilaments after subunit removal was found to be disadvantageous for accumulation of motors at the filament end, in spite of motors not leaving the filament. We described filament depolymerisation as an inverse growth process of an interface and discussed the evolution of the filament end structure as a function of different motor-filament interactions. We showed that diffusion of particles between different protofilaments can change the scaling behaviour of the width and lead to a faster fraying of the edge than in the case of uncoupled protofilaments. We found that the offset between individual protofilaments leads in general to an asymmetric lattice, which in combination with the violation of detailed balance due to subunit removal leads to a ring current of motors around the filament. Finally we were able to approximate the two-dimensional discrete description with the generic one-dimensional mean-field description, introduced in chapter 4, where we used rescaled parameters in order to mimic the two-dimensional dynamics.

---

## Motor induced filament depolymerisation under applied forces

In the preceding chapters we developed and discussed a theory of filament depolymerisation induced by motor proteins which are free to move along filaments and in the surrounding space. In this chapter we will now investigate how filament depolymerisation is influenced if the inducing motor proteins are not free to move in space, but are attached via elastic linkers to a rigid object, for example a bead in an experiment, or chromosomes in a living cell. Due to the elastic linkers, external forces can be exerted on the motor proteins, influencing dynamics and subunit removal.

### 6.1. Generic description

In accordance with the formalism developed in chapter 3, we will consider one filament end and use a semi-infinite, one-dimensional geometry. We will describe motor dynamics and motion of the bead in a moving reference frame in which the depolymerising filament end is at rest for all times. Motor positions on the filament are therefore characterised by the coordinate  $x \geq 0$ . Motor proteins are fixed via elastic linkers of stiffness  $k$  to the bead and we denote the anchoring point of the linkers on the bead with  $x_B$ <sup>1</sup>. The external force acting on the bead is denoted  $f_{\text{ext}}$ . In contrast to the situation where filaments are surrounded by solution, serving as a protein reservoir with protein concentration  $c$ , a conserved number of motor proteins is now irreversibly fixed to the bead. Denoting the density of bound and unbound motor proteins along the filament as  $\rho_b$  and  $\rho_u$  respectively, the total number of proteins,  $N$ , is given by:

$$N = \int (\rho_b + \rho_u) dx \quad . \quad (6.1)$$

---

<sup>1</sup>In the following we will for simplicity assume that all linkers are anchored at the same point on the bead, and that the position of the anchoring point  $x_B$  is identical to the centre of the bead.

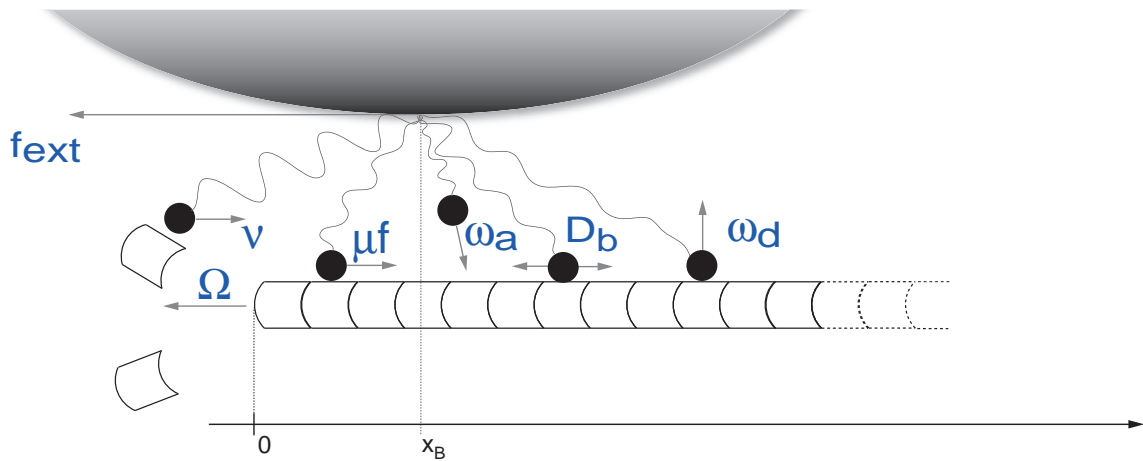


**Figure 6.1:** Illustration of the dynamic processes of motor proteins fixed with elastic linkers to a bead and interacting with a filament. Motors can attach to the filament with a rate  $\omega_a$  and bound motors can detach from it with rate  $\omega_d$ . On the filament motors can diffuse, characterised by the diffusion coefficient  $D_b$ . Forces can be exerted via the elastic linkers on the motor proteins leading to a gliding motion on the filament with velocity  $\mu f(x, x_B)$ . Motors bound at the filament end can induce subunit removal with rate  $\Omega$ . Unbound motors are pulled back into an equilibrium position with rate  $\nu$ .

### 6.1.1. Collective effects of bound motors

Motors bound to the filament can detach from it at a rate, dependent on the force exerted on the proteins by the linkers,  $f(x, x_B) = -k(x - x_B)$ . Following experiments, measuring the distance covered by motor proteins as a function of the applied load (Schnitzer et al., 2000), and in accordance with the rate theory formulated by Kramers (Kramers, 1940), the detachment rate is given by:

$$\omega_d(x, x_B) = \omega_d^0 e^{-\frac{k\epsilon |x - x_B|}{2k_B T}}. \quad (6.2)$$

where  $k_B T$  is the thermal energy and the distance  $\epsilon$  characterises the depth of the binding potential of proteins and the filament<sup>2</sup>. In the absence of any forces, the detachment rate of a single motor protein is given by,  $\omega_d^0$ . This rate can differ at the depolymerising filament end from the value on the filament and is denoted  $\Omega_d^0$ . The attachment rate of unbound motors to the filament, taken to be force- and space-independent, is given by  $\omega_a$  and by  $\Omega_a$  at the filament end.

Bound motors can exhibit directed motion along the filament towards the end,  $v_m$ . This motion will be influenced by the forces exerted on the proteins via the elastic linkers. The magnitude of the exerted force depends on the extension of the individual springs and therefore depends on the difference of the position of the bead on the lattice,  $x_B/a$ , and the position of the respective motor protein on the lattice,  $i$ . The force is always directed such that motor proteins slide towards the position of the bead. It is therefore positive for  $(i - x_B/a) < 0$  and negative for  $(i - x_B/a) > 0$ . Following again experiments indicating that the velocity of a motor decreases linearly with the exerted force opposing motor movement (Svoboda and Block, 1994; Hunt et al., 1994; Visscher et al., 1999), we will use the following force-velocity

<sup>2</sup>For normal kinesin motors, this length is approximately 1 – 2 nm (Schnitzer et al., 2000).

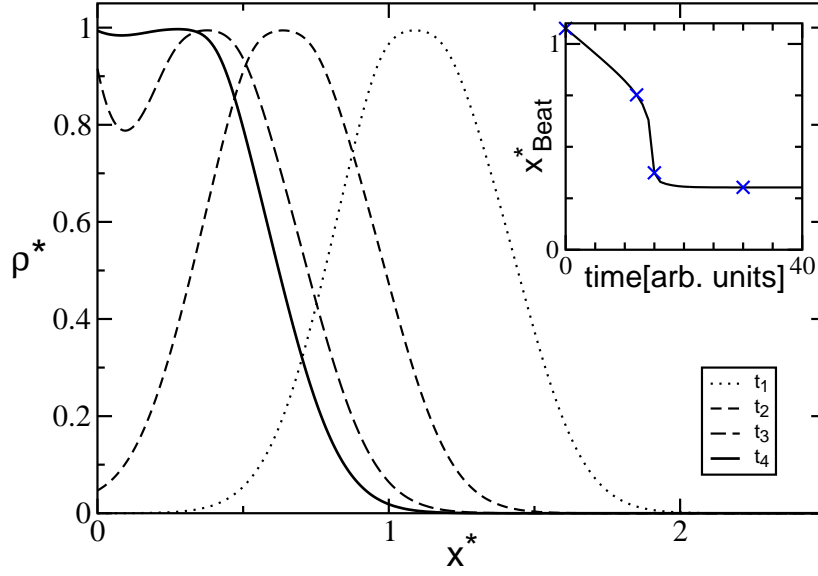


**Figure 6.2:** Density of motors,  $\rho_b^* = \rho_b/\rho_{b,\max}$ , which are fixed to a bead that is pulled by an external force,  $f_{\text{ext}}^* = f_{\text{ext}}/(2k_B T \rho_{\max}) = -1$  towards the edge of the filament as a function of the filament extension  $x^* = x/(a(\bar{\omega}_h/\bar{\omega}_d)^{1/2})$ , at different times, obtained in mean-field approximation of model A. Inset: Position of the bead,  $x_B^* = x_B/(a(\bar{\omega}_h/\bar{\omega}_d)^{1/2})$ , as a function of time. Density profiles are shown for times indicated by the blue crosses. Parameters are:  $\bar{\omega}_a = \bar{\Omega}_a = 0.03\bar{\omega}_h$ ,  $\bar{\omega}_d = \bar{\Omega}_d = 0.008\bar{\omega}_h$ ,  $\bar{\Omega} = 4\bar{\omega}_h$ ,  $\bar{\omega}_f = 0.05\bar{\omega}_h$ ,  $\bar{p} = 1$ ,  $N = 100$ ,  $k^* = ka^2\bar{\omega}_h/(2k_B T \bar{\omega}_d) = 80$ ,  $\xi^* = \xi a(\bar{\omega}_h\bar{\omega}_d)^{1/2}/(2k_B T \rho_{b,\max}) = 0.007$ ,  $\epsilon^* = \epsilon/(a(\bar{\omega}_h/\bar{\omega}_d)^{1/2}) = 0.034$ .

relationship,

$$\begin{aligned} v_m &= v_0 - \mu f(x, x_B) \\ &= v_0 + \mu k(x - x_B) \quad , \end{aligned} \quad (6.3)$$

where  $\mu$  is a motility coefficient (Tawada and Sekimoto, 1991).

Additionally, motors can diffuse along the filament with an effective diffusion coefficient,  $D_b$ , taking into account velocity fluctuations and thermal motion. At the filament end, motors can remove subunits with rate  $\Omega = \Omega_0 + \Omega_1\rho_{b,0} + \Omega_2\rho_{b,0}^2 + \mathcal{O}(\rho_0^3)$  (see Eq.(3.6), leading to a velocity  $v_d = a\Omega/N$  (see Eq.(3.4).

Formulating the dynamics of motor proteins bound to the filament in the form of a continuity equation with additional source and sink terms, leads to:

$$\partial_t \rho_b + \partial_x j_b = \omega_a \left(1 - \frac{\rho_b}{\rho_{b,\max}}\right) \rho_u - \omega_d(x, x_B) \rho_b \quad , \quad (6.4)$$

where the current of bound motors on the filament is given by:

$$j_b = -D_b \partial_x \rho_b - v_d \rho_b - v_m \rho_b \left(1 - \frac{\rho_b}{\rho_{b,\max}}\right) \quad . \quad (6.5)$$

At the filament end,  $x = 0$ , the current on the filament,  $j_b$ , has to equal the net amount of motors attaching to or detaching from the filament end,  $J(\rho_0) = J_0 + J_1\rho_0 + J_2\rho_0^2 + \mathcal{O}(\rho_0^3)$  (see Eq.(3.5), determining the motor density at the end (compare chapter 3).

### 6.1.2. Dynamics of unbound motors

We can formulate the dynamics of unbound motors also in the form of a continuity equation. In this case, attachment and detachment events contribute with signs opposite to those in Eq.(6.4):

$$\partial_t \rho_u + \partial_x j_u = \omega_d(x, x_B) \rho_b - \omega_a \left( 1 - \frac{\rho_b}{\rho_{b, \max}} \right) \rho_u - J(\rho_{b,0}) \delta(x) \quad . \quad (6.6)$$

Here, the term  $J(\rho_{b,0})\delta(x)$  takes into account the possibility of different attachment or detachment rates at the filament end compared to the filament lattice, as well as non-processive depolymerisation, leading to the edge current  $J(\rho_{b,0})$ . The current of unbound motors in the direct vicinity of the filament is given by:

$$j_u = -D_u \partial_x \rho_u - \nu (x - x_B) \rho_u - v_d \rho_u \quad . \quad (6.7)$$

Here,  $D_u$  is an effective diffusion coefficient of motor proteins in the surrounding solution and  $v_d$  the velocity due to motor-induced depolymerisation. After detaching from the filament, motors will be pulled back to an equilibrium position by the relaxing linker elements with rate  $\nu$ , leading to a current of motors as a function of the elongation of the linker elements,  $(x - x_B)$ .

We will assume in the following discussion, that the relaxation rate  $\nu$  of unbound motors is fast compared to the attachment rate  $\omega_a$  and that motors relax instantaneously to an equilibrium position. In this case, we can approximate the actual density distribution of unbound motors along the filament by a distribution around the equilibrium position:

$$\rho_u = N_u B e^{-\frac{k(x-x_B)^2}{2k_B T}} \quad . \quad (6.8)$$

Here,  $N_u$  is the number of unbound motor proteins and  $B = (k/(2\pi k_B T))^{1/2}$  is determined from Eq.(6.1). Inserting Eq.(6.8) in Eq.(6.6) and integrating in respect to  $x$ , yields the time evolution of the number of unbound motor proteins:

$$\begin{aligned} \partial_t N_u &= \omega_d^0 \int \rho_b e^{-\frac{k\epsilon|x-x_B|}{2k_B T}} dx \\ &\quad - \omega_a N_u B \int \left( 1 - \frac{\rho_b}{\rho_{b, \max}} \right) e^{-\frac{k(x-x_B)^2}{2k_B T}} dx \\ &\quad - J(\rho_{b,0}) \end{aligned} \quad (6.9)$$

### 6.1.3. Force balance

The bead in solution is subject to several forces acting on it and governing its dynamics. In addition to the externally applied force,  $f_{\text{ext}}$ , bound motor proteins exert pulling forces on the bead through the elastic linkers, given by  $f_m = k \int (x - x_B) \rho_b dx$ . The movement of the bead, provoked by the above forces, leads to viscous forces acting on the bead in the direction opposing the movement. This Stokes force exerted on the bead is given by,  $f_s = \xi \dot{x}_B$ , where  $\xi$

is the corresponding friction coefficient and  $x_B$  the velocity of the bead in the solution. The equation of motion of the bead is thus given by:

$$\xi \partial_t x_B = k \int (x - x_B) \rho_b dx + f_{\text{ext}} - \xi v_d \quad . \quad (6.10)$$

As we are interested in the interplay of external forces acting on proteins and the depolymerisation activity of these proteins, we have assumed here that  $f_{\text{ext}} \leq 0$ , thus acting along the filament in the direction of the depolymerising edge. The additional viscous force term,  $\xi v_d$ , originates from the description in a reference frame, moving with velocity  $v_d$ .

For the following discussion, we numerically solve Eq.(6.4), (6.9) and Eq.(6.10).

## 6.2. Force-velocity relationships

Applying an external force on the bead leads to a displacement of the bead and the fixed motor proteins in the direction of the applied force (see Fig. 6.2). If the bead is close enough to the edge of the filament for motors to bind at the edge, motors can induce subunit removal. Here we are interested in the interplay of bead position, applied force and depolymerisation velocity. In particular we are interested in how the depolymerisation velocity,  $v_d$ , behaves as a function of the external force,  $f_{\text{ext}}$ . In the discussion which follows, we will choose the specific expressions of the expansion coefficients  $\Omega_i$  and  $J_i$  (see Eq.(3.5) and (3.6)) that were obtained in chapter 4 for model A and model B (see Eq.(4.27)-(4.34)).

### 6.2.1. Depolymerisation velocity

In Fig. 6.3a)-c) (model A) and 6.4a)-c) (model B), the depolymerisation velocity,  $v_d$ , is shown for different processivities,  $\bar{p}$ , as a function of the applied external force,  $f_{\text{ext}}$ . Let us first discuss model A.

#### Model A

In the case of strictly processive motors,  $\bar{p} = 1$ , the speed of depolymerisation decreases first with increasing external force, but increases for large forces shortly before motors break away from the filament (see Fig. 6.3 a)). This interesting behaviour originates from the hindering effect of motor crowding at the filament edge for large motor densities. For small forces, the motor density at the edge increases with increasing  $f_{\text{ext}}$  (see inset of Fig. 6.3 a)), leading to a reduction in subunit removal. As the external force is increased further, motors start to detach and the motor density at the edge starts to diminish, leading to an increase in depolymerisation (compare also Fig. 4.8). The reason why the edge motor density increases first with the external force and then decreases again can be seen in the inset of Fig. 6.3 a), where density profiles of motors on the filament are shown for different external forces. For small forces (black line), the density profile exhibits a maximum approximately at the position of the bead,  $x^* \approx 5$ . For larger external forces, the maximum is shifted towards the edge, and combined with the accumulative effect of processive subunit removal, the density at the edge increases. Once the bead position has approximately reached the filament end, motor density at the end starts to decrease again.

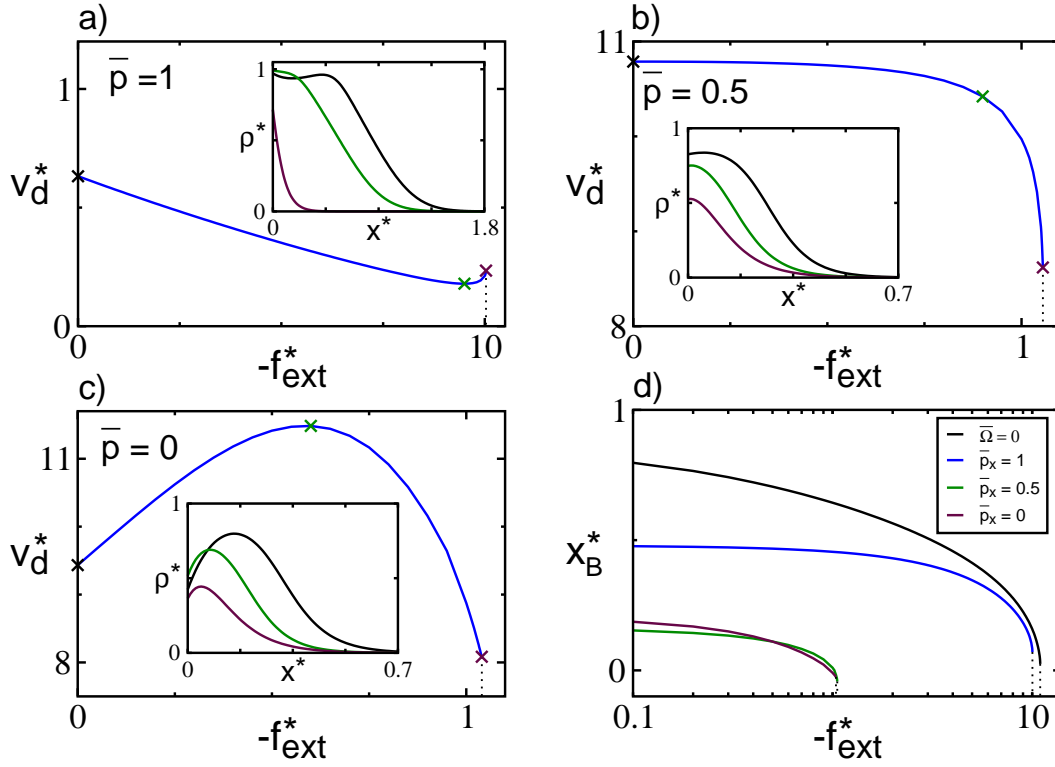


**Figure 6.3:** a)-c): The depolymerisation velocity  $v_d^* = v_d/(a(\bar{\omega}_h\bar{\omega}_d)^{1/2})$  is shown as a function of the applied external force,  $f_{\text{ext}}^* = f_{\text{ext}}/(2k_B T \rho_{\text{max}})$ , for different processivities,  $\bar{p} = 0, 0.5, 1$ , obtained from the mean-field approximation of model A. Insets show density profiles,  $\rho^* = \rho_b/\rho_{b,\text{max}}$ , along the filament,  $x^* = x/(a(\bar{\omega}_h/\bar{\omega}_d)^{1/2})$ , for external forces indicated by the colored crosses. **d)**: Bead displacement,  $x_B^* = x_B/(a(\bar{\omega}_h/\bar{\omega}_d)^{1/2})$ , as a function of the external force,  $f_{\text{ext}}^*$ . Parameters are:  $\bar{\omega}_a = \bar{\Omega}_a = 0.03\bar{\omega}_h$ ,  $\bar{\omega}_d = \bar{\Omega}_d = 0.008\bar{\omega}_h$ ,  $\bar{\Omega} = 2\bar{\omega}_h$ ,  $\bar{\omega}_f = 0.05\bar{\omega}_h$ ,  $N = 100$ ,  $k^* = ka^2\bar{\omega}_h/(2k_B T \bar{\omega}_d) = 80$ ,  $\xi^* = \xi a(\bar{\omega}_h\bar{\omega}_d)^{1/2}/(2k_B T \rho_{b,\text{max}}) = 0.007$ ,  $\epsilon^* = \epsilon/(a(\bar{\omega}_h/\bar{\omega}_d)^{1/2}) = 0.034$ .

Reducing the processivity to  $\bar{p} = 0.5$  results in a higher depolymerisation velocity as now subunits can be removed by motors non-processively, thus without obstruction by crowding of motors at the end. In this case, the accumulative effect of subunit removal is weak and therefore going from the position of the bead towards the filament end, the motor density does not increase again as is the case for  $\bar{p} = 1$ , (compare black lines Fig. 6.3 a) and b)). The edge motor density therefore does not increase with the bead being pulled towards the edge for increasing external force, but is decreased (see inset of Fig. 6.3 b)). As motors are only weakly obstructed from subunit removal by crowding at the end, the velocity reduces with the decreasing edge motor density.

For strictly non-processive motors (see Fig. 6.3 b)),  $\bar{p} = 0$ , subunit removal has a strong diminishing effect on the density at the end. The movement of the bead towards the filament edge for increasing external forces thus first increases the density at the end as the maximum of the profile is pulled towards the edge, but the density is then reduced again as forces get stronger. For non processive motors, depolymerisation is not hindered but increased by crowding at the end, therefore the depolymerisation velocity first increases with the increasing edge motor density and then decreases as well, as the motor density decreases.

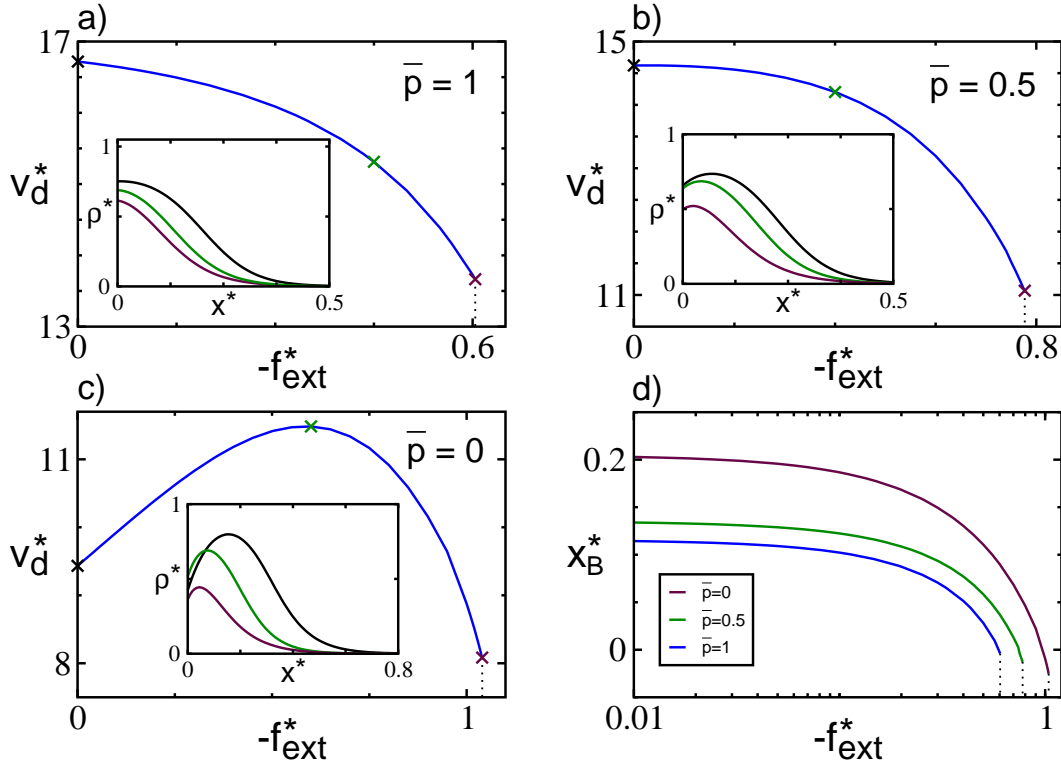


**Figure 6.4:** a)-c): The depolymerisation velocity  $v_d^* = v_d/(a(\bar{\omega}_h\bar{\omega}_d)^{1/2})$  is shown as a function of the applied external force,  $f_{\text{ext}}^* = f_{\text{ext}}/(2k_B T \rho_{\text{b,max}})$ , for different processivities,  $\bar{p} = 0, 0.5, 1$ , obtained from the mean-field approximation of model B. Insets show density profiles,  $\rho_b^* = \rho_b/\rho_{b,\text{max}}$ , along the filament,  $x^* = x/(a(\bar{\omega}_h/\bar{\omega}_d)^{1/2})$ , for external forces indicated by the colored crosses. d): Bead displacement,  $x_B^* = x_B/(a(\bar{\omega}_h/\bar{\omega}_d)^{1/2})$ , as a function of the external force,  $f_{\text{ext}}^*$ . Parameters are:  $\bar{\omega}_a = \bar{\Omega}_a = 0.03\bar{\omega}_h$ ,  $\bar{\omega}_d = \bar{\Omega}_d = 0.008\bar{\omega}_h$ ,  $\bar{\Omega} = 2\bar{\omega}_h$ ,  $\bar{\omega}_f = 0.05\bar{\omega}_h$ ,  $N = 100$ ,  $k^* = ka^2\bar{\omega}_h/(2k_B T \bar{\omega}_d) = 80$ ,  $\xi^* = \xi a(\bar{\omega}_h\bar{\omega}_d)^{1/2}/(2k_B T \rho_{b,\text{max}}) = 0.007$ ,  $\epsilon^* = \epsilon/(a(\bar{\omega}_h/\bar{\omega}_d)^{1/2}) = 0.034$ .

## Model B

In this model, subunit removal is not obstructed by crowding of particles at the filament end. Therefore, the depolymerisation velocity increases with increasing edge motor density and respectively decreases if the motor density decreases (see Fig. 6.4 a-c)). In chapter 4 we showed that subunit removal with  $\bar{p} = 1$  leads to an homogeneous motor distribution along a filament and that in the case of  $\bar{p} < 1$ , motors were depleted at the end. The same effect can be observed here (see insets of Fig. 6.4 a-c)), as the edge motor density is decreasing with decreasing processivity, leading to a reduction of the depolymerisation velocity. The stronger pronouncement of the maximum of the density profiles in the course of reducing the processivity is also a direct consequence of the motor depletion at the end. Motors bound to the filament at values of  $x < x_B$  contribute in pulling the bead towards the edge,  $x = 0$ , while motors bound to the filament at values of  $x > x_B$  pull the bead towards the opposite direction. As motors at the filament end get depleted for  $\bar{p} < 1$ , the bead moves towards larger  $x$  as the processivity is reduced (see also Fig. 6.4 d)). Note, that for  $\bar{p} = 0$ , model A and model B coincide, leading to identical curves in Fig. 6.3 c) and 6.4 c).

### 6.2.2. Critical detachment force

Comparing the critical external forces,  $f_{\text{ext}}^{\text{crit}}$ , for which motors break away from the filament in Fig. 6.3 and 6.4 as a function of the processivity, one finds opposite behaviour in model A and model B. While in model A, the critical force reduces with decreasing processivity, it increases in model B. This behaviour is a direct consequence of the different degree of subunit removal for model A and B for different processivities. In Fig. 6.5 the critical external force is shown for different depolymerisation rates,  $\Omega$ , as a function of the microscopic processivity  $\bar{p}$  for model A and model B (inset). Increasing the depolymerisation rate leads in both models to a increase of the force,  $f_{v_d} = -\xi v_d$ , acting on the bead in direction of the applied external force. Thus less external force is needed for motor molecules to rupture from the filament, leading to the observed decrease of the critical external force for increasing  $\Omega$ . For high rates,  $\Omega$  (see blue lines in Fig. 6.5), the force exerted on the bead by depolymerisation alone is high enough to provoke rupture of motor proteins without any external force applied.

In model A one observes first a decrease and then an increase of the critical force as a function of the processivity,  $\bar{p}$ . Increasing the processivity of motors also increases the motor density at the edge (compare inset of Fig.4.8). As the depolymerisation velocity in model A is given by  $v_d = a(\Omega_1\rho_0 + \Omega_2\rho_0^2)$ <sup>3</sup>, with  $\Omega_1 \geq 0$  and  $\Omega_2 < 0$ , an increase of  $\rho_0$  will lead first to an increase of  $v_d$  and then to a decrease. Following the same argument as for increasing the depolymerisation rate (see above), this behaviour of the depolymerisation velocity then leads as a consequence to the observed behaviour of the critical external force.

The behaviour of the critical external force in model B is explained by the same arguments. Here,  $v_d = a\Omega_1\rho_0$  with  $\Omega_1 \geq 0$ , therefore the depolymerisation velocity does not decrease for increasing edge motor density leading to the observed decrease of the critical external force as a function of the processivity.

## 6.3. Role of fluctuations

In the preceding section we described motor dynamics with a mean-field theory and therefore neglected fluctuations in the number of bound motor proteins. In the case where the number of proteins fixed to a bead,  $N$ , is small, these fluctuations will become important and influence motor and bead dynamics. In order to study these effects, we will extend the discrete stochastic model of chapter 4 to the case of motor proteins being fixed to a bead. As elucidated in chapter 4, motor dynamics are described by a master equation (compare p. 51). Introducing average occupation numbers,  $\langle n_i \rangle$ , of the discrete binding sites,  $i$ , one can deduce evolution equations for the average occupation numbers from the master equation.

### 6.3.1. Evolution equations

#### Binding site occupation

In agreement with the model of chapter 4 we introduce the following rates to describe particle dynamics: hopping to free left and right neighbouring binding sites occurs with rate  $\bar{\omega}_h$ ;

<sup>3</sup>Again we have assumed stabilised filaments, leading to  $\Omega_0 = 0$ , and a subunit to be of length  $a$ .

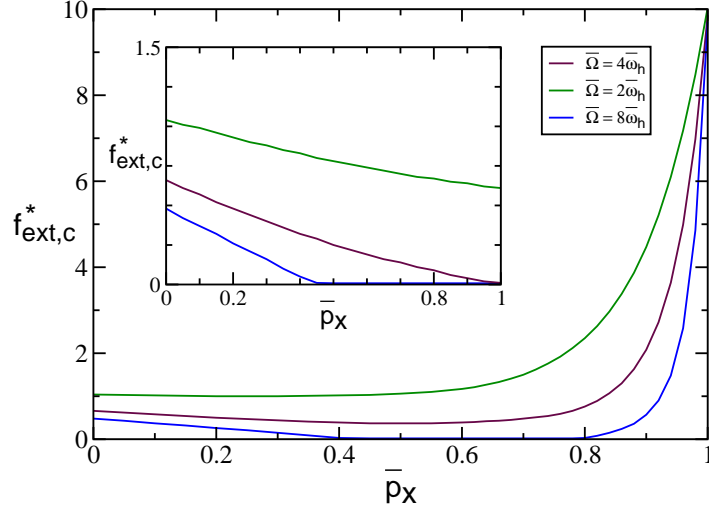


**Figure 6.5:** Critical external force,  $f_{\text{ext,c}}^* = f_{\text{ext,c}}/(2k_{\text{B}}T\rho_{\text{max}})$ , for which motors start to break away from the filament as a function of the processivity of individual motor proteins,  $\bar{p}$ , for different depolymerisation rates,  $\bar{\Omega} = 2\bar{\omega}_h, 4\bar{\omega}_h, 8\bar{\omega}_h$ , obtained from mean-field approximation of model A. Inset: Same situation for model B. Parameters are:  $\bar{\omega}_a = \bar{\Omega}_a = 0.03\bar{\omega}_h$ ,  $\bar{\omega}_d = \bar{\Omega}_d = 0.008\bar{\omega}_h$ ,  $\bar{\omega}_f = 0.05\bar{\omega}_h$ ,  $N = 100$ ,  $k^* = ka^2\bar{\omega}_h/(2k_{\text{B}}T\bar{\omega}_d) = 80$ ,  $\xi^* = \xi a(\bar{\omega}_h\bar{\omega}_d)^{1/2}/(2k_{\text{B}}T\rho_{\text{b,max}}) = 0.007$ ,  $\epsilon^* = \epsilon/(a(\bar{\omega}_h/\bar{\omega}_d)^{1/2}) = 0.034$ .

directed motion towards one end is incorporated by an additional rate  $\bar{\omega}_v$ ; and subunit removal at the end takes place with rate  $\bar{\Omega}$ . Sliding of a particle due to the forces exerted on it by the elastic linkers connecting the particle to the bead is described by a rate  $\bar{\omega}_f$  multiplied by the extension of the respective elastic linker,  $(i - x_{\text{B}}/a)$ . In order to incorporate the equilibrium distribution of unbound motor proteins (see Eq.6.8), we define the following attachment rate of unbound particles to free binding sites on the lattice,

$$\bar{\omega}_a = \bar{\omega}_a^0 \langle n_{\text{u}} \rangle a B e^{\frac{ka^2(i - x_{\text{B}}/a)^2}{2k_{\text{B}}T}}, \quad (6.11)$$

where  $\langle n_{\text{u}} \rangle$ , is the average number of unbound particles and  $\bar{\omega}_a^0$  is the attachment rate of an individual motor protein in the absence of any elastic linkers. Particles can detach from the lattice according to their position in respect to the position of the bead. The corresponding detachment rate is given by,

$$\bar{\omega}_d = \bar{\omega}_d^0 e^{\frac{ka\epsilon|i - x_{\text{B}}/a|}{2k_{\text{B}}T}}, \quad (6.12)$$

where  $\bar{\omega}_d^0$  is again the rate of an individual protein in the absence of any elastic linkers. For the first binding site, the value of the linker-independent rates can be different and we therefore introduce the following attachment,  $\bar{\Omega}_a^0$ , and detachment,  $\bar{\Omega}_d^0$ , rates for individual proteins to and from the first binding site respectively.

The evolution equation of average occupation numbers for binding sites  $i \geq 2$  is then given

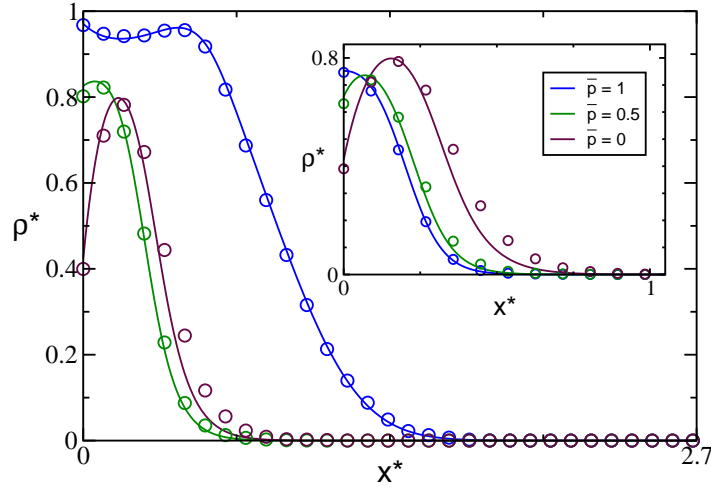


**Figure 6.6:** Motor density,  $\rho_b^* = \rho_b/\rho_{b,\max}$ , along the filament,  $x^* = x/(a(\bar{\omega}_h/\bar{\omega}_d)^{1/2})$ , for different processivities  $\bar{p} = 0, 0.5$  and  $1$  obtained from stochastic simulations of model A (circles) and from the corresponding mean-field equations (lines), if no external force is applied,  $f_{\text{ext}} = 0$ . Inset: The same situation for model B. Parameters are:  $\bar{\omega}_a = \bar{\Omega}_a = 0.03\bar{\omega}_h$ ,  $\bar{\omega}_d = \bar{\Omega}_d = 0.008\bar{\omega}_h$ ,  $\bar{\omega}_f = 0.05\bar{\omega}_h$ ,  $\bar{\Omega} = 2\bar{\omega}_h$ ,  $N = 100$ ,  $k^* = ka^2\bar{\omega}_h/(2k_B T\bar{\omega}_d) = 80$ ,  $\xi^* = \xi a(\bar{\omega}_h\bar{\omega}_d)^{1/2}/(2k_B T\rho_{b,\max}) = 0.007$ ,  $\epsilon^* = \epsilon/(a(\bar{\omega}_h/\bar{\omega}_d)^{1/2}) = 0.034$ .

by:

$$\begin{aligned}
\frac{d}{dt}\langle n_i \rangle &= \bar{\omega}_h(\langle n_{i+1} \rangle - 2\langle n_i \rangle + \langle n_{i-1} \rangle) \\
&+ \bar{\omega}_v(\langle n_{i+1}(1-n_i) \rangle - \langle n_i(1-n_{i-1}) \rangle) \\
&+ \bar{\omega}_f(((i+1) - x_B/a)\langle n_{i+1}(1-n_i) \rangle - (i - x_B/a)\langle n_i(1-n_{i-1}) \rangle) \quad , (i > x_B/a) \\
&+ \bar{\omega}_f((i - x_B/a)\langle n_{i+1}(1-n_i) \rangle - ((i-1) - x_B/a)\langle n_i(1-n_{i-1}) \rangle) \quad , (i < x_B/a) \\
&+ \langle \bar{\Omega}^{A,B} n_1(n_{i+1} - n_i) \rangle \\
&+ \bar{\omega}_a^0 \langle n_u \rangle a B e \frac{ka^2(i - x_B/a)^2}{2k_B T} \langle 1 - n_i \rangle - \bar{\omega}_d^0 e \frac{ka\epsilon|i - x_B/a|}{2k_B T} \langle n_i \rangle \quad . \quad (6.13)
\end{aligned}$$

Here,  $\bar{\Omega}^{A,B}$  is defined by Eq.(4.1) if model A is considered and by Eq.(4.2) in the case of model B. Note that we have to distinguish between the case of  $i > x_B/a$  and  $i < x_B/a$  in the above equation. For the first binding site,  $i = 1$ , the evolution equation reads:

$$\begin{aligned}
\frac{d}{dt}\langle n_1 \rangle &= \bar{\omega}_h\langle n_2 - n_1 \rangle \\
&+ \bar{\omega}_v\langle n_2(1-n_1) \rangle \\
&+ \bar{\omega}_f(2 - x_B/a)\langle n_2(1-n_1) \rangle \quad , (i > x_B/a) \\
&+ \bar{\omega}_f(1 - x_B/a)\langle n_1(1-n_2) \rangle \quad , (i < x_B/a) \\
&- (1 - \bar{p})\bar{\Omega}\langle n_1(1-n_2) \rangle \\
&+ \bar{\omega}_a^0 \langle n_u \rangle a B e \frac{ka^2(1 - x_B/a)^2}{2k_B T} \langle 1 - n_1 \rangle - \bar{\omega}_d^0 e \frac{ka\epsilon|1 - x_B/a|}{2k_B T} \langle n_1 \rangle \quad . \quad (6.14)
\end{aligned}$$

### Unbound motor proteins

In order to complete the discrete stochastic description of the system we need to specify the dynamics of the number of unbound motor proteins and of the bead. The time evolution of the number of unbound particles is directly determined by the discrete form of Eq.(6.9), given by:

$$\begin{aligned} \frac{d}{dt}\langle n_u \rangle &= \frac{\omega_d^0}{a} \sum_{i=1}^{\infty} \langle n_i \rangle e^{-\frac{k\epsilon|i-x_B/a|}{2k_B T}} \Delta x \\ &\quad - \omega_a \langle n_u \rangle B \sum_{i=1}^{\infty} \langle 1 - n_i \rangle e^{-\frac{k(i-x_B/a)^2}{2k_B T}} \Delta x \\ &\quad - \langle j_0^{A,B} \rangle . \end{aligned} \quad (6.15)$$

Here the average net number of particles leaving the lattice from the first binding site,  $\langle j_0^{A,B} \rangle$ , is given by Eq.(4.17) in the case of model A and by Eq.(4.18) in the case of model B.

### Bead position

The time evolution of the bead position is given by the discrete form of Eq.(6.10),

$$\xi \frac{d}{dt} x_B = k \sum_{i=1}^{\infty} (i - x_B/a) \langle n_i \rangle \Delta x + f_{\text{ext}} - \xi \langle v_d^{A,B} \rangle , \quad (6.16)$$

where the average depolymerisation velocity in model A is given by,  $\langle v_d^A \rangle = a\bar{\Omega} \langle n_1(1 - \bar{p}n_2) \rangle$  and by  $\langle v_d^B \rangle = a\bar{\Omega} \langle n_1 \rangle$  for model B.

### 6.3.2. Comparison with generic theory

#### Mean-field approximation

In order to investigate whether our discrete description of bound motor dynamics, Eq.(6.13), reflects the mean-field dynamics of Eq.(6.4) and (6.5), we apply the continuum mean-field approximation introduced in chapter 4

$$\langle n_i \rangle = \int_{(i-1/2)a}^{(i+1/2)a} \rho(x) dx \approx a\rho_b(x) , \quad (6.17)$$

$$\langle n_i n_{i\pm 1} \rangle \approx \langle n_i \rangle \langle n_{i\pm 1} \rangle , \quad (6.18)$$

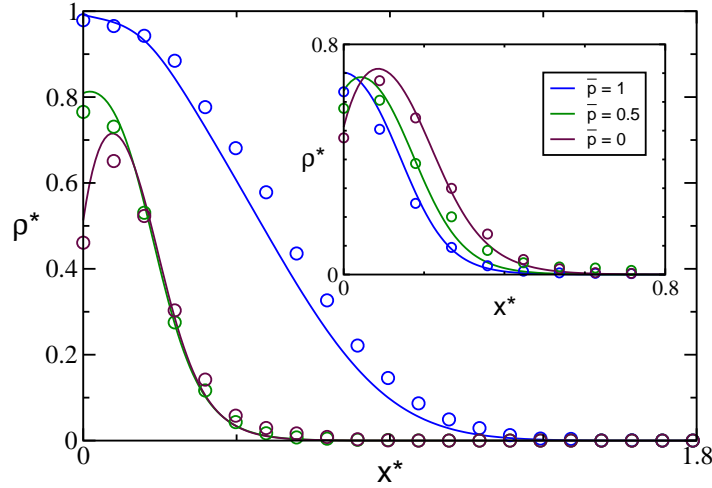


**Figure 6.7:** Motor density,  $\rho_b^* = \rho_b / \rho_{b,max}$ , along the filament,  $x^* = x / (a(\bar{\omega}_h / \bar{\omega}_d)^{1/2})$ , for different processivities  $\bar{p} = 0, 0.5$  and  $1$  obtained from stochastic simulations of model A (circles) and from the corresponding mean-field equations (lines). The external force equals the critical force for which motors start to break off the filament in the computer simulation,  $f_{ext,c}^* = f_{ext,c} / (2k_B T \rho_{max}) = -9.9(\bar{p} = 1), -0.61(\bar{p} = 0.5), -0.54(\bar{p} = 0)$ . Inset: The same situation for model B, with  $f_{ext,c}^* = -0.36(\bar{p} = 1), -0.37(\bar{p} = 0.5), -0.52(\bar{p} = 0)$ . Parameters are:  $\bar{\omega}_a = \bar{\Omega}_a = 0.03\bar{\omega}_h$ ,  $\bar{\omega}_d = \bar{\Omega}_d = 0.008\bar{\omega}_h$ ,  $\bar{\omega}_f = 0.05\bar{\omega}_h$ ,  $\bar{\Omega} = 2\bar{\omega}_h$ ,  $N = 100$ ,  $k^* = ka^2\bar{\omega}_h / (2k_B T \bar{\omega}_d) = 80$ ,  $\xi^* = \xi a(\bar{\omega}_h \bar{\omega}_d)^{1/2} / (2k_B T \rho_{b,max}) = 0.007$ ,  $\epsilon^* = \epsilon / (a(\bar{\omega}_h / \bar{\omega}_d)^{1/2}) = 0.034$ .

to Eq.(6.13) (compare Eq.(4.14), (4.15) and (4.16)), leading to the following equation,

$$\begin{aligned}
\partial_t \rho_b &= a^2 \bar{\omega}_h \partial_x^2 \rho_b \\
&+ a \bar{\omega}_v (1 - 2a\rho_b) \partial_x \rho_b \\
&+ \bar{\omega}_f (\rho_b (1 - a\rho_b) + (x - x_B) (1 - 2a\rho_b) \partial_x \rho_b) \\
&+ a^2 \bar{\Omega}^{A,B} \rho_{b,0} \partial_x \rho_b \\
&+ \omega_a N_u B \int (1 - a\rho_b) e^{-\frac{k(x-x_B)^2}{2k_B T}} - \omega_d^0 e^{-\frac{k\epsilon|x-x_B|}{2k_B T}} \rho_b \quad . \quad (6.19)
\end{aligned}$$

Introducing again macroscopic parameters,  $D = a^2 \bar{\omega}_h$ ,  $v_0 = a \bar{\omega}_v$ ,  $\mu k = \bar{\omega}_f$  and  $v_d = a \bar{\Omega}^{A,B}$  and using that  $\rho_{b,max} = 1/a$ , we find that Eq.(6.19) is identical to Eq.(6.4) after inserting Eq.(6.5), thus our discrete description is exactly reflecting the dynamics described with in the generic framework of section 6.1 (see also Fig.6.6 and Fig. 6.7).

### Force-velocity relationships

In the following discussion we compare the depolymerisation velocity and the displacement of the bead as a function of the applied external force obtained in stochastic simulations with results obtained in mean-field approximation. Comparing these results, one has to keep in mind that due to the stochasticity of the simulation, the critical external force, for example, for which motors break away from the filament, is not given by a single well defined value, but rather by continuous distributions. The peak and width of these distributions can in general be influenced by the duration of the simulation time.

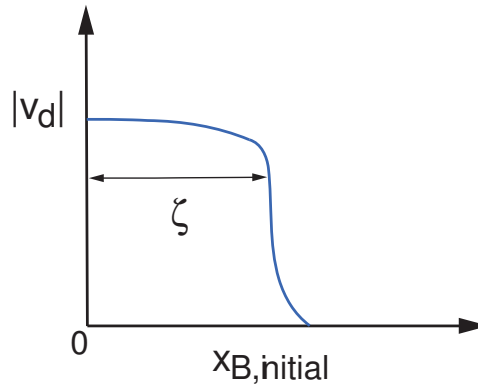


**Figure 6.8:** Illustration of the dependence of the depolymerisation velocity,  $v_d$ , on the initial position of the bead along the filament. If fluctuations are strong, for example in the case of only a small number of motors attached to the bead, motors can detach completely from the filament before reaching the filament end. The average distance covered by motor proteins on the filament,  $\zeta$ , depends on parameter values of the motor-filament interactions, the number of proteins on the bead and the external force.

**Influence of observation time** Let us take the critical external force,  $f_{\text{ext},c}$ , as an example. Increasing the duration of simulation,  $t_{\text{sim}} \rightarrow \infty$ , the distribution of forces will be shifted towards smaller values, as the probability for motor proteins to detach completely from the filament simply due to fluctuations will increase. On the other hand, decreasing the time of simulation will reduce the probability for complete detachment of motors from the filament. In order to compare simulation data with experimental data, one therefore has to adjust these times to realistic values <sup>4</sup>.

**Influence of initial bead position** In a similar way, the initial bead position can also have an influence on results. If the initial position of the bead from the filament end is increased, the probability for motor proteins to detach completely from the filament due to fluctuations before reaching the end will also increase. The average distance,  $\zeta$ , covered by bound motors before detaching completely from the filament is dependent on parameter values of the interaction rates of motors with the filament, like for example the force dependent detachment rate,  $\bar{\omega}_d(x)$ , the number of motor proteins on the bead and the external force,  $f_{\text{ext}}$ . In order to obtain consistent results, the initial bead position has to be chosen such that  $x_B < \zeta$ .

In Fig. 6.10 and 6.9 the bead displacement and the depolymerisation velocity as a function of the applied external force is shown. Computer simulations of the discrete model are compared with the corresponding mean-field calculations for different processivities in model A and model B. One can see, that the bead displacements obtained in computer simulations are in very good agreement with the mean-field results in the case of small externally applied forces, but show deviations for higher forces. Increasing the external force, one finds that motors break off the filament at lower forces in the stochastic model than they do in the mean-field description. This effect becomes more visible as the processivity,  $\bar{p}$ , is decreased

<sup>4</sup>For the following discussion, simulation times correspond approximately to 3 min.

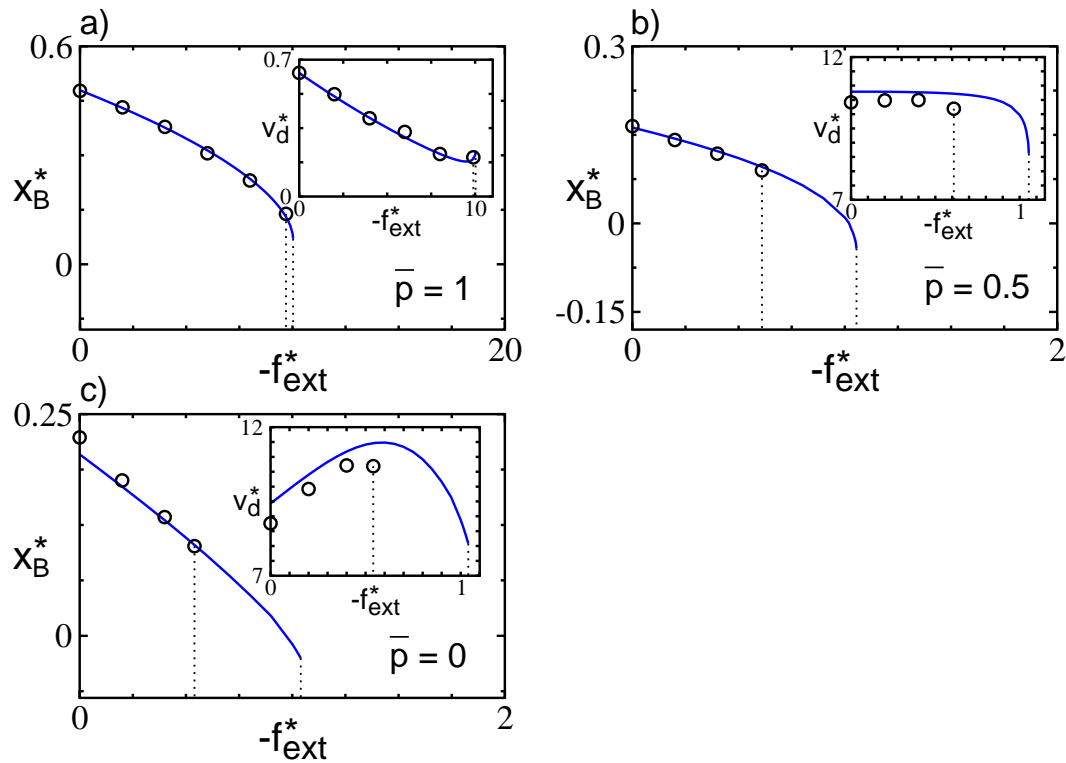


**Figure 6.9: a)-c):** The bead position,  $x_B^* = x_B / (a(\bar{\omega}_h/\bar{\omega}_d)^{1/2})$ , is shown as a function of the applied external force,  $f_{\text{ext}}^* = f_{\text{ext}} / (2k_B T \rho_{\text{max}})$ , for different processivities,  $\bar{p} = 0, 0.5, 1$ . Results from stochastic simulations of model A (circles) are compared with results from the corresponding mean-field equations (lines). Insets show the depolymerisation velocity  $v_d^* = v_d / (a(\bar{\omega}_h \bar{\omega}_d)^{1/2})$  as a function of the applied external force,  $f_{\text{ext}}^*$  for the same situations. Parameters are:  $\bar{\omega}_a = \bar{\Omega}_a = 0.03\bar{\omega}_h$ ,  $\bar{\omega}_d = \bar{\Omega}_d = 0.008\bar{\omega}_h$ ,  $\bar{\Omega} = 2\bar{\omega}_h$ ,  $\bar{\omega}_f = 0.05\bar{\omega}_h$ ,  $N = 100$ ,  $k^* = ka^2\bar{\omega}_h / (2k_B T \bar{\omega}_d) = 80$ ,  $\xi^* = \xi a(\bar{\omega}_h \bar{\omega}_d)^{1/2} / (2k_B T \rho_{b,\text{max}}) = 0.007$ ,  $\epsilon^* = \epsilon / (a(\bar{\omega}_h/\bar{\omega}_d)^{1/2}) = 0.034$ .

and is a direct result of the reduction of bound motors on the filament as the external force is increased leading to a crucial influence of fluctuation.

Comparing the results for the depolymerisation velocity one also finds good agreement between stochastic simulations and mean-field calculations, especially for highly processive motor proteins. The slightly stronger deviation than in the case of the bead displacement arises from differences in the motor density at the edge of the filament. As already discussed in chapter 4, one expects differences at this particular point on the filament between a discrete description and a meanfield approach, where peculiarities of a single binding site are neglected.

## 6.4. Summary

We developed a theory for subunit removal by motor proteins on which an external force is exerted. We have here concentrated on a situation corresponding to an experiment where motor proteins are fixed via elastic linkers to a bead on which a force can be exerted. We found that the depolymerisation velocity can increase or decrease if the applied external force is increased, depending on the processivity of the motor proteins and whether crowding of

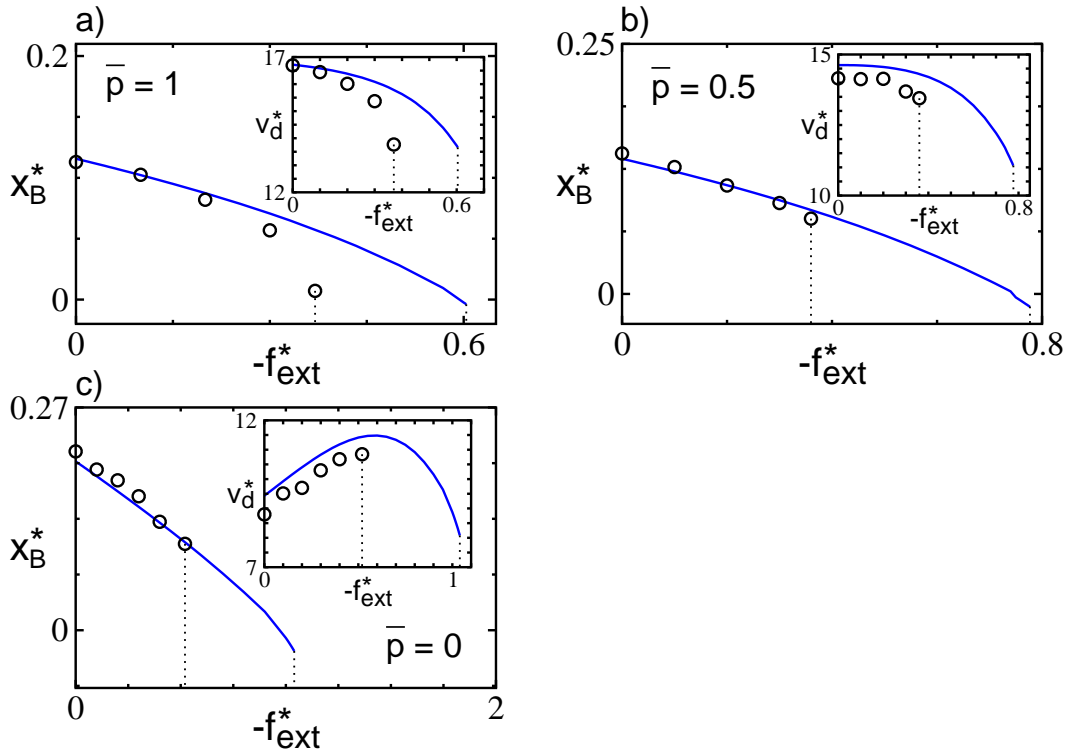


**Figure 6.10: a)-c):** The bead position,  $x_B^* = x_B/(a(\bar{\omega}_h/\bar{\omega}_d)^{1/2})$ , is shown as a function of the applied external force,  $f_{\text{ext}}^* = f_{\text{ext}}/(2k_B T \rho_{\text{max}})$ , for different processivities,  $\bar{p} = 0, 0.5, 1$ . Results from stochastic simulations of model B (circles) are compared with results from the corresponding mean-field equations (lines). Insets show the depolymerisation velocity  $v_d^* = v_d/(a(\bar{\omega}_h \bar{\omega}_d)^{1/2})$  as a function of the applied external force,  $f_{\text{ext}}^*$  for the same situations. Parameters are:  $\bar{\omega}_a = \bar{\Omega}_a = 0.03\bar{\omega}_h$ ,  $\bar{\omega}_d = \bar{\Omega}_d = 0.008\bar{\omega}_h$ ,  $\bar{\Omega} = 2\bar{\omega}_h$ ,  $\bar{\omega}_f = 0.05\bar{\omega}_h$ ,  $N = 100$ ,  $k^* = ka^2\bar{\omega}_h/(2k_B T \bar{\omega}_d) = 80$ ,  $\xi^* = \xi a(\bar{\omega}_h \bar{\omega}_d)^{1/2}/(2k_B T \rho_{b,\text{max}}) = 0.007$ ,  $\epsilon^* = \epsilon/(a(\bar{\omega}_h/\bar{\omega}_d)^{1/2}) = 0.034$ .

motors is hindering depolymerisation (model A) or not (model B). Increasing the processivity of motors in model B leads to a decrease in the critical external force which is needed for motors to break away from the filament. In model A the critical external force also decreases at first for increasing processivity but then strongly increases for high processivities. We saw that the corresponding mean-field approximation of model A and model B are in good agreement with results from stochastic simulations for small external forces, but show deviations for the critical external force at which motors break away from the filament.



---

## Summary and Perspectives

In the presented work we discussed different aspects of the dynamic behaviour of motor proteins which induce the shortening of the ends of filaments to which they bind. For this, we have developed a generic theory of motor-induced filament depolymerisation (Klein et al., 2005). Although this work has been motivated by recent experiments with members of the kinesin subfamily KIN-13 (Desai et al., 1999; Hunter et al., 2003), the developed description is valid irrespective of details of the mechanism of subunit removal and of the structure of the depolymerising filament end. It is therefore not restricted to motors of the KIN-13 family which interact with microtubules but can be applied in general to associated proteins which regulate the dynamics of filament ends. Actin depolymerisation by actin-depolymerisation factor/cofilin as well as the polymerisation of actin by formin are further examples of such processes (Pruyne et al., 2002; Sagot et al., 2002).

Our phenomenological description revealed that the experimentally observed accumulation of motor proteins at both depolymerising filament ends can occur through a dynamic process, even if the binding affinity of motors to the ends is not larger than to the rest of the filament. In this process, motors which bind along the filament are subsequently captured by the retracting filament ends. We furthermore show that a positive effective processivity of subunit removal is essential to achieve this dynamic accumulation of motors at the ends. This effective processivity, describing the collective behaviour of subunit removing proteins, is a direct result of the steric exclusion of motors bound near the end. We found that for high effective processivities a dynamic instability appears, where two stable states with different motor densities at the filament end coexist. A signature of this dynamic instability could appear for real microtubule depolymerisation by KIN-13 motor proteins in the mitotic spindle, leading to bistability and switch-like changes of depolymerisation velocities. In the mitotic spindle this instability could be relevant for chromosome oscillations, which have been observed (Skibbens et al., 1993).

In our discussion we focused on excluded volume effects at the filament end and considered the case where motors do not exhibit directed motion towards one of the ends of the filament, as was observed experimentally for members of the KIN-13 subfamily. Directed motion in general depends on the density of motors on the filament (Lipowsky et al., 2001; Kruse and

Sekimoto, 2002) and excluded volume effects in the bulk are known to lead to unexpected motor behaviour in this case, for example the occurrence of domain walls which separate coexisting regions of low and high densities on the filament (Parmeggiani et al., 2003; Nishinari et al., 2005). In the case of motors not only showing depolymerisation activities at filament ends but also exhibiting directed motion on the filament the interplay between bulk- and end-excluded volume effects could lead to new phenomena. Examples for motor proteins showing depolymerisation activity and directed motion on microtubules are members of the KIN-8 subfamily (Pereira et al., 1997; Rischitor et al., 2004), for which detailed results from *in vitro* experiments are unfortunately still lacking. Although this work has focused on motors which show negligible directed motion, finite directed motion is completely incorporated in our framework and our description is therefore also applicable to motors showing such behaviour.

In order to gain better insight into the cooperativity and processivity of motors bound at the end of a filament, we developed a more microscopic description of subunit removal of a single protofilament. In this discrete stochastic model, motors are represented by identical particles which occupy discrete binding sites on a lattice, symbolising the filament. We introduced two scenarios, model A and model B, in which interactions between motor proteins at the filament end lead to different rates of subunit removal and different effective processivities. The differences between these two models are observable, for example, by looking at the depolymerisation velocity as a function of the motor concentration. For model A, the velocity exhibits a maximum for intermediate motor concentrations before saturating for higher motor concentrations, while in model B the maximum velocity is always given by the saturation value at high motor concentrations. In addition, dynamic motor accumulation at filament ends is only possible in model A, while in model B motors are depleted at the end. We can relate our results to experiments, as the depolymerisation velocity as a function of the motor concentration has been measured for MCAK proteins (Hunter et al., 2003). The observed velocity is consistent with both models A and B since it does not exclude the possibility of a maximal velocity for intermediate motor concentrations. The observed accumulation at the end suggests that a mechanism similar to model A is more likely to be at work. Indeed, experiments indicate that a collection of MCAK motors processively depolymerise microtubules (Hunter et al., 2003) consistent with model A. Present data cannot rule out a mechanism akin to model B where motor accumulation is still possible if the affinity of motors to the filament end is high. In future experiments, model B could be ruled out if a maximum of the depolymerisation velocity at intermediate motor concentration would be observed as suggested by our theory. The members XKCM1 and XKIF2 of the KIN-13 family, can depolymerise microtubules with or without accumulation of motors at the end, depending on the conditions under which microtubules have been stabilised (Desai et al., 1999). Furthermore, it has been suggested that processivity is reduced under conditions where motors do not accumulate (Desai et al., 1999). Thus, stabilisation of microtubules could influence the microscopic mechanisms of collective subunit removal by a change in the microtubule lattice structure, leading to reduced processivity or a mechanism similar to model B. Experimentally determining the values of the parameters of our theory - diffusion coefficient, attachment and detachment rate and the cutting rate - would allow us to discuss in our framework whether the observed differences in the behaviour of different KIN-13 motor proteins are related to differences in the processivity or in the cutting mechanisms of these motors.

Given our interest in how the presence of multiple protofilaments influences subunit re-

removal and motor dynamics, we extended our discrete stochastic model of one single protofilament to the situation of a periodic parallel alignment of any number of protofilaments with motors being able to change protofilaments. Simulations of this extended model showed that processive motor proteins which rebind on adjacent protofilaments after subunit removal, rather than on the protofilament the subunit was removed from, diminish the effect of dynamic accumulation at the end. This is in contrast to the situation of one single protofilament, where processive subunit removal lead to accumulation. We could show, that the asymmetry of the lattice, resulting from a shift of the protofilaments in respect to each other, in combination with subunit removal leads to a ring current of motors perpendicular to the axis of the protofilaments. Examining the structure of the ends of the parallel aligned protofilaments we found two distinct scaling behaviours of the width of the edge in time, depending on motor dynamics.

As a completion of our theoretical investigations of motor-induced subunit removal we considered the case of motor proteins being fixed by elastic linkers to a bead. The interplay of external forces acting on the bead and being exerted via the elastic linkers on the proteins and the collective behaviour of proteins removing subunits could be observed by discussing the depolymerisation velocity as a function of the external force.

In conclusion, we presented a theoretical description of some of the key aspects of motor-induced filament depolymerisation, providing us with a better understanding of the phenomenon of motor-induced filament depolymerisation. Our results will assist in the interpretation of recent experimental results and we are confident that our work will motivate further experiments, capable of testing predictions made in our theory.



## Parameter determination in the generic description

### Selfconsistent determination of the edge motor density

As shown in chapter 3, the density of motor proteins at the depolymerising end has to be calculated selfconsistently from the general steady state solution, Eq.(3.14), and the boundary condition at  $x = 0$ , Eq.(3.10). This leads to a polynomial in  $\rho_0$ , whose order depends on the order of the expansion of the edge motor current  $J(\rho_0)$ , Eq.(3.5) and the depolymerisation rate  $\Omega(\rho_0)$ , Eq.(3.6). In the case of an expansion of  $J(\rho_0)$  and  $\Omega(\rho_0)$  up to second order, one gets a polynomial of fifth order, whose coefficients read:

$$\Theta_0 = J_0^2 \rho_{\max}^2 + J_0 \Omega_0 \rho_{\max} \rho_\infty + J_0 v_0 \rho_{\max}^2 \rho_\infty - D \omega_a c \rho_{\max} \rho_\infty^2 - D \omega_d \rho_{\max}^2 \rho_\infty^2 \quad ,$$

$$\Theta_1 = J_0 \Omega_0 \rho_{\max} + 2J_0 J_1 \rho_{\max}^2 + J_0 v_0 \rho_{\max}^2 + \Omega_0^2 \rho_\infty + J_1 \Omega_0 \rho_{\max} \rho_\infty + 2v_0 \Omega_0 \rho_{\max} \rho_\infty + J_0 \Omega_1 \rho_{\max} \rho_\infty + 2D \omega_a c \rho_{\max} \rho_\infty + J_1 v_0 \rho_{\max}^2 \rho_\infty + v_0^2 \rho_{\max}^2 \rho_\infty + 2D \omega_d \rho_{\max}^2 \rho_\infty$$

$$\Theta_2 = J_1 \Omega_0 \rho_{\max} + J_0 \Omega_1 \rho_{\max} - D \omega_a c \rho_{\max} + J_1^2 \rho_{\max}^2 + 2J_0 J_2 \rho_{\max}^2 + J_1 v_0 \rho_{\max}^2 - D \omega_d \rho_{\max}^2 + 2\Omega_0 \Omega_1 \rho_\infty + J_2 \Omega_0 \rho_{\max} \rho_\infty + J_1 \Omega_1 \rho_{\max} \rho_\infty + 2v_0 \Omega_1 \rho_{\max} \rho_\infty + J_0 \Omega_2 \rho_{\max} \rho_\infty + j_2 v_0 \rho_{\max}^2 \rho_\infty \quad ,$$

$$\Theta_3 = J_2 \Omega_0 \rho_{\max} + J_1 \Omega_1 \rho_{\max} + J_0 \Omega_2 \rho_{\max} + 2J_1 J_2 \rho_{\max}^2 + J_2 v_0 \rho_{\max}^2 + \Omega_1^2 \rho_\infty + 2\Omega_0 \Omega_2 \rho_\infty + J_2 \Omega_1 \rho_{\max} \rho_\infty + J_1 \Omega_2 \rho_{\max} \rho_\infty + 2v_0 \Omega_2 \rho_{\max} \rho_\infty \quad ,$$

$$\begin{aligned}
\Theta_4 &= J_2\Omega_1\rho_{\max} + J_1\Omega_2\rho_{\max} + J_2^2\rho_{\max}^2 + 2\Omega_1\Omega_2\rho_{\infty} + J_2\Omega_2\rho_{\max}\rho_{\infty} \quad , \\
\Theta_5 &= J_2\Omega_2\rho_{\max} + \Omega_2^2\rho_{\infty} \quad ,
\end{aligned} \tag{A.1}$$

## Constants of stability analysis

Calculating the coefficients of Eq.(3.27) explicitly, one gets the following expressions:

$$\begin{aligned}
\Gamma_0 &= \frac{1}{2} \quad , \\
\Gamma_1 &= \frac{1}{2} \left( \left( v_0 + \frac{\Omega_0}{\rho_{\max}} + 2J_1 \right) + \left( \frac{3\Omega_1}{\rho_{\max}} + 4J_2 \right) \rho_{s,0} + \frac{5\Omega_2}{\rho_{\max}} \rho_{s,0}^2 \right) \quad , \\
\Gamma_2 &= \frac{1}{2\lambda} (\Omega_1 + 2\Omega_2\rho_{s,0}) \left( \frac{\rho_{s,0} - \rho_{\infty}}{\rho_{\max}} \right) \quad , \\
\Gamma_3 &= \frac{1}{2\lambda} (\Omega_1 + 2\Omega_2\rho_{s,0}) \left( \frac{\rho_{s,0} - \rho_{\infty}}{\rho_{\max}} \right) \left( (v_0 + v_d)^2 + 4D \left( \frac{\omega_a c}{\rho_{\max}} + \omega_d \right) \right)^{1/2}
\end{aligned} \tag{A.2}$$

## Determination of $\zeta_c$ for $\zeta \in \mathbb{C}$

In order to calculate  $\zeta_c$  in the case of complex eigenvalues we use  $\zeta = \zeta_R + i\zeta_I$ , in Eq.(3.25),

$$\begin{aligned}
k_{\pm} &= \frac{2D}{(v_0 + v_d) \pm \left( (v_0 + v_d)^2 + 4D \left( \frac{\omega_a c}{\rho_{\max}} + \omega_d + (\zeta_R + i\zeta_I) \right) \right)^{1/2}} \\
&= \frac{2D}{(v_0 + v_d) \pm \left( \left( \left( (v_0 + v_d)^2 + 4D \left( \frac{\omega_a c}{\rho_{\max}} + \omega_d + \zeta_R \right) \right)^2 + (4D\zeta_I)^2 \right)^{1/2} e^{-i\phi} \right)^{1/2}} \\
&= \frac{2D}{(v_0 + v_d) \pm \left( \left( \left( (v_0 + v_d)^2 + 4D \left( \frac{\omega_a c}{\rho_{\max}} + \omega_d + \zeta_R \right) \right)^2 + (4D\zeta_I)^2 \right)^{1/4} \left( \cos\left(\frac{\phi}{2}\right) - i \sin\left(\frac{\phi}{2}\right) \right) \right)} .
\end{aligned} \tag{A.3}$$

Here, the phase  $\phi$  is defined through

$$\phi = \arctan \left( \frac{4D\zeta_I}{(v_0 + v_d)^2 + 4D \left( \frac{\omega_a c}{\rho_{\max}} + \omega_d + \zeta_R \right)} \right) . \tag{A.4}$$

For more clarity, we can write Eq.(A.3) as:

$$k_{\pm} = \frac{2D}{\operatorname{Re}[z] \mp i\operatorname{Im}[z]} = \frac{2D\operatorname{Re}[z]}{\operatorname{Re}[z]^2 + \operatorname{Im}[z]^2} \pm \frac{\operatorname{Im}[z]}{\operatorname{Re}[z]^2 + \operatorname{Im}[z]^2} \quad , \tag{A.5}$$

where

$$Re[z] = (v_0 + v_d) \pm \left( \left( (v_0 + v_d)^2 + 4D \left( \frac{\omega_a c}{\rho_{\max}} + \omega_d + \zeta_R \right) \right)^2 + (4D\zeta_I)^2 \right)^{1/4} \cos\left(\frac{\phi}{2}\right) \quad (\text{A.6})$$

and

$$Im[z] = (v_0 + v_d) \mp \left( \left( (v_0 + v_d)^2 + 4D \left( \frac{\omega_a c}{\rho_{\max}} + \omega_d + \zeta_R \right) \right)^2 + (4D\zeta_I)^2 \right)^{1/4} \sin\left(\frac{\phi}{2}\right) . \quad (\text{A.7})$$

Thus we see, that the real part of  $k_{\pm}$  is solely determined by the sign of  $Re[z]$ . Due to Eq.(A.4) one sees immediately from Eq.(A.6), that  $Re[k_+] > 0$  for all values of  $\zeta$ .

The real part of  $k_-$  can switch sign, depending on  $\zeta_R$  and  $\zeta_I$ . One sees, that for  $\zeta_I = 0$ , one recovers the same value of  $\zeta_c$ , as stated in chapter 3.

## Dimensionless variables

Most of our results are presented for dimensionless variables. For this, we introduced new dimensionless variables,

$$t^* = \omega_d t \quad (\text{A.8})$$

$$x^* = \frac{x}{\sqrt{D/\omega_d}} \quad (\text{A.9})$$

$$\rho^* = \rho/\rho_{\max} . \quad (\text{A.10})$$

With these, we can rewrite Eq.(3.9) and Eq.(3.10) and get

$$\partial_{t^*} \rho^* - \partial_{x^*}^2 \rho^* - (v_m^* + v_d^*) \partial_{x^*} \rho^* + (1 + c^*) \rho^* - c^* = 0 , \quad (\text{A.11})$$

where

$$v_m^* = v_0^* (1 - 2\rho^*) , \quad (\text{A.12})$$

$$v_0^* = \frac{v_0}{\sqrt{D\omega_d}} , \quad (\text{A.13})$$

$$v_d^* = \Omega_0^* + \Omega_1^* \rho_0^* + \Omega_2^* \rho_0^{*2} , \quad (\text{A.14})$$

$$\Omega_0^* = \frac{\Omega_0}{\rho_{\max} \sqrt{D\omega_d}} , \quad (\text{A.15})$$

$$\Omega_1^* = \frac{\Omega_1}{\sqrt{D\omega_d}} , \quad (\text{A.16})$$

$$\Omega_2^* = \frac{\Omega_2 \rho_{\max}}{\sqrt{D\omega_d}} , \quad (\text{A.17})$$

$$c^* = \frac{\omega_a c}{\omega_d \rho_{\max}} , \quad (\text{A.18})$$

$$(\text{A.19})$$

and

$$\partial_{x^*} \rho_0^* = -J^*(\rho_0^*) - v_d^* \rho_0^* \quad (\text{A.20})$$

with

$$J^*(\rho_0^*) = J_0^* + J_1^* \rho_0^* + J_2^* \rho_0^{*2} \quad , \quad (\text{A.21})$$

$$J_0^* = \frac{J_0}{\rho_{\max} \sqrt{D\omega_d}} \quad , \quad (\text{A.22})$$

$$J_1^* = \frac{J_1}{\sqrt{D\omega_d}} \quad , \quad (\text{A.23})$$

$$J_2^* = \frac{J_2 \rho_{\max}}{\sqrt{D\omega_d}} \quad . \quad (\text{A.24})$$

$$(\text{A.25})$$

## Dimensionless variables in the case of applied forces

We introduce new dimensionless variables for the time  $t$ , the space coordinate  $x$  and the density variables  $\rho_b, \rho_u$ :

$$t^* = t\omega_d^0 \quad (\text{A.26})$$

$$x^* = x / \sqrt{\frac{D_b}{\omega_d^0}} \quad (\text{A.27})$$

$$\rho_b^* = \rho_b / \rho_{b,\max} \quad (\text{A.28})$$

$$\rho_u^* = \rho_u / \rho_{b,\max} \quad (\text{A.29})$$

$$(\text{A.30})$$

With these we get the following equations for the density of bound motors:

$$\partial_{t^*} \rho_b^* + \partial_{x^*} j_b^* = \omega_a^* (1 - \rho_b^*) \rho_u^* - \omega_d(x)^* \rho_b^* \quad (\text{A.31})$$

$$j_b^* = -\partial_{x^*} \rho_b^* - v_d^* \rho_b^* + (v_0^* + f^*) \left( \rho_b^* - \frac{\rho_b^{*2}}{2} \right) \quad , \quad (\text{A.32})$$

while the density of unbound motors obeys:

$$\partial_{t^*} \rho_u^* + \partial_{x^*} j_u^* = \omega_d(x)^* \rho_b^* - \omega_a^* (1 - \rho_b^*) \rho_u^* - j_b^*(\rho_{b,0}^*) \delta^*(x^*) \quad (\text{A.33})$$

$$j_u^* = -\partial_{x^*} \rho_u^* - \nu^* (x^* - x_B^*) \rho_u^* - v_d^* \rho_u^* \quad . \quad (\text{A.34})$$

The new dimensionless variables are given by:

$$\omega_a^* = \omega_a / \omega_d^0 \quad (\text{A.35})$$

$$\omega_d(x)^* = e^{k^* \epsilon^* |x^* - x_B^*|} \quad (\text{A.36})$$

$$\epsilon^* = \epsilon / \sqrt{\frac{D_b}{\omega_d^0}} \quad (\text{A.37})$$

$$k^* = k D_b / (2 k_B T \omega_d^0) \quad (\text{A.38})$$

$$\nu^* = \nu / \omega_d^0 \quad (\text{A.39})$$

$$v_d^* = \Omega_0^* + \Omega_1^* \rho_{b,0}^* + \Omega_2^* \rho_{b,0}^{*2} \quad (\text{A.40})$$

$$v_0^* = v_0 / \sqrt{D_b \omega_d^0} \quad (\text{A.41})$$

$$f^* = \frac{-\mu k (\bar{x} - \bar{x}_B)}{\omega_d^0} \quad (\text{A.42})$$

where the dimensionless expansion coefficients are defined as:

$\Omega_0^* = \Omega_0 / (\rho_{b,\max} \sqrt{D_b \omega_d^0})$ ,  $\Omega_1^* = \Omega_1 / \sqrt{D_b \omega_d^0}$ ,  $\Omega_2^* = \Omega_2 \rho_{b,\max} / \sqrt{D_b \omega_d^0}$ . The equilibrium distribution reads:

$$\rho_u^* = N_u B^* e^{-k^* (x^* - x_B^*)^2} \quad , \quad (\text{A.43})$$

with  $B^* = \sqrt{k^* / \pi}$ .

The equation of motion for the anchoring point is then given by:

$$\xi^* \partial_{t^*} x_B^* = k^* \int (x^* - x_B^*) \rho_b^* dx^* + f_{\text{ext}}^* - \xi^* v_d^* \quad , \quad (\text{A.44})$$

with

$$\xi^* = \frac{\xi \sqrt{D_b \omega_d^0}}{2 k_B T \rho_{b,\max}} \quad (\text{A.45})$$

$$f_{\text{ext}}^* = \frac{f_{\text{ext}}}{2 k_B T \rho_{b,\max}} \quad . \quad (\text{A.46})$$

The fraction of unbound motors evolves in time corresponding to:

$$\begin{aligned} \partial_{t^*} N_u = & \int \rho_b^* e^{k^* \epsilon^* |x^* - x_B^*|} dx^* - \omega_a^* N_u B^* \int (1 - \rho_b^*) e^{-k^* (x^* - x_B^*)^2} dx^* \\ & - j_b^*(\rho_{b,0}) \quad . \end{aligned} \quad (\text{A.47})$$



## Master and evolution equations for the one-dimensional discrete model

### Dynamic equations for average occupation numbers

Starting from the master equation, Eq(4.4), we will in the following derive the equations, governing the dynamics of average occupation numbers. The master equation for the  $i$ th site reads:

$$\begin{aligned}
\partial_t P(n_i) = & \bar{\omega}_h (P(n_{i-1} = 1, n_i = 0) + P(n_i = 0, n_{i+1} = 1) \\
& - P(n_{i-1} = 0, n_i = 1) - P(n_i = 1, n_{i+1} = 0)) \\
& - \bar{\omega}_v (P(n_i = 0, n_{i+1} = 1) - P(n_i = 1, n_{i-1} = 0)) \\
& + \bar{p}\bar{\Omega} (P(n_1 = 1, n_2 = 0, n_{i+1} = 1) - P(n_1 = 1, n_2 = 0, n_i = 1)) \\
& + (1 - \bar{p})\bar{\Omega} (P(n_1 = 1, n_{i+1} = 1) - P(n_1 = 1, n_i = 1)) \\
& + \bar{\omega}_a P(n_i = 0) - \bar{\omega}_d P(n_i = 1) \quad , \tag{B.1}
\end{aligned}$$

Using the fact, that

$$P(n_i) = P(n_i, n_{i+1} = 1) + P(n_i, n_{i+1} = 0) \quad , \tag{B.2}$$

one can rewrite Eq.(B.1):

$$\begin{aligned}
\partial_t P(n_i) = & \bar{\omega}_h (P(n_{i-1} = 1) - P(n_{i-1} = 1, n_i = 1) + P(n_{i+1} = 1) - P(n_i = 1, n_{i+1} = 1) \\
& - P(n_i = 1) - P(n_i = 1, n_{i-1} = 1) + P(n_i = 1) - P(n_i = 1, n_{i+1} = 1)) \\
& - \bar{\omega}_v (P(n_{i+1} = 1) - P(n_{i+1} = 1, n_i = 1) - P(n_i = 1) + P(n_i = 1, n_{i-1} = 1)) \\
& + \bar{p}\bar{\Omega} (P(n_1 = 1, n_{i+1} = 1) - P(n_1 = 1, n_2 = 1, n_{i+1} = 1) \\
& - P(n_1 = 1, n_i = 1) + P(n_1 = 1, n_2 = 1, n_i = 1)) \\
& + (1 - \bar{p})\bar{\Omega} (P(n_1 = 1, n_{i+1} = 1) - P(n_1 = 1, n_i = 1)) \\
& + \bar{\omega}_a (1 - P(n_i = 1)) - \bar{\omega}_d P(n_i = 1) \quad , \tag{B.3}
\end{aligned}$$

Using now the definition of the average occupation of the binding sides,

$$\langle n_i \rangle = \sum_{n_i=0}^1 n_i P(n_i) = P(n_i = 1) \quad , \quad (\text{B.4})$$

$$\begin{aligned} \langle n_i n_{i\pm 1} \rangle &= \sum_{n_{i\pm 1}=0}^1 \sum_{n_i=0}^1 n_i n_{i\pm 1} P(n_i, n_{i\pm 1}) \\ &= P(n_i = 1, n_{i\pm 1} = 1) \quad , \end{aligned} \quad (\text{B.5})$$

we can rewrite Eq.(B.3) in terms of average occupation numbers and get the dynamic equation for the average occupation numbers, for  $i \geq 2$ :

$$\begin{aligned} \frac{d\langle n_i \rangle}{dt} &= \bar{\omega}_h (\langle n_{i+1} \rangle - 2\langle n_i \rangle + \langle n_{i-1} \rangle) \\ &\quad + \bar{\omega}_v (\langle n_{i+1} (1 - n_i) \rangle - \langle n_i (1 - n_{i+1}) \rangle) \\ &\quad + \bar{\omega}_a c \langle 1 - n_i \rangle - \bar{\omega}_d \langle n_i \rangle \\ &\quad + \langle \bar{\Omega}^{A,B} n_1 (n_{i+1} - n_i) \rangle \quad . \end{aligned} \quad (\text{B.6})$$

Rewriting Eq.(4.5) for the first binding site in the same way,

$$\begin{aligned} \partial_t P(n_1) &= \bar{\omega}_h (P(n_2 = 1) - P(n_1 = 1, n_2 = 1) - P(n_1 = 1) - P(n_1 = 1, n_2 = 1)) \\ &\quad + \bar{\omega}_v (P(n_2 = 1) - P(n_1 = 1, n_2 = 1)) \\ &\quad + (1 - \bar{p}) \bar{\Omega} (P(n_1 = 1, n_{i+1} = 1) - P(n_1 = 1, n_i = 1)) \\ &\quad + \bar{\Omega}_a (1 - P(n_1 = 1)) - \bar{\Omega}_d P(n_i = 1) \quad , \end{aligned} \quad (\text{B.7})$$

we get for the rate of change of the average occupation number of the binding site at the filament end,  $i = 1$ ,

$$\begin{aligned} \frac{d\langle n_1 \rangle}{dt} &= \bar{\omega}_h \langle n_2 - n_1 \rangle \\ &\quad + \bar{\omega}_v \langle n_2 - n_1 \rangle \\ &\quad + \bar{\Omega}_a c \langle 1 - n_1 \rangle - \bar{\Omega}_d \langle n_1 \rangle \\ &\quad - (1 - \bar{p}) \bar{\Omega} \langle n_1 (1 - n_2) \rangle \quad . \end{aligned} \quad (\text{B.8})$$

## Subunit labelling and rate determination on an array of sublattices

Sublattices arranged in parallel in  $y$ -direction are labelled  $j = 1, \dots, Y$  and binding sites in  $x$ -direction on a sublattice are labelled  $i = 1, 2, \dots$ . Due to differences in the amount of subunit removal on the individual sublattices, neighbouring binding sites on adjacent sublattices will in general have different coordinates  $i$  in  $x$ -direction. Denoting the number of removed subunits from the  $j$ th and the  $(j \pm 1)$ th protofilament with  $m_j$  and  $m_{j \pm 1}$  respectively, the neighbouring binding sites of site  $(i, j)$  on adjacent sublattices are given by:

**( $j + 1$ )-th sublattice:**

$$(i, j) \rightarrow (i + \Delta m_{j,j+1} - 1, j + 1) \quad \text{with} \quad \Delta m_{j,j+1} \geq 2 - i \quad , \quad (\text{C.1})$$

(left neighbouring site)

$$(i, j) \rightarrow (i + \Delta m_{j,j+1}, j + 1) \quad \text{with} \quad \Delta m_{j,j+1} \geq 1 - i \quad , \quad (\text{C.2})$$

(right neighbouring site)

(C.3)

**( $j - 1$ )-th sublattice:**

$$(i, j) \rightarrow (i + \Delta m_{j,j-1}, j - 1) \quad \text{with} \quad \Delta m_{j,j-1} \geq 1 - i \quad , \quad (\text{C.4})$$

(left neighbouring site)

$$(i, j) \rightarrow (i + \Delta m_{j,j-1} + 1, j - 1) \quad \text{with} \quad \Delta m_{j,j-1} \geq -i \quad , \quad (\text{C.5})$$

(right neighbouring site)

with  $\Delta m_{j,j \pm 1} = m_j - m_{j \pm 1}$ .

Extra care has to be taken between the 1st and  $Y$ th-sublattice. As the offset between these two sublattices is given by  $(Y - 1)\delta$  instead of just  $\delta$ , labelling of neighbouring binding sites not

only depends on the difference of the amount of removed subunits between the corresponding sublattices, but also on the offset and the number of sublattices,  $Y$ . The neighbouring binding sites of site  $(i, j = Y)$  on the first sublattice are given by:

**(1)-st sublattice:**

$$(i, Y) \rightarrow (i + \Delta m_{y,1} + [(Y - 1)\delta/a], 1) \quad \text{with} \quad \Delta m_{y,1} \geq 1 - i - [(Y - 1)\delta/a] \quad , \quad (\text{C.6})$$

(left neighbouring site)

$$(i, Y) \rightarrow (i + \Delta m_{y,1} + [(Y - 1)\delta/a] + 1), \quad \text{with} \quad \Delta m_{y,1} \geq -i - [(Y - 1)\delta/a] \quad . \quad (\text{C.7})$$

(right neighbouring site)

The neighbouring binding sites of  $(i, j = 1)$  on the last protofilament are given by:

**(Y)-th sublattice:**

$$(i, 1) \rightarrow (i + \Delta m_{1,y} - [(Y - 1)\delta/a] - 1, Y) \quad \text{with} \quad \Delta m_{1,y} \geq 2 - i + [(Y - 1)\delta/a] \quad , \quad (\text{C.8})$$

(left neighbouring site)

$$(i, 1) \rightarrow (i + (m_1 - m_Y) - [(Y - 1)\delta/a], Y) \quad \text{with} \quad \Delta m_{1,y} \geq 1 - i + [(Y - 1)\delta/a] \quad , \quad (\text{C.9})$$

(right neighbouring site)

where the Gauss brackets,  $[(Y - 1)\delta/a]$ , denote the largest integer less than or equal to  $(Y - 1)\delta/a$ .

## Hopping rates and processivity at the seam

A simple geometrical consideration, leads to the following hopping rates between binding sites on the  $Y$ th and the 1st protofilament:

$$\bar{\omega}_{h,Y}^{l,1} = \bar{\omega}_{h,1}^{r,Y} = \bar{\omega}_{h,y}(1 - ((Y - 1)\delta/a - [(Y - 1)\delta/a])) \quad , \quad (\text{C.10})$$

$$\bar{\omega}_{h,Y}^{r,1} = \bar{\omega}_{h,1}^{l,Y} = \bar{\omega}_{h,y}((Y - 1)\delta/a - [(Y - 1)\delta/a]) \quad , \quad (\text{C.11})$$

where  $[\dots]$ , are again the Gauss brackets.

For rebinding at the seam between  $Y$ th and 1st filament, the same considerations as for the hopping rate lead to:

$$\bar{p}_y^{Y \rightarrow 1, l} = \bar{p}_y^{1 \rightarrow Y, r} = \frac{1}{4} \bar{p}_y (1 - ((Y - 1)\delta/a - [(Y - 1)\delta/a])) \quad , \quad (\text{C.12})$$

$$\bar{p}_y^{Y \rightarrow 1, r} = \bar{p}_y^{1 \rightarrow Y, l} = \frac{1}{4} \bar{p}_y ((Y - 1)\delta/a - [(Y - 1)\delta/a]) \quad . \quad (\text{C.13})$$

Note, that because of the seam, the diagonal symmetry of the array is broken, leading to the following inequalities in the hopping rate between sublattices,

$$\bar{\omega}_{h,Y}^{l,1} \neq \bar{\omega}_{h,Y}^{r,Y-1} \quad , \quad (\text{C.14})$$

$$\bar{\omega}_{h,Y}^{r,1} \neq \bar{\omega}_{h,Y}^{l,Y-1} \quad . \quad (\text{C.15})$$

$$(\text{C.16})$$

and

$$\bar{\omega}_{h,1}^{1,2} \neq \bar{\omega}_{h,1}^{r,Y} \quad , \quad (\text{C.17})$$

$$\bar{\omega}_{h,1}^{r,2} \neq \bar{\omega}_{h,1}^{1,Y} \quad . \quad (\text{C.18})$$

and in the probability to rebind on adjacent sublattices after subunit removal:

$$\bar{p}_y^{Y \rightarrow 1,1} \neq \bar{p}_y^{Y \rightarrow Y-1,r} \quad , \quad (\text{C.19})$$

$$\bar{p}_y^{Y \rightarrow 1,r} \neq \bar{p}_y^{Y \rightarrow Y-1,1} \quad , \quad (\text{C.20})$$

and

$$\bar{p}_y^{1 \rightarrow 2,1} \neq \bar{p}_y^{1 \rightarrow Y,r} \quad , \quad (\text{C.21})$$

$$\bar{p}_y^{1 \rightarrow 2,r} \neq \bar{p}_y^{1 \rightarrow Y,1} \quad . \quad (\text{C.22})$$



## Master equations for the two-dimensional discrete model

### Master equations for model A

Filament end,  $i = 1$ :

$$\begin{aligned}
\partial_t P(n_{1,j}; m_j) = & \bar{\omega}_{h,x} (P(n_{2,j} = 1, n_{1,j} = 0; m_j) - P(n_{1,j} = 1, n_{2,j} = 0; m_j)) \\
& + \bar{\omega}_{h,y} (P(n_{1,j} = 0, n_{m_j - m_{j+1} + 1, j+1} = 1; m_{j-1} \geq m_{j+1}) \\
& \quad + P(n_{1,j} = 0, n_{m_j - m_{j+1}, j+1} = 1; m_{j-1} > m_{j+1}) \\
& \quad + P(n_{1,j} = 0, n_{m_j - m_{j-1} + 2, j-1} = 1; m_j + 1 \geq m_{j-1}) \\
& \quad + P(n_{1,j} = 0, n_{m_j - m_{j-1} + 1, j-1} = 1; m_j + 1 > m_{j-1}) \\
& \quad - P(n_{1,j} = 1, n_{m_j - m_{j+1} + 1, j+1} = 0; m_{j-1} \geq m_{j+1}) \\
& \quad - P(n_{1,j} = 1, n_{m_j - m_{j+1}, j+1} = 0; m_{j-1} > m_{j+1}) \\
& \quad - P(n_{1,j} = 1, n_{m_j - m_{j-1} + 2, j-1} = 0; m_j + 1 \geq m_{j-1}) \\
& \quad - P(n_{1,j} = 1, n_{m_j - m_{j-1} + 1, j-1} = 0; m_j + 1 > m_{j-1})) \\
& + \bar{\omega}_v P(n_{2,j} = 1, n_{1,j} = 0; m_j) \\
& + \bar{\Omega}_a c P(n_{1,j} = 0) - \bar{\Omega}_d P(n_{1,j} = 1) \\
& - (1 - \bar{p}(\delta)) \bar{\Omega}_j(M) P(n_{1,j} = 1, n_{2,j} = 0; m_{j-1}) \\
& + \bar{p}_y(\delta) \bar{\Omega}_{j+1}(M) (P(n_{1,j+1} = 1, n_{1,j} = 0; m_{j+1} - 1 = m_j) \\
& \quad + P(n_{1,j+1} = 1, n_{1,j} = 0; m_{j+1} = m_j))
\end{aligned}$$

(D.1)



## Master equations for model B

Filament end,  $i = 1$ :

$$\begin{aligned}
\partial_t P(n_{1,j}; m_j) = & \bar{\omega}_{h,x} (P(n_{2,j} = 1, n_{1,j} = 0; m_j) - P(n_{1,j} = 1, n_{2,j} = 0; m_j)) \\
& + \bar{\omega}_{h,y} (P(n_{1,j} = 0, n_{m_j - m_{j+1} + 1, j+1} = 1; m_{j-1} \geq m_{j+1}) \\
& \quad + P(n_{1,j} = 0, n_{m_j - m_{j+1}, j+1} = 1; m_{j-1} > m_{j+1}) \\
& \quad + P(n_{1,j} = 0, n_{m_j - m_{j-1} + 2, j-1} = 1; m_j + 1 \geq m_{j-1}) \\
& \quad + P(n_{1,j} = 0, n_{m_j - m_{j-1} + 1, j-1} = 1; m_j + 1 > m_{j-1}) \\
& \quad - P(n_{1,j} = 1, n_{m_j - m_{j+1} + 1, j+1} = 0; m_{j-1} \geq m_{j+1}) \\
& \quad - P(n_{1,j} = 1, n_{m_j - m_{j+1}, j+1} = 0; m_{j-1} > m_{j+1}) \\
& \quad - P(n_{1,j} = 1, n_{m_j - m_{j-1} + 2, j-1} = 0; m_j + 1 \geq m_{j-1}) \\
& \quad - P(n_{1,j} = 1, n_{m_j - m_{j-1} + 1, j-1} = 0; m_j + 1 > m_{j-1})) \\
& + \bar{\omega}_v P(n_{2,j} = 1, n_{1,j} = 0; m_j) \\
& + \bar{\Omega}_a c P(n_{1,j} = 0) - \bar{\Omega}_d P(n_{1,j} = 1) \\
& - (1 - \bar{p}(\delta)) \bar{\Omega}_j(M) P(n_{1,j} = 1, n_{2,j} = 0; m_{j-1}) \\
& + \bar{p}_y(\delta) \bar{\Omega}_{j+1}(M) (P(n_{1,j+1} = 1, n_{1,j} = 0; m_{j+1} - 1 = m_j) \\
& \quad + P(n_{1,j+1} = 1, n_{1,j} = 0; m_{j+1} = m_j)) \\
& + \bar{p}_y(\delta) \bar{\Omega}_{j-1}(M_j) (P(n_{1,j-1} = 1, n_{1,j} = 0; m_{j-1} - 1 = m_j) \\
& \quad + P(n_{1,j-1} = 1, n_{1,j} = 0; m_{j-1} = m_j + 1)) \\
& - \bar{p}_y(\delta) \bar{\Omega}_j(M) (P(n_{1,j} = 1, n_{2,j} = 0; m_j - 1 > m_{j+1}) \\
& \quad - P(n_{1,j} = 1, n_{2,j} = 0; m_j - 1 \geq m_{j+1}) \\
& \quad - P(n_{1,j} = 1, n_{2,j} = 0; m_j \geq m_{j-1}) \\
& \quad - P(n_{1,j} = 1, n_{2,j} = 0; m_j > m_{j-1}))
\end{aligned} \tag{D.3}$$

Lattice bulk,  $i \geq 2$ :

$$\begin{aligned}
\partial_t P(n_{i,j}; m_j) = & \bar{\omega}_{h,x} (P(n_{i+1,j} = 1, n_{i,j} = 0; m_j) + P(n_{i-1,j} = 1, n_{i,j} = 0; m_j) \\
& \quad - P(n_{i,j} = 1, n_{i+1,j} = 0; m_j) - P(n_{i,j} = 1, n_{i-1,j} = 0; m_j)) \\
& \bar{\omega}_{h,y} (P(n_{i,j} = 0, n_{i+m_j - m_{j+1} - 1, j+1} = 1; m_j - m_{j+1} \geq 2 - i) \\
& \quad + P(n_{i,j} = 0, n_{i+m_j - m_{j+1}, j+1} = 1; m_j - m_{j+1} \geq 1 - i) \\
& \quad + P(n_{i,j} = 0, n_{i+m_j - m_{j-1}, j-1} = 1; m_j - m_{j-1} \geq 1 - i) \\
& \quad + P(n_{i,j} = 0, n_{i+m_j - m_{j-1} + 1, j-1} = 1; m_j - m_{j-1} \geq -i) \\
& \quad - P(n_{i,j} = 1, n_{i+m_j - m_{j+1} - 1, j+1} = 0; m_j - m_{j+1} \geq 2 - i) \\
& \quad - P(n_{i,j} = 1, n_{i+m_j - m_{j+1}, j+1} = 0; m_j - m_{j+1} \geq 1 - i) \\
& \quad - P(n_{i,j} = 1, n_{i+m_j - m_{j-1}, j-1} = 0; m_j - m_{j-1} \geq 1 - i) \\
& \quad - P(n_{i,j} = 1, n_{i+m_j - m_{j-1} + 1, j-1} = 0; m_j - m_{j-1} \geq -i))
\end{aligned} \tag{D.4}$$

$$\begin{aligned}
& +\bar{\omega}_v (P(n_{i+1,j} = 1, n_{i,j} = 0; m_j) - P(n_{i,j} = 1, n_{i-1,j} = 0; m_j)) \\
& +\bar{\omega}_a c P(n_{i,j} = 0; m_j) - \bar{\omega}_d P(n_{i,j} = 1; m_j) \\
& +\bar{\Omega}_j(M) (P(n_{1,j} = 1, n_{i+1} = 1; m_j - 1) \\
& \quad - P(n_{1,j} = 1, n_i = 1; m_j - 1)) \\
& +\bar{p}_y(\delta)\bar{\Omega}_{j+1}(M) (P(n_{1,j+1} = 1, n_{i,j} = 0; m_j - m_{j+1} = 2 - i) \\
& \quad + P(n_{1,j+1} = 1, n_{i,j} = 0; m_j - m_{j+1} = 1 - i)) \\
& +\bar{p}_y(\delta)\bar{\Omega}_{j-1}(M_j) (P(n_{1,j-1} = 1, n_{i,j} = 0; m_j - m_{j-1} = 1 - i) \\
& \quad + P(n_{1,j-1} = 1, n_{i,j} = 0; m_j - m_{j-1} = -i))
\end{aligned}$$

(D.5)

---

## Random deposition model

A very basic growth model of an interface is the so called random deposition model (RD). In this model, particles are dropped at random positions on a surface. The particles fall vertically, unless reaching a column of particles already accumulated or the surface. In this model, no spatial correlations between the different columns exist and each column grows independently from the neighbouring columns. In this simple case, one can analytically calculate the growth exponent  $\beta$ . Taking a one-dimensional interface of size  $Y$ , a particle accumulates with probability  $p = 1/Y$  everywhere along the interface. The probability to find a column of height  $h$  after  $N$  particles have been dropped, is then given by:

$$P(h, N) = \binom{N}{h} p^h (1-p)^{N-h} \quad (\text{E.1})$$

Using the definition of the first and second moment,

$$\langle h \rangle = \sum_{h=1}^N h P(h, N) \quad , \quad (\text{E.2})$$

$$\langle h^2 \rangle = \sum_{h=1}^N h^2 P(h, N) \quad , \quad (\text{E.3})$$

one gets for the width of the interface:

$$w^2(t) \equiv \langle h^2 \rangle - \langle h \rangle = \frac{N}{L} \left( 1 - \frac{1}{L} \right) \quad . \quad (\text{E.4})$$

Defining a time,  $t = N/L$ , by the mean-number of deposited layers, one gets,  $w^2(t) \sim t^{1/2}$ , and therefor  $\beta = 0.5$  (Barabasi and Stanley, 1995).

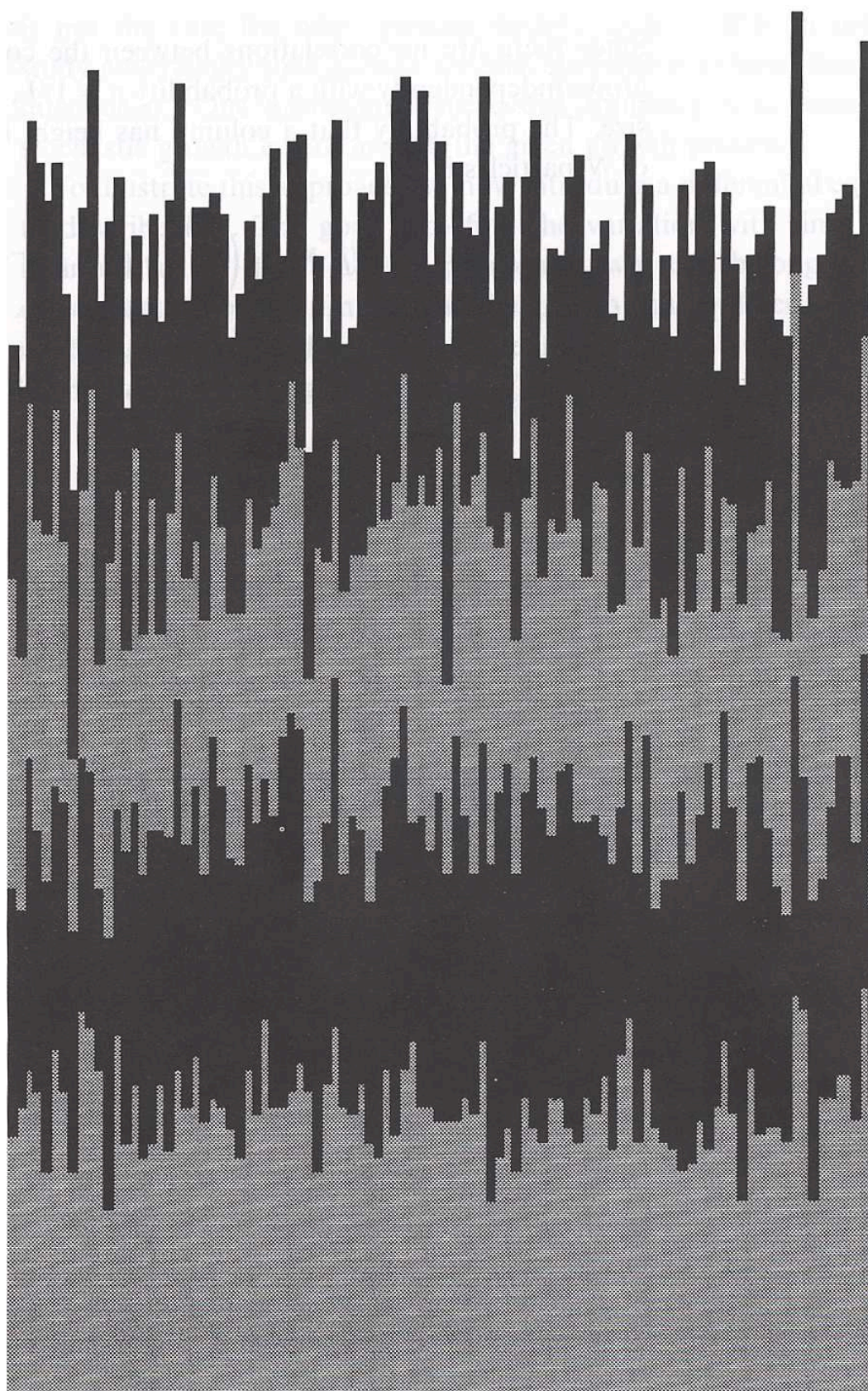


**Figure E.1:** Snapshot of a typical interface, generated by the random deposition model. After 4000 deposited particles, the colour was changed. Taken from (Barabasi and Stanley, 1995)

---

---

# Bibliography

- Y. Aghababaie, G. I. Menon, and M. Plischke. Universal properties of interacting brownian motors. *Physical Review E*, 59(3):2578, 1999.
- B. Alberts, A. Johnson, J. Lewis, M. Raff, K. Roberts, and P. Walter. *Molecular Biology Of The Cell*. Garland Science, 2002.
- P. D. Andrews, Y. Ovechkina, N. Morrice, M. Wagenbach, K. Duncan, L. Wordeman, and J. R. Swedlow. Aurora b regulates mcaK at the mitotic centromere. *Developmental Cell*, 6(2):253, 2004.
- C. L. Asbury, A. N. Fehr, and S. M. Block. Kinesin moves by an asymmetric hand-over-hand mechanism. *Science*, 302(5653):2130, 2003.
- R. D. Astumian and M. Bier. Fluctuation driven ratchets - molecular motors. *Physical Review Letters*, 72(11):1766, 1994.
- A.-L. Barabasi and H. Stanley. *Fractal Concepts In Surface Growth*. Cambridge University Press, 1995.
- S. T. Brady. A novel brain atpase with properties expected for the fast axonal-transport motor. *Nature*, 317(6032):73, 1985.
- D. Bray. *Cell Movements. From Molecules to Motility, 2nd edition*. Garland Publishing, New York, 2001.
- L. Cassimeris and J. Morabito. Tognp, the human homolog of xmap215/dis1, is required for centrosome integrity, spindle pole organization, and bipolar spindle assembly. *Molecular Biology Of The Cell*, 15(4):1580, 2004.
- S. R. de Groot and P. Mazur. *Non-Equilibrium Thermodynamics*. Dover Publications, New York, 1984.
- B. Derrida and M. Evans. The asymmetric exclusion model: exact results through a matrix approach. In: *Nonequilibrium Statistical Mechanics in One Dimension*, ed. V. Privman, page 277, 1997.
- A. Desai, S. Verma, T. J. Mitchison, and C. E. Walczak. Kin i kinesins are microtubule-destabilizing enzymes. *Cell*, 96(1):69, 1999.

## 120 BIBLIOGRAPHY

- M. Dogterom. Polymerization forces. in *Physics of bio-molecules and cells, Les Houches, Session LXXV*, 2001.
- M. Dogterom, J. W. Kerssemakers, G. Romet-Lemonne, and M. E. Janson. Force generation by dynamic microtubules. *Current Opinion In Cell Biology*, 17(1):67, 2005.
- M. Dogterom and S. Leibler. Physical aspects of the growth and regulation of microtubule structures. *Physical Review Letters*, 70(9):1347, 1993.
- M. Dogterom and B. Yurke. Measurement of the force-velocity relation for growing microtubules. *Science*, 278(5339):856, 1997.
- S. a. Endow, R. Chandra, D. J. Komma, a. H. Yamamoto, and E. D. Salmon. Mutants of the drosophila *ncd* microtubule motor protein cause centrosomal and spindle pole defects in mitosis. *Journal of Cell Science*, 107:859, 1994a.
- S. a. Endow, S. J. Kang, L. L. Satterwhite, M. D. Rose, V. P. Skeen, and E. D. Salmon. Yeast *kar3* is a minus-end microtubule motor protein that destabilizes microtubules preferentially at the minus ends. *Embo Journal*, 13(11):2708, 1994b.
- H. Flyvbjerg, T. E. Holy, and S. Leibler. Stochastic dynamics of microtubules - a model for caps and catastrophes. *Physical Review Letters*, 73(17):2372, 1994.
- H. Flyvbjerg, T. E. Holy, and S. Leibler. Microtubule dynamics: Caps, catastrophes, and coupled hydrolysis. *Physical Review E*, 54(5):5538, 1996.
- D. K. Fygenson, J. F. Marko, and A. Libchaber. Mechanics of microtubule-based membrane extension. *Physical Review Letters*, 79(22):4497, 1997.
- J. Gaetz and T. M. Kapoor. Dynein/dynactin regulate metaphase spindle length by targeting depolymerizing activities to spindle poles. *Molecular Biology Of The Cell*, 15:396A, 2004.
- R. Gandhi, S. Bonaccorsi, D. B. Wentworth, M. Gatti, and A. J. Pereira. The *kfp67a* astral microtubule motor is required for proper spindle assembly during mitosis and male meiosis. *Molecular Biology of the Cell*, 13:322A, 2002.
- N. J. Ganem and D. A. Compton. The kini kinesin *kif2a* is required for bipolar spindle assembly through a functional relationship with *mcak*. *Journal Of Cell Biology*, 166(4):473, 2004.
- I. R. Gibbons. Cilia and flagella of eukaryotes. *Journal Of Cell Biology*, 91(3):S107, 1981.
- I. R. Gibbons and a. J. Rowe. Dynein - a protein with adenosine triphosphatase activity from cilia. *Science*, 149(3682):424, 1965.
- F. Gittes, B. Mickey, J. Nettleton, and J. Howard. Flexural rigidity of microtubules and actin-filaments measured from thermal fluctuations in shape. *Journal of Cell Biology*, 120(4):923, 1993.
- P. Hanggi, F. Marchesoni, and F. Nori. Brownian motors. *Annalen Der Physik*, 14(1-3):51, 2005.

- Y. Harada, A. Noguchi, A. Kishino, and T. Yanagida. Sliding movement of single actin-filaments on one-headed myosin-filaments. *Nature*, 326(6115):805, 1987.
- M. Hatsumi and S. a. Endow. Mutants of the microtubule motor protein, nonclaret disjunctional, affect spindle structure and chromosome movement in meiosis and mitosis. *Journal of Cell Science*, 101:547, 1992.
- J. Helenius, G. Brouhard, Y. Kalaidzidis, S. Diez, and J. Howard. The depolymerizing kinesin mcak uses 1-dimensional diffusion to rapidly target the ends of microtubules. submitted.
- T. Hill. Theoretical formalism for the sliding filament model of contraction of striated muscle. part i. *Prog. Biophys. Mol. Biol.*, 28:267, 1974.
- T. Hill. *Linear Aggregation Theory in Cell Biology*. Springer -Verlag, New York, Berlin, Heidelberg, 1987.
- E. Hirakawa, H. Higuchi, and Y. Y. Toyoshima. Processive movement of single 22s dynein molecules occurs only at low atp concentrations. *Proceedings of the National Academy of Sciences of the United States of America*, 97(6):2533, 2000.
- N. Hirokawa. Kinesin and dynein superfamily proteins and the mechanism of organelle transport. *Science*, 279(5350):519, 1998.
- T. E. Holy and S. Leibler. Dynamic instability of microtubules as an efficient way to search in-space. *Proceedings Of The National Academy Of Sciences Of The United States Of America*, 91(12):5682, 1994.
- N. Homma, Y. Takei, Y. Tanaka, T. Nakata, S. Terada, M. Kikkawa, Y. Noda, and N. Hirokawa. Kinesin superfamily protein 2a (kif2a) functions in suppression of collateral branch extension. *Cell*, 114(2):229, 2003.
- J. Howard. *Mechanics of motor proteins and the cytoskeleton*. 2001.
- A. J. Hunt, F. Gittes, and J. Howard. The force exerted by a single kinesin molecule against a viscous load. *Biophysical Journal*, 67(2):766, 1994.
- A. W. Hunter, M. Caplow, D. L. Coy, W. O. Hancock, S. Diez, L. Wordeman, and J. Howard. The kinesin-related protein mcak is a microtubule depolymerase that forms an atp-hydrolyzing complex at microtubule ends. *Molecular Cell*, 11(2):445, 2003.
- A. W. Hunter and L. Wordeman. How motor proteins influence microtubule polymerization dynamics. *Journal of Cell Science*, 113(24):4379, 2000.
- H. E. Huxley. The double array of filaments in cross-striated muscle. *Journal of Biophysical and Biochemical Cytology*, 3(5):631, 1957.
- S. Inoue and E. D. Salmon. Force generation by microtubule assembly disassembly in mitosis and related movements. *Molecular Biology Of The Cell*, 6(12):1619, 1995.
- F. Julicher, A. Ajdari, and J. Prost. Modeling molecular motors. *Reviews Of Modern Physics*, 69(4):1269, 1997.

- Kinesin-Homepage. <http://www.proweb.org/kinesin/index.html>.
- G. A. Klein, K. Kruse, G. Cuniberti, and F. Julicher. Filament depolymerization by motor molecules. *Physical Review Letters*, 94(10), 2005.
- S. L. Kline-Smith, A. Khodjakov, P. Hergert, and C. E. Walczak. Depletion of centromeric mcaak leads to chromosome congression and segregation defects due to improper kinetochore attachments. *Molecular Biology Of The Cell*, 15(3):1146, 2004.
- S. L. Kline-Smith and C. E. Walczak. Mitotic spindle assembly and chromosome segregation: Refocusing on microtubule dynamics. *Molecular Cell*, 15(3):317, 2004.
- S. Klumpp and R. Lipowsky. Phase transitions in systems with two species of molecular motors. *Europhysics Letters*, 66(1):90, 2004.
- A. B. Kolomeisky and M. E. Fisher. Force-velocity relation for growing microtubules. *Biophysical Journal*, 80(1):149, 2001.
- A. B. Kolomeisky and B. Widom. A simplified "ratchet" model of molecular motors. *Journal of Statistical Physics*, 93(3-4):633, 1998.
- H. a. Kramers. Brownian motion in a field of force and the diffusion model of chemical reactions. *Physica*, 7:284, 1940.
- S. J. Kron and J. A. Spudich. Fluorescent actin-filaments move on myosin fixed to a glass-surface. *Proceedings Of The National Academy Of Sciences Of The United States Of America*, 83(17):6272, 1986.
- K. Kruse and K. Sekimoto. Growth of fingerlike protrusions driven by molecular motors. *Physical Review E*, 66(3):031904, 2002.
- W. Kuehne, Wagenschieber, H. Kuehne, C. Kofoid, and L. Museum. Untersuchungen ber das protoplasma und die contractilititt. 1864.
- W. J. Lan, X. Zhang, S. L. Kline-Smith, S. E. Rosasco, G. A. Barrett-Wilt, J. Shabanowitz, C. E. Walczak, and P. T. Stukenberg. Aurora b phosphorylates centromeric mcaak and regulates its localization and microtubule depolymerization activity. *Current Biology*, 14(4):273, 2004.
- C. J. Lawrence, R. K. Dawe, K. R. Christie, D. W. Cleveland, S. C. Dawson, S. A. Endow, L. S. B. Goldstein, H. V. Goodson, N. Hirokawa, J. Howard, R. L. Malmberg, J. R. McIntosh, H. Miki, T. J. Mitchison, Y. Okada, A. S. N. Reddy, W. M. Saxton, M. Schliwa, J. M. Scholey, R. D. Vale, C. E. Walczak, and L. Wordeman. A standardized kinesin nomenclature. *Journal of Cell Biology*, 167(1):19, 2004.
- S. Leibler and D. A. Huse. A physical model for motor proteins. *Comptes Rendus De L Academie Des Sciences Serie Iii-Sciences De La Vie-Life Sciences*, 313(1):27, 1991.
- S. Leibler and D. A. Huse. Porters versus rowers - a unified stochastic-model of motor proteins. *Journal Of Cell Biology*, 121(6):1357, 1993.

- R. Lipowsky, S. Klumpp, and T. M. Nieuwenhuizen. Random walks of cytoskeletal motors in open and closed compartments. *Physical Review Letters*, 8710(10):108101, 2001.
- H. Lodish, A. Berk, P. Matsudaira, C. Kaiser, M. Krieger, M. Scott, S. Zipursky, and J. Darnell. *Molecular Cell Biology*. W.H. Freeman and Company, New York, 2003.
- M. O. Magnasco. Forced thermal ratchets. *Physical Review Letters*, 71(10):1477, 1993.
- T. Maney, M. Wagenbach, and L. Wordeman. Molecular dissection of the microtubule depolymerizing activity of mitotic centromere-associated kinesin. *Journal of Biological Chemistry*, 276(37):34753, 2001.
- A. D. Mehta, R. S. Rock, M. Rief, J. A. Spudich, M. S. Mooseker, and R. E. Cheney. Myosin-v is a processive actin-based motor. *Nature*, 400(6744):590, 1999.
- H. Miki, M. Setou, K. Kaneshiro, and N. Hirokawa. All kinesin superfamily protein, kif, genes in mouse and human. *Proceedings of the National Academy of Sciences of the United States of America*, 98(13):7004, 2001.
- T. Mitchison and M. Kirschner. Dynamic instability of microtubule growth. *Nature*, 312(5991):237, 1984.
- H. Miyata, S. Nishiyama, K. Akashi, and K. Kinosita. Protrusive growth from giant liposomes driven by actin polymerization. *Proceedings Of The National Academy Of Sciences Of The United States Of America*, 96(5):2048, 1999.
- A. Mogilner and G. Oster. The polymerization ratchet model explains the force-velocity relation for growing microtubules. *European Biophysics Journal With Biophysics Letters*, 28(3):235, 1999.
- A. Moore and L. Wordeman. C-terminus of mitotic centromere-associated kinesin (mcak) inhibits its lattice-stimulated atpase activity. *Biochemical Journal*, 383:227, 2004.
- C. A. Moores, M. Yu, J. Guo, C. Beraud, R. Sakowicz, and R. A. Milligan. A mechanism for microtubule depolymerization by kini kinesins. *Molecular Cell*, 9(4):903, 2002.
- Myosin-Homepage. <http://www.mrc-lmb.cam.ac.uk/myosin/myosin.html>.
- P. Nelson. *Biological physics - energy, information, life*. 2004.
- H. Niederstrasser, H. Salehi-Had, E. C. Gan, C. Walczak, and E. Nogales. Xkcm1 acts on a single protofilament and requires the c terminus of tubulin. *Journal Of Molecular Biology*, 316(3):817, 2002.
- K. Nishinari, Y. Okada, A. Schadschneider, and D. Chowdhury. Intracellular transport of single-headed molecular motors kif1a. *Physical Review Letters*, 95(11), 2005.
- Y. Noda, R. Satoyoshitake, S. Kondo, M. Nangaku, and N. Hirokawa. Kif2 is a new microtubule-based anterograde motor that transports membranous organelles distinct from those carried by kinesin heavy-chain or kif3a/b. *Journal of Cell Biology*, 129(1):157, 1995.

- T. Ogawa, R. Nitta, Y. Okada, and N. Hirokawa. A common mechanism for microtubule destabilizers - m type kinesins stabilize curling of the protofilament using the class-specific neck and loops. *Cell*, 116(4):591, 2004.
- R. Ohi, M. L. Coughlin, W. S. Lane, and T. J. Mitchison. An inner centromere protein that stimulates the microtubule depolymerizing activity of a kinl kinesin. *Developmental Cell*, 5(2):309, 2003.
- R. Ohi, T. Sapra, J. Howard, and T. J. Mitchison. Differentiation of cytoplasmic and meiotic spindle assembly mca functions by aurora b-dependent phosphorylation. *Molecular Biology Of The Cell*, 15(6):2895, 2004.
- K. Oiwa and H. Sakakibara. Recent progress in dynein structure and mechanism. *Current Opinion in Cell Biology*, 17(1):98, 2005.
- Y. Ovechkina, M. Wagenbach, and L. Wordeman. K-loop insertion restores microtubule depolymerizing activity of a "neckless" mca mutant. *Journal Of Cell Biology*, 159(4):557, 2002.
- Y. Ovechkina and L. Wordeman. Unconventional motoring: An overview of the kin c and kin i kinesins. *Traffic*, 4(6):367, 2003.
- D. Pantaloni, C. Le Clainche, and M. F. Carrier. Cell biology - mechanism of actin-based motility. *Science*, 292(5521):1502, 2001.
- A. Parmeggiani, T. Franosch, and E. Frey. Phase coexistence in driven one-dimensional transport. *Physical Review Letters*, 90(8):086601, 2003.
- A. Parmeggiani, T. Franosch, and E. Frey. Totally asymmetric simple exclusion process with langmuir kinetics. *Physical Review E*, 70(4):046101, 2004.
- A. Parmeggiani, F. Julicher, A. Ajdari, and J. Prost. Energy transduction of isothermal ratchets: Generic aspects and specific examples close to and far from equilibrium. *Physical Review E*, 60(2):2127, 1999.
- a. J. Pereira, B. Dalby, R. J. Stewart, S. J. Doxsey, and L. S. B. Goldstein. Mitochondrial association of a plus end-directed microtubule motor expressed during mitosis in drosophila. *Journal of Cell Biology*, 136(5):1081, 1997.
- C. S. Peskin, G. B. Ermentrout, and G. F. Oster. *in Cell Mechanics and Cellular Engineering*. Springer, New York, 1994.
- C. S. Peskin, G. M. Odell, and G. F. Oster. Cellular motions and thermal fluctuations - the brownian ratchet. *Biophysical Journal*, 65(1):316, 1993.
- T. D. Pollard and G. G. Borisy. Cellular motility driven by assembly and disassembly of actin filaments. *Cell*, 112(4):453, 2003.
- J. Prost, J. F. Chauwin, L. Peliti, and A. Ajdari. Asymmetric pumping of particles. *Physical Review Letters*, 72(16):2652, 1994.

- D. Pruyne, M. Evangelista, C. S. Yang, E. F. Bi, S. Zigmond, A. Bretscher, and C. Boone. Role of formins in actin assembly: Nucleation and barbed-end association. *Science*, 297(5581):612, 2002.
- S. L. Reck-Peterson, M. J. Tyska, P. J. Novick, and M. S. Mooseker. The yeast class v myosins, myo2p and myo4p, are nonprocessive actin-based motors. *Journal of Cell Biology*, 153(5):1121, 2001.
- P. Reimann. Brownian motors: noisy transport far from equilibrium. *Physics Reports-Review Section Of Physics Letters*, 361(2-4):57, 2002.
- P. E. Rischitor, S. Konzack, and R. Fischer. The kip3-like kinesin kipb moves along microtubules and determines spindle position during synchronized mitoses in aspergillus nidulans hyphae. *Eukaryotic Cell*, 3(3):632, 2004.
- D. Riveline, C. H. Wiggins, R. E. Goldstein, and A. Ott. Elastohydrodynamic study of actin filaments using fluorescence microscopy. *Physical Review E*, 56(2):R1330, 1997.
- G. C. Rogers, S. L. Rogers, T. A. Schwimmer, S. C. Ems-McClung, C. E. Walczak, R. D. Vale, J. M. Scholey, and D. J. Sharp. Two mitotic kinesins cooperate to drive sister chromatid separation during anaphase. *Nature*, 427(6972):364, 2004.
- I. Sagot, A. A. Rodal, J. Moseley, B. L. Goode, and D. Pellman. An actin nucleation mechanism mediated by bni1 and profilin. *Nature Cell Biology*, 4(8):626, 2002.
- H. Sakakibara, H. Kojima, Y. Sakai, E. Katayama, and K. Oiwa. Inner-arm dynein c of chlamydomonas flagella is a single-headed processive motor. *Nature*, 400(6744):586, 1999.
- M. S. Savoian, M. K. Gatt, M. G. Riparbelli, G. Callaini, and D. M. Glover. Drosophila klp67a is required for proper chromosome congression and segregation during meiosis i. *Journal Of Cell Science*, 117(16):3669, 2004.
- M. Schliwa. *Molecular Motors*, edited by Manfred Schliwa. WILEY-VCH GmbH & Co., Weinheim, 2003.
- M. J. Schnitzer, K. Visscher, and S. M. Block. Force production by single kinesin motors. *Nature Cell Biology*, 2(10):718, 2000.
- G. Schuetz. In: Exactly solvable models for many-body systems far from equilibrium, ed. c. domb and j.l. lebowitz. *Phase Transitions and critical Phenomena, Vol.19*, page 1, 2001.
- C. Shingyoji, H. Higuchi, M. Yoshimura, E. Katayama, and T. Yanagida. Dynein arms are oscillating force generators. *Nature*, 393(6686):711, 1998.
- R. V. Skibbens, V. P. Skeen, and E. D. Salmon. Directional instability of kinetochore motility during chromosome congression and segregation in mitotic newt lung-cells - a push-pull mechanism. *Journal of Cell Biology*, 122(4):859, 1993.
- Y. H. Song and E. Mandelkow. Recombinant kinesin motor domain binds to beta-tubulin and decorates microtubules with a b-surface lattice. *Proceedings of the National Academy of Sciences of the United States of America*, 90(5):1671, 1993.

- E. B. Stukalin and A. B. Kolomeisky. Simple growth models of rigid multifilament biopolymers. *Journal Of Chemical Physics*, 121(2):1097, 2004.
- K. Svoboda and S. M. Block. Force and velocity measured for single kinesin molecules. *Cell*, 77(5):773, 1994.
- K. Svoboda, C. F. Schmidt, B. J. Schnapp, and S. M. Block. Direct observation of kinesin stepping by optical trapping interferometry. *Nature*, 365(6448):721, 1993.
- A. Szent-Gyorgyi. *Stud. Inst. Med. Chem. Univ. Szeged*, page 67, 1941.
- K. Tawada and K. Sekimoto. Protein friction exerted by motor enzymes through a weak-binding interaction. *Journal Of Theoretical Biology*, 150(2):193, 1991.
- R. D. Vale. The molecular motor toolbox for intracellular transport. *Cell*, 112(4):467, 2003.
- R. D. Vale, T. S. Reese, and M. P. Sheetz. Identification of a novel force-generating protein, kinesin, involved in microtubule-based motility. *Cell*, 42(1):39, 1985.
- G. S. van Doorn, C. Tanase, B. M. Mulder, and M. Dogterom. On the stall force for growing microtubules. *European Biophysics Journal With Biophysics Letters*, 29(1):2, 2000.
- N. Van Kampen. *Stochastic Processes In Physics And Chemistry*. Elsevier Science Pub Co, 2001.
- P. Venier, a. C. Maggs, M. F. Carlier, and D. Pantaloni. Analysis of microtubule rigidity using hydrodynamic flow and thermal fluctuations. *Journal of Biological Chemistry*, 269(18):13353, 1994.
- K. Visscher, M. J. Schnitzer, and S. M. Block. Single kinesin molecules studied with a molecular force clamp. *Nature*, 400(6740):184, 1999.
- C. E. Walczak, T. J. Mitchison, and A. Desai. Xkcm1: A xenopus kinesin-related protein that regulates microtubule dynamics during mitotic spindle assembly. *Cell*, 84(1):37, 1996.
- C. M. Waterman-Storer, J. Gregory, S. F. Parsons, and E. D. Salmon. Membrane/microtubule tip attachment complexes (tacs) allow the assembly dynamics of plus ends to push and pull membranes into tubulovesicular networks in interphase xenopus egg extracts. *Journal Of Cell Biology*, 130(5):1161, 1995.
- C. M. Waterman-Storer and E. D. Salmon. Endoplasmic reticulum membrane tubules are distributed by microtubules in living cells using three distinct mechanisms. *Current Biology*, 8(14):798, 1998.
- L. Wordeman. Microtubule-depolymerizing kinesins. *Current Opinion in Cell Biology*, 17(1):82, 2005.
- L. Wordeman and T. J. Mitchison. Identification and partial characterization of mitotic centromere-associated kinesin, a kinesin-related protein that associates with centromeres during mitosis. *Journal Of Cell Biology*, 128(1-2):95, 1995.
- T. Yanagida, M. Nakase, K. Nishiyama, and F. Oosawa. Direct observation of motion of single f-actin filaments in the presence of myosin. *Nature*, 307(5946):58, 1984.

- A. Yildiz and P. R. Selvin. Kinesin: walking, crawling or sliding along? *Trends in Cell Biology*, 15(2):112, 2005.



---

# Acknowledgements

The first person to thank is Frank Jülicher, who not only gave me the opportunity to carry out this work, but also supported and guided my scientific work in the last three years with numerous discussions and impulses.

The next person I own my gratitude is Karsten Kruse who always had the time and patience to discuss about my project and fortunately also about non-scientific subjects.

My fellow combatants on the way to higher academic worth, Thomas, Björn, Nils, Frank, Andreas, Alexander, Tobias, Florian and Nili are responsible for making the last years at the institute an enjoyable and memorable time. I especially like to remember our cake-and-coffee meetings in the afternoons, and various late night excursions into saxony's well-known, healthy haute cuisine.

Specail thanks go to Nadine, who helped me with every imaginable administrative and organisational problem a PhD-student can face.

At the MPI-CBG, I would like to thank Joe Howard, Stefan Diez, Tanuj, Jonne and Gary for various discussions and explanations about the experiments which motivated this work.

I would like to thank Giovanni Cunniberti for several discussions at the beginning of my work and for several stays in the lovely town of Regensburg.

To end, my special, deep gratitude goes to my friends and family who supported me in the last years in every possible way.



---

# Versicherung

Hiermit versichere ich, dass ich die vorliegende Arbeit ohne unzulässige Hilfe Dritter und ohne Benutzung anderer als der angegebenen Hilfsmittel angefertigt habe; die aus fremden Quellen direkt oder indirekt übernommenen Gedanken sind als solche kenntlich gemacht. Die Arbeit wurde bisher weder im Inland noch im Ausland in gleicher oder ähnlicher Form einer anderen Prüfungsbehörde vorgelegt.

Die vorliegende Arbeit wurde vom 1.08.2002 bis 1.11.2005 unter wissenschaftlicher Betreuung durch Prof. Dr. Frank Jülicher am Max-Planck-Institut für Physik komplexer Systeme in Dresden durchgeführt.

Ich versichere, dass ich bisher keine erfolglosen Promotionsverfahren unternommen habe. Ich erkenne die Promotionsordnung der Fakultät Mathematik und Naturwissenschaften der Technischen Universität Dresden an.

Dresden, den 1.11.2005,

Gernot A. Klein